

GLOBAL TRENDS IN EDDY KINETIC ENERGY FROM SATELLITE ALTIMETRY

A thesis submitted to the

School of Environmental Sciences

of the

University of East Anglia

in partial fulfilment of the requirements for the degree of

Doctor of Philosophy

By

Christopher John O'Donnell

January 2015

© This copy of the thesis has been supplied on condition that anyone who consults it is understood to recognise that its copyright rests with the author and that use of any information derived there from must be in accordance with current UK Copyright Law. In addition, any quotation or extract must include full attribution.

Abstract

The temporal changes in the oceanic eddy kinetic energy (EKE) including trends and variability are presented and the dynamical mechanisms are investigated. The domain is near-global with a focus on the North Atlantic, North Pacific and Southern Oceans. Altimeter-derived geostrophic surface velocities are used to compute an 18 year time series of EKE on a $1/3^{\circ}$ grid. Linear trends are best-fit to the 18-year time series and their statistical significance assessed using bootstrap techniques. Near-global mean EKE trends are non-statistically significant. However, on a regional scale, statistically significant trends are found in all of the major ocean basins. Widespread negative trends occur primarily in the northern and southern subtropical Pacific as well as the central North Atlantic, while positive trends occur primarily in the North Atlantic subtropical gyre, much of the northeast North Atlantic, the southeast Indian Ocean and in several regions in the Southern Ocean. Buoyancy forcing and non-local wind forcing related to the PDO are significant in the North Pacific. In the North Atlantic, changes in wind stress curl as well as changes in local wind speed are implicated, where a di-polar pattern of correlations with the NAO is observed. In the Southern Ocean, changes in local and/or remote winds appear as the dominant mechanism south of 30°S . On a global scale, EKE trends are slightly positive (0.15% of the mean per decade) but non-statistically significant. EKE has decreased in the northern hemisphere and increased in the southern hemisphere despite an increase in hemispheric mean wind speed in both northern and southern hemispheres. Changing wind speeds are influential across all the ocean basins but other mechanisms are significant including shifting wind stress curl fields, buoyancy forcing, indirect (non-local) winds and intrinsic variability. Statistically significant correlations between annual mean EKE and major modes of climate variability are evident in all the ocean basins.

Acknowledgements

I would like to give special thanks to my supervisor Prof. Karen Heywood, firstly, for providing me with this opportunity, and secondly, for her mentoring and support during my time at UEA. I would also like to give special thanks to my other supervisors, Prof. Dave Stevens, who has always found the time for me despite his time-consuming responsibilities as head of the school of Mathematics, and Dr. Emily Shuckburgh, whose contribution has been greatly appreciated.

I would also like to express my gratitude to Dr. Gillian Damerell, who has helped me with Matlab and Latex coding on numerous occasions. I am also grateful to all the individuals at AVISO, who are collectively responsible for producing the altimeter data, without which this study would never have been possible.

I want to thank all my family, in particular, my parents for supporting me. Finally, I want to thank Bel for being a wonderful mother to our children and for putting up with me.

My research was funded by the Natural Environment Research Council (NERC) and is a case study with the British Antarctic Survey (BAS) as part of the DIMES project.

LIST OF ACRONYMS

ACC	Antarctic Circumpolar Current
ADT	Absolute Dynamic Topography
AzC	Azores Current
CC	California Current
DIMES	Diapycnal and Isopycnal Mixing Experiment in the Southern Ocean
ECMWF	European Centre for Medium-range Weather Forecasting
ENSO	El Niño Southern Oscillation
EKE	Eddy Kinetic Energy
ENP	Eastern North Pacific
HLCC	Hawaiian Lee Counter-Current
KE	Kuroshio Extension
NAO	North Atlantic Oscillation
NBSAF	Northern Boundary of the Sub-antarctic Front
PDO	Pacific Decadal Oscillation
PF	Polar Front
PSA	Pacific-South America wave train
SACCF	Southern ACC Front
SAF	Sub-antarctic Front
SAM	Southern Annular Mode
SASD	South Atlantic Subtropical Dipole Mode
SASH	South Atlantic Subtropical High
SLP	Sea Level Pressure
SSH	Sea Surface Height
SST	Sea Surface Temperature
STF	Sub-tropical Front
STCC	Sub-tropical Counter-current
TP	TOPEX/Poseidon

Contents

Abstract	iii
Acknowledgements	iv
LIST OF ACRONYMS	v
1 Introduction	1
1.1 Introduction	1
1.2 Historical Eddy Observations	3
1.3 Eddy Characteristics	4
1.4 Mechanisms of eddy generation	6
1.4.1 Mechanism M1: Direct (local) changes in wind.	7
1.4.2 Mechanism M2: Indirect (remote) changes in wind.	7
1.4.3 Mechanism M3: Shifting wind stress curl fields.	8
1.4.4 Mechanism M4: Wind stress curl intensification.	8
1.4.5 Mechanism M5: Local Baroclinicity.	8
1.4.6 Mechanism M6: Intrinsic variability	9
1.5 Scientific motivation and goals	10
1.6 Thesis outline	11
2 Data and Methods	13
2.1 Altimetry	13

2.2	Eddy kinetic energy	16
2.2.1	EKE Filtering	17
2.3	Statistical Analysis	23
2.4	Wind data	27
2.5	Climate modes	28
3	The North Atlantic	31
3.1	Introduction	31
3.1.1	History	31
3.1.2	Seasonal variability	33
3.1.3	Interannual variability	34
3.2	Results and Discussion	37
3.2.1	EKE Trends	37
3.2.2	Atmospheric Trends	45
3.3	EKE variability and the NAO	49
3.3.1	The North Atlantic subtropical Gyre	51
3.3.2	The Gulf Stream	52
3.3.3	Central North Atlantic and Azores Current	55
3.3.4	The northeast North Atlantic	56
3.4	Summary	60
4	The North Pacific	63
4.1	Introduction	63
4.2	Results and Discussion	67
4.2.1	EKE trends	67
4.2.2	Atmospheric trends	74
4.2.3	EKE and atmospheric variability	79
4.2.4	The Kuroshio Extension	81
4.2.5	The STCC region	83

4.2.6	The eastern North Pacific	84
4.3	Conclusions	86
5	The Southern Ocean	89
5.1	Introduction	89
5.2	Results and Discussion	96
5.2.1	EKE Trends	96
5.2.2	Atmospheric Trends	103
5.2.3	EKE and Atmospheric Variability	108
5.2.4	The DIMES Experiment Region	113
5.3	Summary	115
6	Summary and Global Perspective	116
6.1	Introduction	116
6.2	Results and Discussion	117
6.2.1	Global EKE trends	117
6.2.2	Atmospheric trends	121
6.2.3	EKE variability and climate modes	126
6.3	Conclusions and Future work	129
6.4	Outlook	131
Bibliography		133

List of Tables

1.1	Table of mechanisms.	10
-----	------------------------------	----

List of Figures

1.1	Eddy propagation characteristics	5
1.2	Eddy trajectories, 1992 to 2008	6
2.1	Schematic of Jason-2 altimeter	14
2.2	Comparison of TPJ1 EKE with merged EKE from Chelton (2007) . .	15
2.3	Comparison of trends from different satellite products	16
2.4	Time-mean EKE in the North Atlantic with spatial filtering.	19
2.5	Residual EKE after spatial filtering in the North Atlantic	20
2.6	Time-mean EKE in the North Atlantic with temporal filtering.	21
2.7	Residual EKE after temporal filtering in the North Atlantic	22
2.8	Correlation length of EKE time series	24
2.9	Frequency distribution of fictitious trends	25
2.10	Arakawa B-Grid	28
2.11	Indices, ENSO, PDO, NAO and SAM	29
3.1	Time mean EKE for the North Atlantic	37
3.2	EKE time series for the North Atlantic	38
3.3	North Atlantic annual EKE anomalies 1993-2010	39
3.4	EKE trends in the Southern Ocean 1993-2010	40
3.5	North Atlantic EKE decadal trends.	42
3.6	North Atlantic UEKE and VEKE trends.	43
3.7	EKE timeseries for 6 regions of the North Atlantic.	44
3.8	Trend in wind speed for the North Atlantic	46

3.9	Trend in wind stress curl	48
3.10	EKE/NAO Correlation coefficients	50
3.11	Yearly paths of the Gulf Stream	53
3.12	Annual mean EKE anomalies for the Gulf stream region	54
3.13	Annual mean SSH fields for the northeast North Atlantic.	57
3.14	Hovemoller diagram of wind stress curl.	58
3.15	NA wind curl composites	60
3.16	North Atlantic summary schematic.	61
4.1	EKE temporal mean for the North Pacific	67
4.2	EKE time series for the North Pacific	68
4.3	Annual EKE anomalies for the North Pacific	69
4.4	EKE trend map for the North Pacific	71
4.5	North Pacific EKE decadal trends.	72
4.6	EKE trend (normalised) for the North Pacific	73
4.7	EKE time series for the Kuroshio, STCC and ENP regions	74
4.8	Wind speed trend for the North Pacific	75
4.9	WSC trends for the North Pacific	78
4.10	EKE/PDO correlation coefficients	80
4.11	EKE time series for Kuroshio upstream and downstream	82
4.12	Time series of EKE, ENP and CC regions	85
4.13	North Pacific summary schematic.	87
5.1	Southern Ocean bathymetry	90
5.2	SAM and ENSO wind correlations	94
5.3	Southern Ocean EKE temporal mean	95
5.4	EKE time series for the Southern Ocean	97
5.5	SO annual EKE anomalies 1993-1998	99
5.6	EKE trends in the Southern Ocean 1993-2010	100
5.7	Southern Ocean EKE decadal trends.	101

5.8	Southern Ocean UEKE trend	102
5.9	EKE time series for regions of the Southern Ocean	104
5.10	Wind speed maps for the Southern Ocean	105
5.11	Wind stress curl maps for the Southern Ocean	107
5.12	Correlations of Southern Ocean EKE with SAM and ENSO	110
5.13	Zonal mean EKE trends in the Southern Ocean	111
5.14	Trend in circumpolar mean current speed	112
5.15	The Dimes region	114
6.1	Global and hemispheric EKE time series	117
6.2	Global EKE and wind speed anomalies	118
6.3	Global EKE trend map	120
6.4	Trend in slope variance from Stammer (2006)	121
6.5	Wind speed temporal mean and trend	123
6.6	WSC temporal mean and trend	124
6.7	Decadal zero wind stress curl changes	125
6.8	Zonal mean EKE trends.	126
6.9	Global EKE indices correlations	127

Chapter 1

Introduction

1.1 Introduction

The world's oceans are in constant motion and this motion, like the atmosphere, is fundamentally turbulent. As well as the large-scale mean circulation which includes the mean currents such as the Gulf Stream and Kuroshio currents, the oceans swirl and meander on smaller scales; the oceanic analogy to weather in the atmosphere. This transient variability includes linear Rossby waves and non-linear eddies (Chelton et al., 2007). It is typically referred to collectively as mesoscale variability. The oceanic mesoscale variability generally refers to space scales of 50 - 500 km and time scales of 20 - 150 days (Wyrtki et al., 1976). The kinetic energy of the mesoscale motions, or eddy kinetic energy (EKE), is considered to be more than an order of magnitude larger than the kinetic energy of the mean ocean circulation (Wyrtki et al., 1976; Richardson, 1983; Chelton et al., 2007).

The oceans cover more than 70% of the Earth's surface. Due to the high specific heat capacity of the oceans compared with the atmosphere, the oceans play a vital role in the regulation of climate. Our understanding of the role of eddies in the global ocean is therefore essential for understanding the ocean's role in climate. For example, they are the primary mechanism for the meridional transport of heat across the

Antarctic Circumpolar Current (ACC) (Hogg et al., 2008). Eddies also play a vital role in the energy and momentum budget of the global ocean (Gill et al., 1974; Ferrari and Wunsch, 2009), interacting with and feeding energy and momentum back into the mean flow (Morrow et al., 1994). As eddies can transport momentum, heat, mass and chemical constituents of seawater they consequently play a role in the general circulation, large-scale water mass distribution and biological processes (Robinson, 1984). Consequently, long term changes in EKE have the potential to influence global ocean processes including ocean circulation and climate.

The primary source of EKE generation in the ocean is the instabilities of the mean currents (Stammer and Wunsch, 1999). This flow instability takes two forms and the mechanism for eddy generation where ocean currents are strong is commonly a combination of both. Firstly, strong horizontally sheared motions result in barotropic instability where the energy source for generating eddies is the mean flow kinetic energy. Secondly, the presence of vertical shear in strong ocean fronts results in baroclinic instability where the energy required for eddy generation comes from the stored potential energy due to tilt in the isopycnal surfaces. Both of these formation processes lead to hot spots of eddy energy in the vicinity of western boundary currents and the ACC.

Recent studies have revealed processes including eddies at scales smaller than mesoscale termed sub-mesoscale processes. Observational studies and numerical studies have revealed that their dynamics are distinct from those of the largely quasi-geostrophic mesoscale processes. Sub-mesoscale processes make an important contribution to the vertical flux of mass, buoyancy, and tracers in the upper ocean. They flux potential vorticity through the mixed layer, enhance communication between the pycnocline and surface, and play a crucial role in changing the upper-ocean stratification and mixed-layer structure on a timescale of days. A review of sub-mesoscale processes by Thomas (2008) presents a synthesis of upper-ocean sub-mesoscale processes.

1.2 Historical Eddy Observations

During the 1970s, the development of eddy-resolving general circulation models underwent rapid advancement and development. Holland (1978) showed using a quasi-geostrophic general ocean circulation model, with fine horizontal resolution, that mesoscale eddies spontaneously arise due to instabilities of the ocean currents, which ultimately determine the character of the mean flow. The eddies were found to limit the amplitude of the mean flow in the upper ocean. Eddies were also found to transfer momentum and eddy energy to the abyssal ocean, creating deep, time-mean, abyssal gyres. Global observations of surface currents made by merchant ships were used to calculate the kinetic energy of the mean flow as well as EKE, which was interpreted as the kinetic energy of the fluctuations (Wyrtki et al., 1976). During this time the sparse distribution of in situ observational data meant that a detailed understanding of global mesoscale activity remained elusive.

In the late 1970s the launch of satellite-borne altimeters provided the first opportunity to study synoptic mesoscale characteristics from a global perspective. It was demonstrated by Menard (1983) that velocity anomalies associated with mesoscale motions are related to anomalies in sea-surface height (SSH) through geostrophy. Despite the poor performance of the first altimeter (GEOS-3), data from the much improved Seasat altimeter was used to generate the first global maps of mesoscale variability (Cheney and Marsh, 1983). Following the success of Seasat, Geosat was developed for the specific role of mapping mesoscale eddies. Data from this satellite facilitated the the first global-scale studies of the dynamical properties of eddies (Zlotnicki et al., 1989).

A new era in the study of mesoscale eddies began in the early 1990s with the launch of 2 new satellite altimeters; ERS-1 and TOPEX/Poseidon (TP). Professor Walter Munk, in a testimony before the United States Commission on Ocean Policy in April 2002, referred to the TOPEX/Poseidon altimeter as “the most successful ocean

experiment of all time”. A new data set was created by merging the data from both TP and ERS-1, using an objective analysis technique (Ducet et al., 2000), by Archiving, Validation and Interpretation of Satellite Oceanography (AVISO) in France. In recent years this data set has been maintained and improved with additional altimeters to the present day and is the data set with which all the oceanographic data analysis in this thesis is based.

1.3 Eddy Characteristics

By far the strongest signal in the SSH variability is associated with eddies (Fu et al., 2010). Using ten years of SSH fields, a study investigating mesoscale variability in the global ocean revealed that more than 50% of the SSH variability over much of the global ocean is accounted for by eddies with amplitudes of 5 - 25 cm and diameters of 100 - 200 km (Chelton et al., 2007). These eddies were shown to propagate nearly due westward, with preferences for slight poleward and equatorward deflection of cyclonic and anticyclonic eddies, respectively (figure 1.1a). Eddy propagation speeds were found to be slower than the zonal phase speeds of non-dispersive baroclinic Rossby waves, predicted by the classical theory, equatorward of about 25° . In the Antarctic Circumpolar Current (ACC) nearly all of the observed eddies were advected eastward. Elsewhere, eddy speeds were very similar to the westward phase speeds of classical Rossby waves (figure 1.1b).

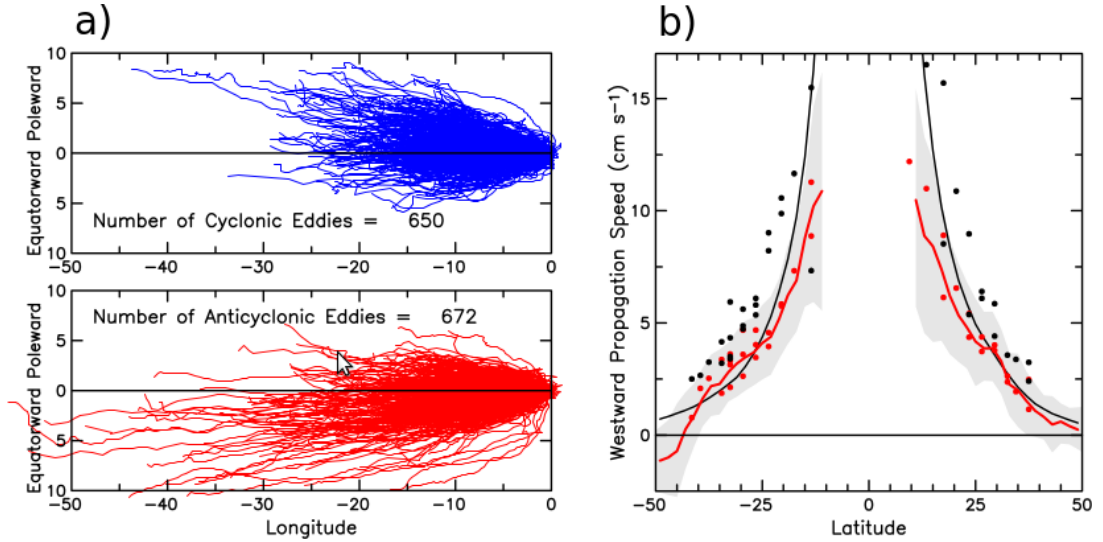


Figure 1.1: a) The global propagation characteristics of long-lived cyclonic and anticyclonic eddies with lifetimes ≥ 12 weeks. (a) The relative changes in longitude (negative westward) and latitude (poleward versus equatorward). (b) The latitudinal variation of the westward zonal propagation speeds of large-scale SSH (black dots) and small-scale eddies (red dots) along selected zonal sections. The global zonal average of the propagation speeds of all of the eddies with lifetimes ≥ 12 weeks is shown in panel b by the red line, with gray shading to indicate the central 68% of the distribution in each latitude band, and the propagation speed of non-dispersive baroclinic Rossby waves (black line). Modified from Chelton et al. (2007).

In a global observational study of eddies (Chelton et al., 2011), an automated process for identifying and tracking eddies yielded 35,891 eddies with lifetimes of ≥ 16 weeks over a period of 16 years (figure 1.2). These long-lived eddies were shown to have an average lifetime of 32 weeks and an average propagation distance of 550 km. Eddies identified and tracked by Chelton et al. (2011) were found to originate nearly everywhere in the ocean. Overall, cyclonic eddies slightly outnumbered anticyclonic eddies, however, there was a preference for eddies with long lifetimes and large propagation distances to be anticyclonic.

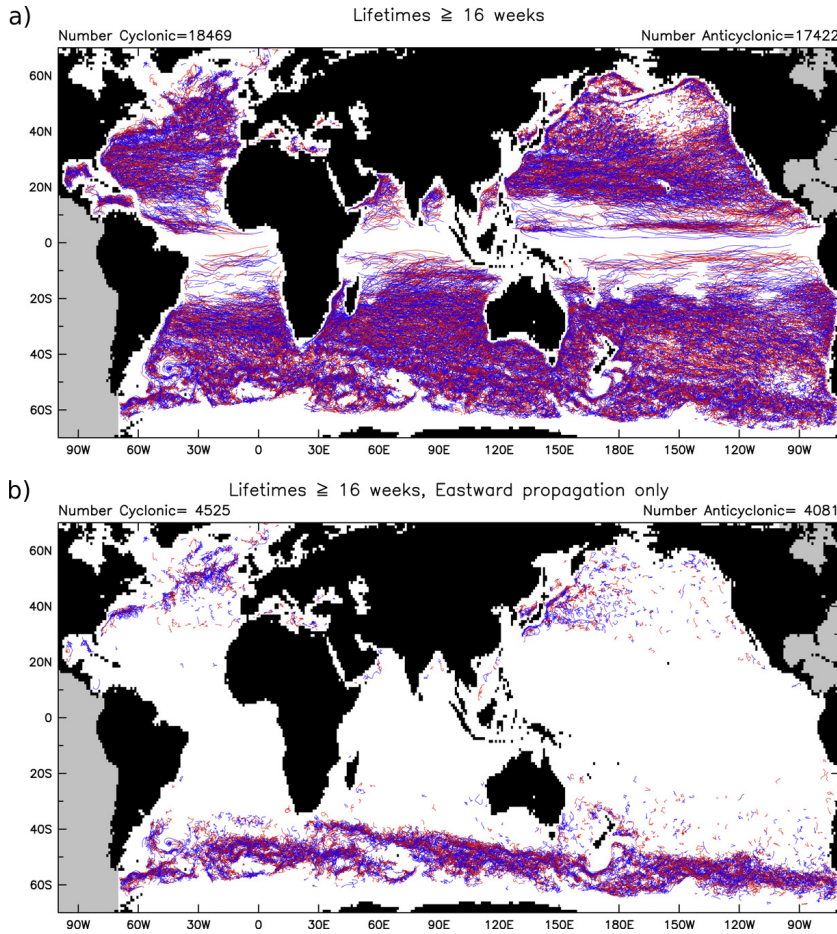


Figure 1.2: The trajectories of cyclonic (blue lines) and anticyclonic (red lines) eddies over the 16-year period October 1992 to December 2008 for (a) lifetimes ≥ 16 weeks and (b) lifetimes ≥ 16 weeks for only those eddies for which the net displacement was eastward. The numbers of eddies of each polarity are labelled at the top of each panel. From Chelton et al. (2011).

1.4 Mechanisms of eddy generation

In the analysis chapters of this thesis, references are frequently made to a number of different mechanisms responsible for EKE variability and trends. In order to both provide clarity and to avoid repetition, this section provides a preliminary description and explanation of each mechanism. Each mechanism is described in the following sub-sections (1.4.1 to 1.4.6) and a summary is shown in table 1.1.

1.4.1 Mechanism M1: Direct (local) changes in wind.

Most of the eddy energy of the oceans is generated by instabilities of the mean flow (Stammer and Wunsch, 1999), but fluctuating winds can also provide a direct forcing mechanism, particularly in regions characterised by low EKE (e.g. Frankignoul and Müller (1979); Müller and Frankignoul (1981); Stammer and Wunsch (1999)). Local wind stress at the ocean surface transfers momentum to the ocean. This can generate surface horizontal velocity shear which can produce eddies. The seasonality of EKE in the sub-polar North Atlantic has been suggested to be indicative of a significant local generation mechanism by fluctuating winds (Heywood et al., 1994). Localised eddy generation due to wind is known to exist in the lee of island chains such as the Canary Islands in the North Atlantic (Aristegui et al., 1994) and the Hawaiian Archipelago in the North Pacific (Jia et al., 2011). Two mechanisms of eddy generation in the wake of the Hawaiian islands were examined with numerical model experiments (Jia et al., 2011). The first, eddy generation by an oceanic flow around an oceanic barrier, was found to contribute an insignificant amount of EKE in the region. The second, eddy generation and shedding by an atmospheric flow around an atmospheric barrier, based on oceanic upwelling and downwelling induced by surface wind shear, provided an explanation of why eddy occurrences in the lee of the Hawaiian Islands coincided with periods of strong trade winds. Eddy generation characteristics in the model experiments were consistent with this mechanism, in terms of time of occurrence, strength and the resulting EKE.

1.4.2 Mechanism M2: Indirect (remote) changes in wind.

Once generated, eddies can both propagate and be advected over large distances. Advection rates are dependent on surface velocities, whereas propagation is nearly always due west at approximately the phase speed of non-dispersive baroclinic Rossby waves, with preferences for slight poleward and equatorward deflection of cyclonic

and anticyclonic eddies, respectively (Chelton et al., 2007). Consequently, a non-local wind forcing is a plausible mechanism for EKE changes.

1.4.3 Mechanism M3: Shifting wind stress curl fields.

The oceanic gyre circulation is wind-driven, where the meridional boundaries of the subtropical and subpolar gyres are controlled by the zonally integrated wind stress curl (WSC) (Munk, 1950). A shift in the position of WSC fields can subsequently lead to a shift in the position of the path of the wind driven currents. This can have a direct effect on EKE in the path of the current, as the enhanced EKE within the current path shifts with the current.

Sea-floor bathymetry can transfer barotropic (e.g. tidal) energy to smaller baroclinic (e.g. eddies) scales (Treguier and Hua, 1988). The sea-floor can also generate eddies where mean currents interact with (flow over or around) bathymetric features (Gille et al., 2000). In regions where eddies are generated in this manner, changes in the position of the mean currents due to shifting WSC patterns can also have an indirect effect by shifting the current path to and from a position where it interacts with bathymetry.

1.4.4 Mechanism M4: Wind stress curl intensification.

An increase (decrease) in the intensity of WSC will lead to an increase (decrease) in the strength of the wind-driven currents. This, in turn, can lead to increased (decreased) EKE in a number of ways including increased flow instability and increased flow interaction with bathymetry.

1.4.5 Mechanism M5: Local Baroclinicity.

Baroclinic instability is one of the primary mechanisms for eddy generation (Stammer and Wunsch, 1999). The existence of a baroclinic environment requires the existence

of horizontal density gradients. When horizontal density gradients increase (due to temperature and salinity fluxes) the buoyancy force is increased, increasing the available potential energy for eddy generation.

1.4.6 Mechanism M6: Intrinsic variability

When considering the physical processes responsible for any observed changes, it is necessary to make an important distinction between 'forced' variability that results from a change in the forcing and 'intrinsic' variability that results from the existence of the forcing even if that forcing does not change. Modelling studies have demonstrated that in presence of stochastic, seasonal, or constant atmospheric forcing, oceanic non-linearity can intrinsically generate and sustain variability of the horizontal circulation at interannual time scales (e.g. Hogg and Blundell (2006), Berloff et al. (2007)). Both idealised and more 'realistic' model studies suggest that, at high Reynolds number and with a sufficiently strong atmospheric forcing, the oceanic variability is likely a complex combination of direct responses to the atmosphere and of intrinsic fluctuations (Dijkstra and Ghil, 2005). Using a $1/4^\circ$ global ocean–sea ice general circulation model, Penduff et al. (2011) evaluated the local contributions of direct atmospheric forcing and intrinsic oceanic processes on interannual sea level anomalies. This study revealed that the intrinsic part of the total interannual SLA variance exceeds 40% over half of the open-ocean area and exceeds 80% over one fifth of it. This intrinsic contribution was particularly strong in eddy-active regions, as well as within the 20° to 35° latitude bands. The atmosphere was shown to directly force most of the interannual SLA variance at low latitudes and in most mid-latitude eastern basins, in particular north of about 40°N in the Pacific.

1.5 Scientific motivation and goals

Previous studies have utilised altimetric data to investigate the annual changes in EKE in a global context. Stammer and Wunsch (1999) was the first study of its kind to investigate the global temporal changes in EKE, using four years of TOPEX/Poseidon data from 1993 to 1997. On a global average, no evidence was found for any trends in global mean EKE over the 4 year altimetric record. Trends did emerge however on a regional basis. Most of the changes in mid- and low-latitudes were related to the intense currents of the general circulation, with no obvious direct connection to annual changes in the wind field (mechanism M1). In most regions, the eddy source terms were associated with the ocean flow field (baroclinic and barotropic instability) and most of the seasonal and secular changes of the EKE variability were associated with similar fluctuations in the strength and stability properties of these currents, and in the strength of the interactions with local bottom topography. Exceptions included a few places with high wind energy, notably in the North Pacific and in the northern North Atlantic, where a significant correlation of altimetric EKE with the NCEP wind stress fields was found both on annual and interannual time scales.

With more than a decade of altimeter data, Stammer et al. (2006) revisited the earlier results with the goal of obtaining a statistically more stable estimate of the time-mean EKE. In addition, this study used the changes in EKE to estimate decadal-scale changes in mixing and in their potential impact on the general circulation.

Table 1.1: A summary of the hypothesised forcing mechanisms for EKE variability and trends, including the oceanic effect.

	Forcing	Ocean Effect
M1	Local wind	Local eddy generation
M2	Remote wind	Eddy advection or propagation
M3	Shifting WSC	Shifting currents
M4	WSC intensification	Increased current strength
M5	Local Baroclinicity	More available PE, increase in baroclinicity
M6	Intrinsic	low-frequency variability

The Eddy mixing coefficient (κ) was determined as a linear function of EKE and a geographically-varying time-mean baroclinic time scale. The resulting trends in κ should therefore be related to trends in EKE. Their results suggested that there was a decline in κ from 1993 - 2003 over large parts of the western Pacific Ocean, in some regions by as much as 50% of the time-mean value. Increased κ was found in the Kuroshio and Gulf Stream regions, as well as in the Agulhas region, east of Australia, and at several locations along the ACC. Somewhat enhanced κ was also apparent in the eastern tropical Pacific.

Two decades on from the launch of TP and ERS-1, numerous altimetric studies have contributed to our understanding of global mesoscale variability. Despite this, two important questions have yet to be addressed: Firstly, are there any regions of the ocean characterised by statistically significant trends in EKE during the altimetry record? Secondly, what can be determined about the physical mechanisms responsible for the observed EKE trends? This thesis will address both of these questions. The first question is explored by studying the 18 year trends in altimeter derived EKE from 1993 to 2010. EKE trends are investigated on a regional-scale, a basin-wide scale, a hemispheric-wide scale and a global scale. Following on from this analysis, the dynamical causes of the trends are investigated using atmospheric re-analysis data. This thesis will also investigate the global pattern of EKE interannual variability, including the correlations between this variability and the major modes of climate variability in different regions.

1.6 Thesis outline

In Chapter 2, the data and methods are explained. I will explain and justify the reasons for choosing oceanic and atmospheric data sets for my analysis. The data processing steps and techniques are also outlined and explained in this chapter. In order to organise the results and discussion methodically, the results are organised into chapters

based on geographical location. Chapter 3 is the first results chapter where the focus is on the North Atlantic Ocean. In chapter 4 results are presented for the North Pacific Ocean and in chapter 5 results are presented for the Southern Ocean. In chapter 6, a synthesis of the results is presented from a global perspective.

Chapter 2

Data and Methods

2.1 Altimetry

SSH is measured using active remote sensing satellites which transmit an electromagnetic pulse in the microwave frequency band which reflects off the sea surface and back to detectors on the satellites. The distance to the sea surface (and hence SSH) is a simple linear function of the speed of the pulse and the time delay between transmission and detection. The 'raw' data acquired by the satellites undergo a number of processing steps and corrections to remove unwanted signals from both oceanic (such as tidal corrections) and atmospheric (such as ionospheric corrections) origins. Details of the altimetric data processing steps are described by Fu and Cazenave (2000).

Figure 2.1 illustrates how the altimeter measures SSH. This illustration shows that SSH is made up of a combination of two separate phenomena; The marine geoid and ocean surface topography. The marine geoid represents the surface that a resting ocean would conform to were there no fluid motion in the oceans. Due to the Earth's surface gravity anomalies, the marine geoid is not flat. The ocean surface topography, also referred to as dynamic height or dynamic topography, represents the departure of the ocean's surface from the geoid, resulting from motion. Early studies showed that altimetric data analysis allows determination of dynamic heights of the sea surface

with respect to the marine geoid (Cheney and Marsh, 1981; Douglas and Gaborski, 1979; Huang et al., 1978; Mather et al., 1979). The dynamic height results not only from mesoscale motions, but also the motion of the mean currents.

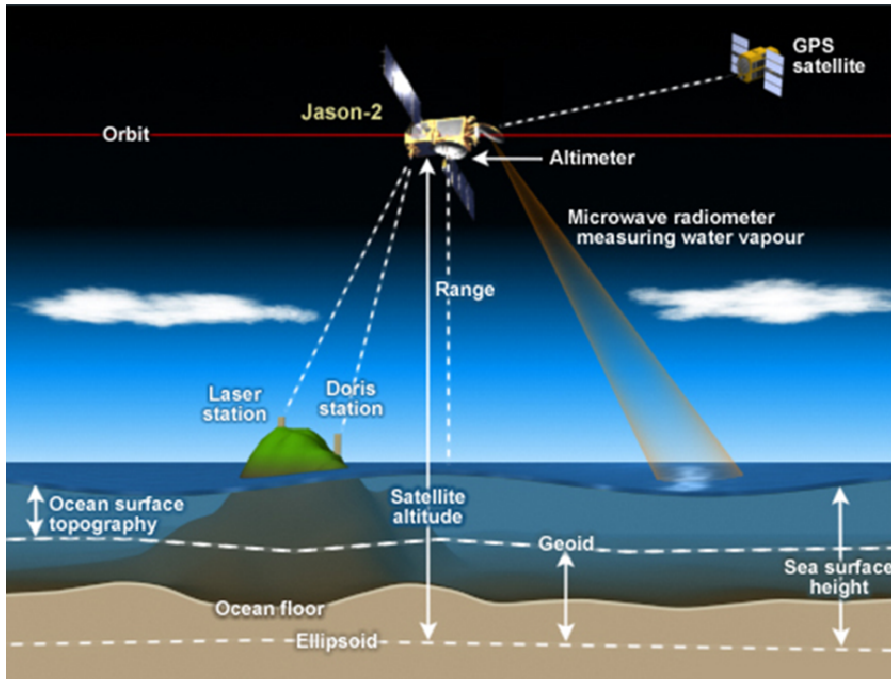


Figure 2.1: Schematic diagram illustrating the method of SSH measurement by the Jason-2 altimeter.

The post-processing SSH product used in this thesis is provided by AVISO (Archiving, Validation and Interpretation of Satellite Oceanography, available online at <http://www.aviso.oceanobs.com>). The raw SLA product is computed from the difference of the instantaneous SSH minus a temporal reference. The method for producing the temporal reference is detailed in the AVISO User Handbook (available online at <http://www.aviso.oceanobs.com>). These data are obtained on a $1/3^\circ$ Mercator grid at 7-day intervals from January 1993 to December 2010. The delayed-time (M)SLA 'Ref' product (ref-SSH) was chosen for this study. The ref-SSH satellite product is a homogeneous data set based on two simultaneous satellite missions; TOPEX/Poseidon and ERS-1 from October 1992 to August 2002, Jason-1 and ERS-2 from August 2002 to June 2003 and Jason-1 and Envisat from June 2003 to December

2010. The authors of previous studies (e.g. Meredith and Hogg (2006)) have chosen to use data from the TOPEX/Posiedon and Jason1 (TPJ1) satellites only. This is due to the fact that for several months in 1994, TOPEX/Posiedon data alone was used in the merged multi-satellite product. The resulting different spatial/temporal sampling was affected by around 30% globally (Ducet et al., 2000).

The resolution of the merged TPJ1 and ERS-1/2 data is about double that of the TPJ1 data alone (Chelton and Schlax, 2003), which presents a markedly different picture of SSH (Figure 2.2). The merged data reveal many isolated eddy-like cyclonic and anticyclonic features (negative and positive SSH, respectively) that are poorly resolved in the TPJ1 data alone.

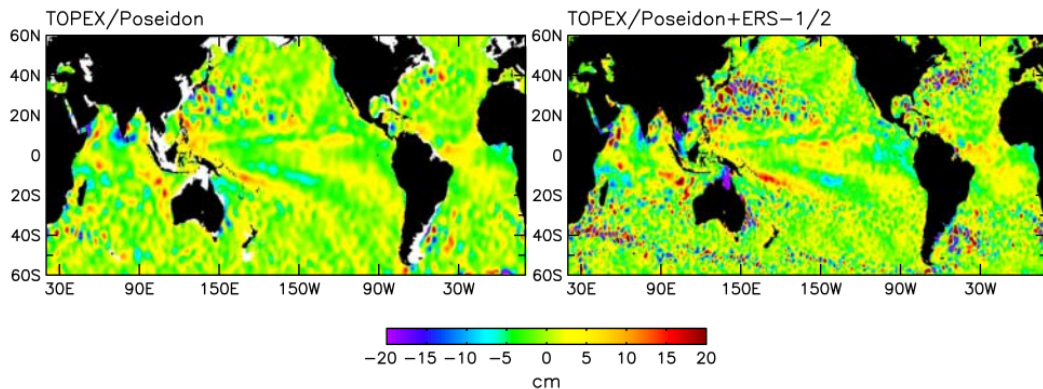


Figure 2.2: North Pacific SSH on 21 August 1996 from the T/P data alone and from the merged T/P and ERS-1/2 data. From Chelton et al. (2007).

We can also demonstrate (figure 2.3) that the global trends in EKE which form the main topic of this thesis are not sensitive to different satellite configurations (i.e. products). In each region in figure 2.3, the magnitude of the annual mean EKE derived from the merged satellite data is significantly higher than that of the TPJ1 data. The gradient of the linear trend line for each region is virtually the same for all the regions, indicating that the trends are not sensitive to the different data sets.

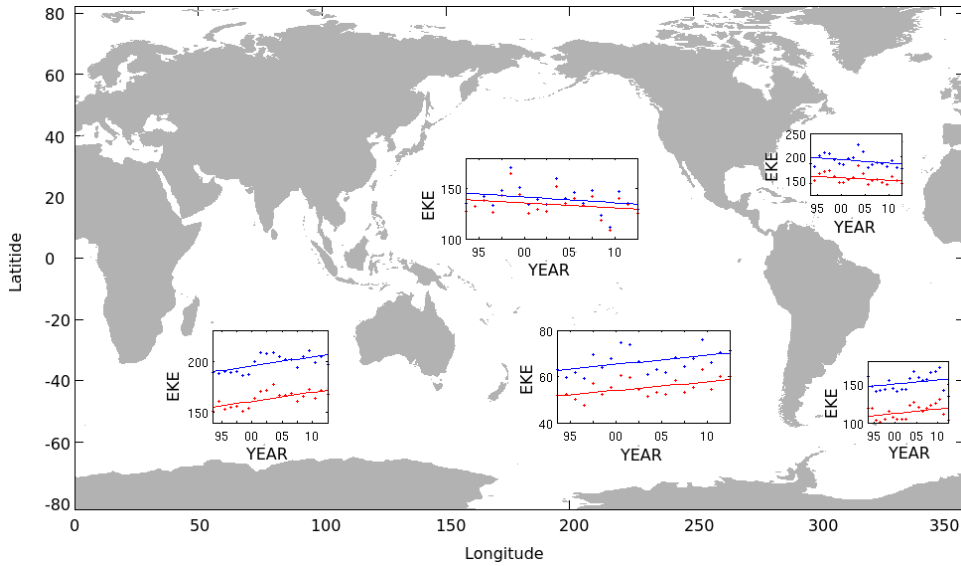


Figure 2.3: Time series of EKE averaged over each boxed region, showing the comparison between EKE from the merged satellite data (blue stars) with trend (blue line) and EKE from the TPJ1 satellite data (red stars) and trend (red line).

2.2 Eddy kinetic energy

Calculating EKE from sea level anomalies

The ability of radar altimetry to map the EKE field was first demonstrated by Menard (1983) who, considering the eddy field in geostrophic balance, derived surface eddy velocities from the geostrophic relation. An estimation of the EKE was then deduced assuming the velocity variability was quasi-isotropic. In this thesis, eighteen year time series of weekly near global EKE fields are computed from the sea-level anomaly (SLA) fields. EKE is calculated by deriving surface geostrophic velocity anomalies from the SLA gradients, and then calculating half the sum of the average eastward and northward velocity anomalies squared (equation 1).

$$\text{EKE} = \frac{1}{2} \left[\left(\frac{g}{f} \frac{\partial h'}{\partial x} \right)^2 + \left(\frac{g}{f} \frac{\partial h'}{\partial y} \right)^2 \right] \quad (1)$$

where g is the acceleration due to gravity (9.81 m s^{-2}), f is the Earth's planetary vorticity or Coriolis parameter; $f = 2\Omega \sin(\theta)$, where Ω is the Earth's angular velocity ($7.3 \text{ e}^{-5} \text{ rad s}^{-1}$), θ is latitude and $\frac{\partial h'}{\partial y}$ and $\frac{\partial h'}{\partial x}$ are the meridional and zonal slope of the sea surface respectively.

The result is a near-global data set of EKE on a $1/3^\circ \times 1/3^\circ$ Mercator grid at weekly intervals spanning the period from October 1992 to December 2010. Due to the seasonal variability of sea ice cover, some regions in the high latitudes have incomplete time series. In this study these regions have been masked and simply removed from our analysis to avoid biasing our results. The regions within 3° north and south of the equator have also been removed for our analysis, as the geostrophic assumption breaks down due to a vanishing Coriolis parameter near the equator as the sine of the latitude approaches zero (see equation 1).

2.2.1 EKE Filtering

The oceanic mesoscale variability captured by the altimeters and represented in the SSH anomaly fields includes a number of different mesoscale phenomena such as eddies, shifting current paths and meandering jets, Rossby waves and equatorial Kelvin waves, each of which has its own frequency and wavenumber characteristics. In later chapters, in order to isolate the contribution of eddies in the SSH fields from other mesoscale signals, we have filtered the SSH fields prior to calculating geostrophic velocities.

Previous studies have also attempted to isolate the eddy-like signals in the SSH data using spatial and temporal filtering techniques. Scharffenberg and Stammer (2010) used a variable wavenumber filter set to be a function of latitude to isolate eddy signals in the SSH data. Other studies including Qiu and Chen (2005) used a 300 day high pass filter, to filter the SSH fields in the frequency domain. Other recent studies of EKE variability such as Volkov (2005), Meredith and Hogg (2006) and Zhai et al. (2008) have chosen not to filter the SSH fields for their analysis.

The methods of spatial and temporal filtering in this thesis follow the methods detailed in Boland (2013). The space filtering is performed at each time step using a 2D high-pass wavenumber filter. Figure 2.4 shows the degree to which the time-mean EKE field in the North Atlantic changes with varying wavenumber filters from 1° to 6° .

Figure 2.5 shows the residual values normalised by the mean, representing how much (as a percentage) of the unfiltered field (upper left panel) has been removed by the filter. When a 1° filter is used, nearly all the signal is removed. However, a weak signal remains in the Gulf Stream extension. The signal increases progressively from 1.5° s to 3.5° where the EKE field begins to resemble the unfiltered field in magnitude and the major current systems can be identified. From 4° to 6° the signal does not show an obvious increase but the residuals show the changes more clearly.

Temporal filtering is performed at each location using a low-pass butterworth filter. Figure 2.6 shows the degree to which EKE in the same domain changes with varying frequency filters from 1 month to 11 months and figure 2.7, the subsequent residual fields.

A one month high-pass filter removes the majority of the signal although the Gulf Stream is clearly visible in this field. With the frequency filter increasing steadily from 2 to 5 months, the major current systems become observable. The signal does not appear to change very much from 6 to 11 months but once again the residuals show the signal continues to increase at each time step, in fact the residuals clearly show that even at 11 months a significant portion of the EKE signal is still removed by the filtering. This is most prominent in the northeast where in some locations more than 50% of the EKE signal has been removed.

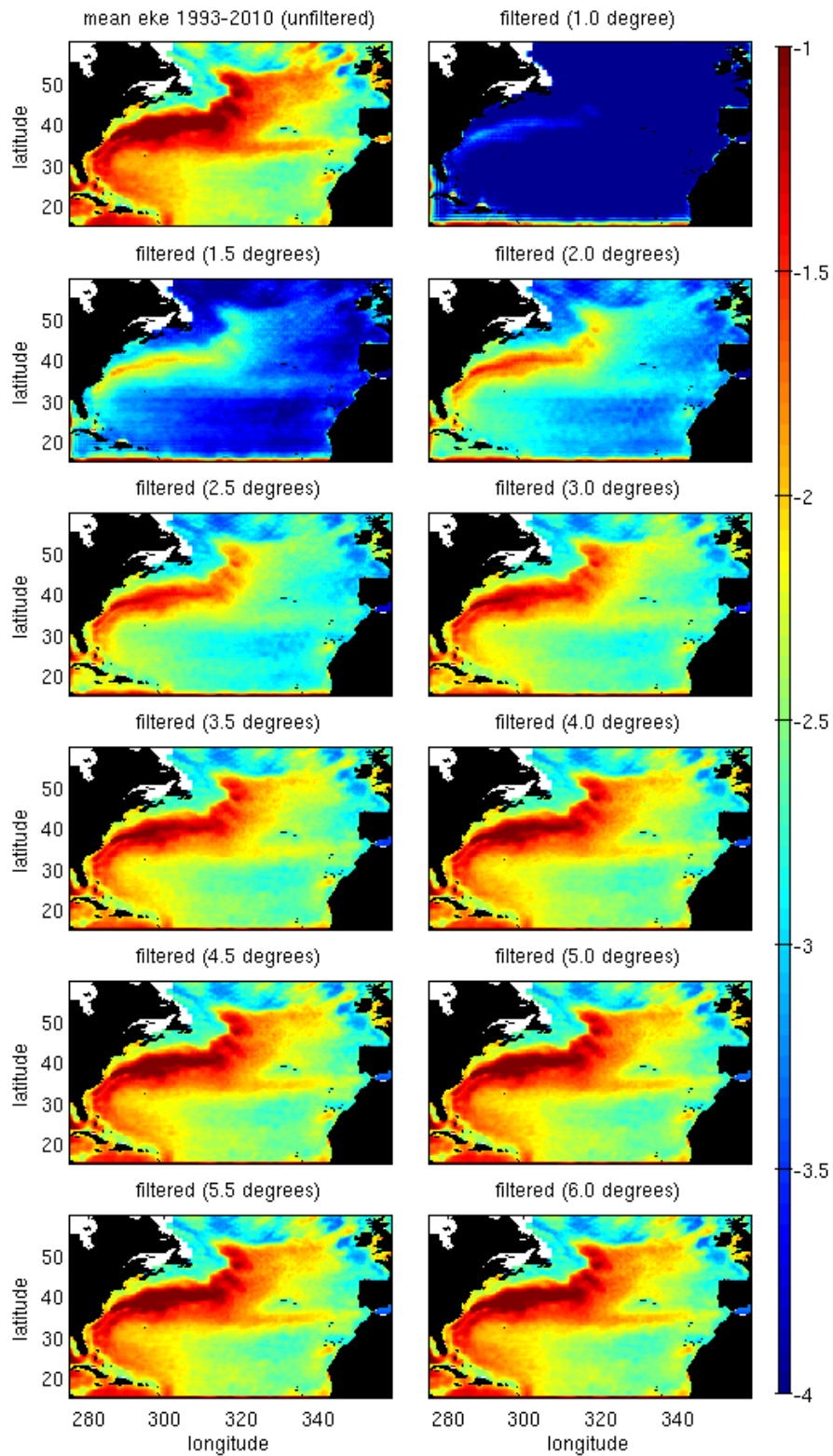


Figure 2.4: \log_{10} of time mean EKE ($m^2 s^{-2}$) in the North Atlantic (1993 – 2010) calculated from high-pass filtered SLA fields with varying filters from 1° to 6°.

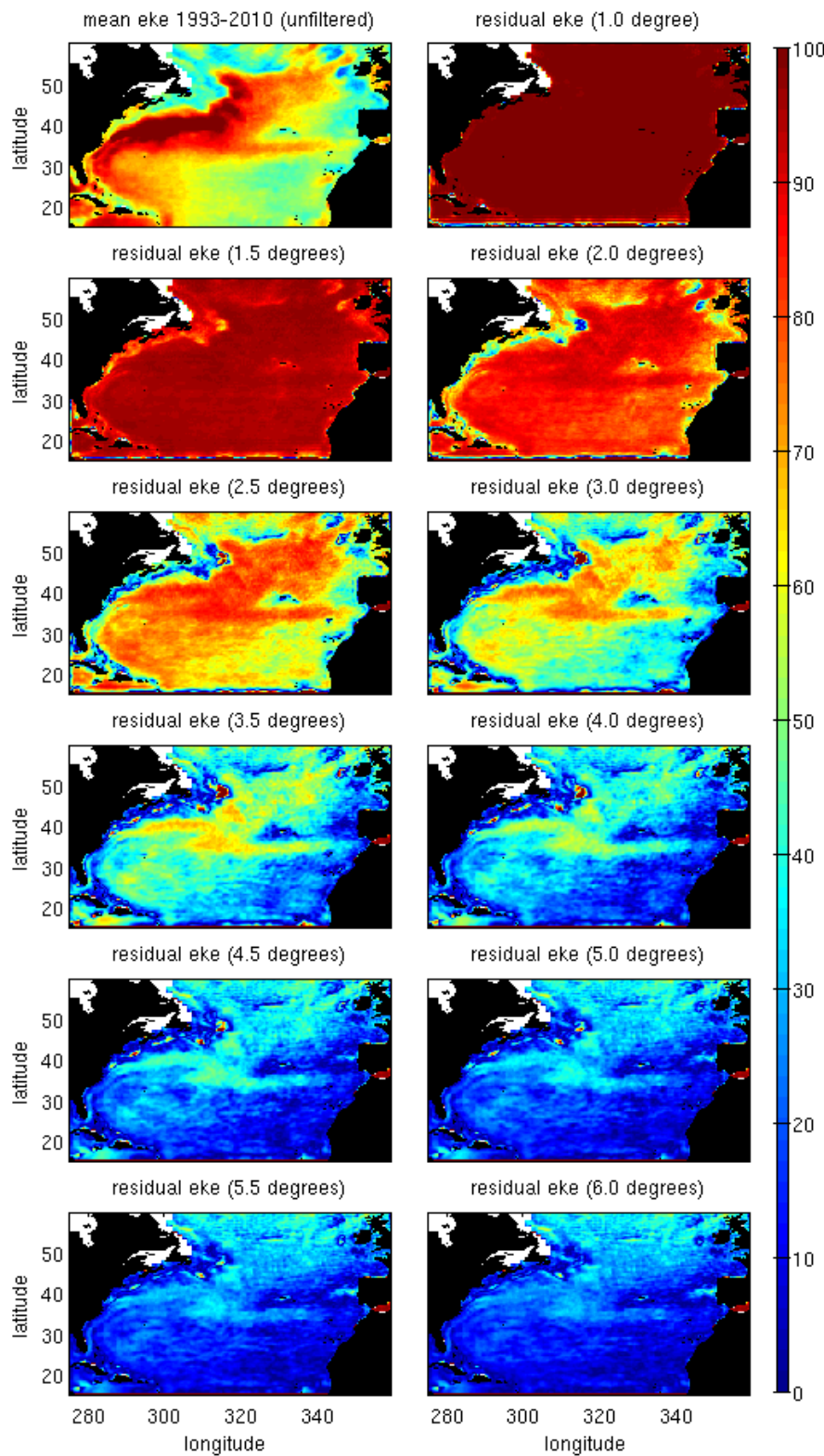


Figure 2.5: Residual time-mean EKE ($m^2 s^{-2}$) in the North Atlantic (1993 – 2010) calculated by removing the filtered fields in each panel of figure 2.4 from the unfiltered field (top left panel). The scale is normalised by the unfiltered field and multiplied by 100 to represent a percentage of the top left panel.

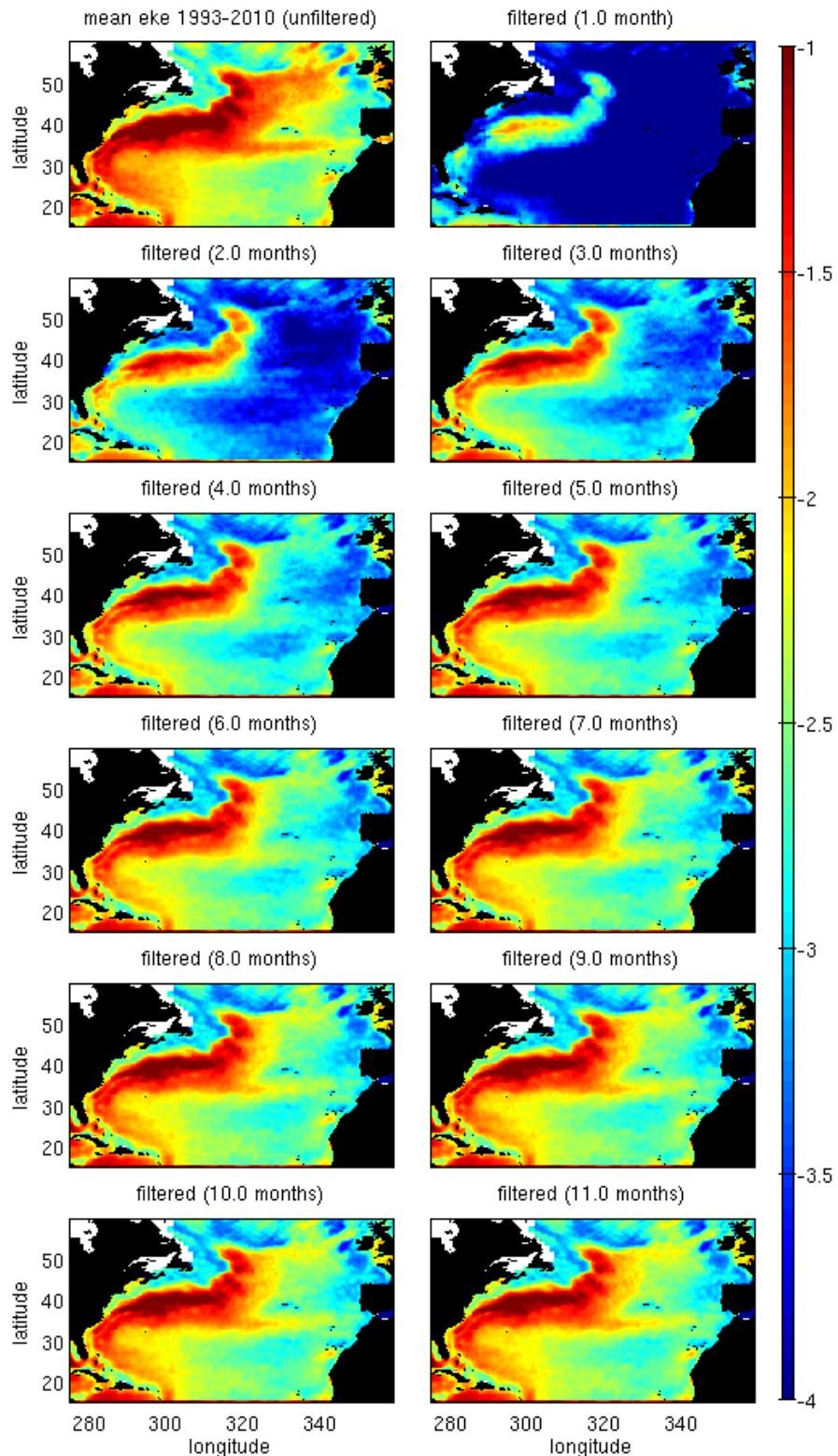


Figure 2.6: \log_{10} of time mean EKE ($m^2 s^{-2}$) in the North Atlantic (1993 – 2010) calculated from SLA fields with varying frequency filters from 1 month to 11 months.

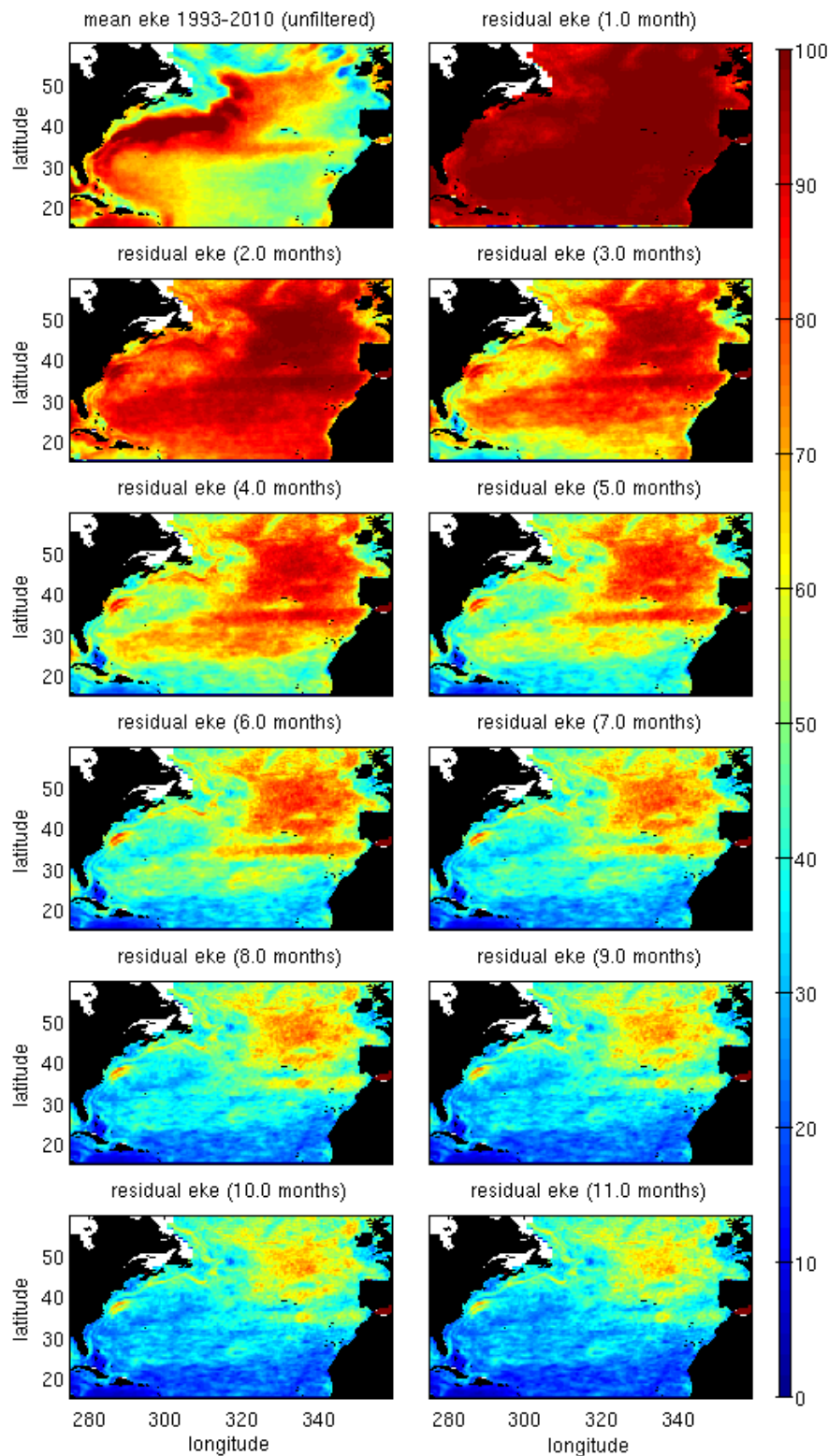


Figure 2.7: Same as figure 2.5 but for time filtered residuals from figure 2.6.

2.3 Statistical Analysis

Statistical significance of trends

Trends are determined as the gradient of a least squares linear fit to each time series. The term 'Statistically significant' refers to a result or outcome (trend or correlation coefficient) which falls within a given significance level. For this thesis we have chosen to use the 90% significance level. This means we are 90% confident that a result deemed statistically significant has not arisen by chance.

In the case of trends, the statistical significance can be typically quantified using a bootstrapping method (Efron, 1979). This method involves the re-sampling of the time series several thousand times. A frequency distribution of these fictitious trends is then used to identify the standard deviation (std) of the bootstrapped trends. Any real trend from the original time series greater than +2 std or less than -2 std of the re-sampled trends is typically deemed to be statistically significant. This method assumes that all the data points are independent.

In the case of EKE, data points in the time series may not be independent but instead may contain auto-correlation. Auto-correlation exists when data points in a data series have some degree of relation to their neighbouring data points. In such a case, a simple bootstrapping method is not appropriate. Instead a block bootstrap (Efron, 1979) must be used that accounts for the autocorrelation when determining significance.

This method works by dividing the time series into 'chunks' of data, the length of which must be sufficient to preserve the autocorrelation. Each block can then be considered independent from its neighbouring blocks and each time series can then be re-sampled. The following steps show how this method has been employed in this thesis to determine trend significance at each location:

- 1) Calculate the decorrelation time scale of EKE time series. This is determined by correlating a data set with itself at varying lags until the correlation reaches zero. An

example of a time series (figure 2.8a) clearly shows a significant degree of dependency of each data point with its neighbours. This results in the very high autocorrelation values (figure 2.8b) at small lags (>0.4 at up to 10 week lag) which continue to reduce until reaching zero at 21 week lag. This sets the decorrelation time scale at 21 weeks (21 data points).

2) A trend line is then fitted to the time series by calculating the linear coefficients based on a least squares linear fit. The magnitude of the trend is expressed as the gradient of the trend line.

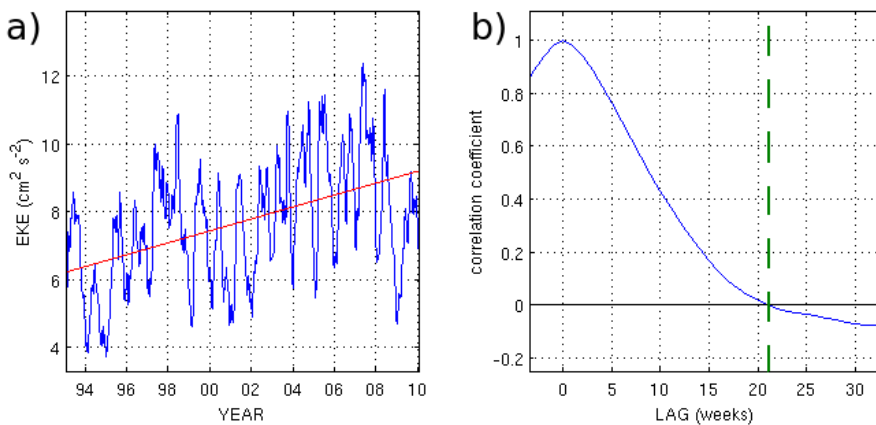


Figure 2.8: (a) An example of a time series of weekly EKE (blue line) with linear trend (red line). (b) The normalised autocorrelation coefficients at varying lags. The dashed green line in b) identifies the lag at which the correlation reaches zero.

3) The time series is then re-sampled 1000 times by randomly selecting blocks of data from the original data series (In this example data blocks are 21 data points long). On each occasion, the magnitude of the trend is calculated. This generates a series of 1000 fictitious trends, of which simple statistical values such as mean, standard deviation, and percentiles can be established. Ninety percent of these fictitious trends will lie within \pm the 95th percentile if the process is random and the distribution is Gaussian (figure 2.9).

4) Finally, the statistical significance is established as significant where the fitted

trend is outside the bounds of ± 95 th percentile of the bootstrapped trends and non-statistically significant if it is not. The frequency distribution of bootstrapped trends from the time series in figure 2.8 is shown in figure 2.9, where the fitted trend (red line) lies outside the bounds of the 95th percentile (green line) and is hence 'significant'.

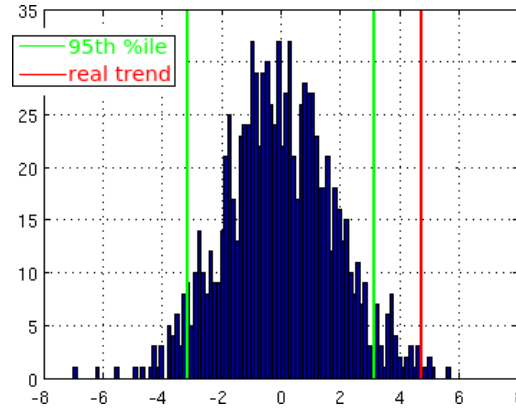


Figure 2.9: Frequency distribution showing the Gaussian nature of trends generated from EKE timeseries in 2.8a re-sampled 1000 times. The real trend (red line) is clearly outside the significance boundaries set by the 5th and 95th percentiles (green lines).

Statistical significance of correlations

The correlation coefficient between two time series x and y (r_{xy}), is calculated as shown in equation 2, where σ_{xy} is the covariance of x with y and $std(x)$ and $std(y)$ are the standard deviations of x and y respectively. Typically, a p-value is used to determine the statistical significance of a correlation. Once again, this is only appropriate when data points in each data set are independent. When auto-correlation is present, this must be accounted for when determining the statistical significance.

$$\sigma_{xy} = \mathbb{E} ([x - \bar{x}] [y - \bar{y}]) \quad (2)$$

$$r_{xy} = \frac{\sigma_{xy}}{std(x) std(y)}$$

In this thesis we have employed the method from Von Storch and Zwiers (2001) as follows.

- 1) Define the decorrelation length scale, τ_D ,

$$\tau_D = 1 + 2 \sum_{k=1}^{\infty} \rho(k) \quad (3)$$

where k is the lag, $\rho(k)$ is the autocorrelation function.

- 2) The time series has n data points. The number of independent realisations (n') is then:

$$n' = \frac{n}{\tau_D} \quad (4)$$

- 3) The Fisher-Z transformation is

$$Z = \frac{1}{2} \ln \left(\frac{1+r}{1-r} \right) = \tanh^{-1} r \quad (5)$$

where the correlation coefficient between two time series is r .

For two randomly generated white-noise time series, Z is normally distributed with mean zero, and standard deviation $\sigma = 1/(n-3)^{1/2}$.

- 4) The critical correlation coefficient at the 90% significance level is

$$r_{90} = \pm \tanh \frac{1.68}{(n-3)^{1/2}} \quad (6)$$

To calculate the critical correlation coefficient for two time series that have non-zero autocorrelations, we use n' instead of n . If both time series have autocorrelations, we calculate the decorrelation time scale separately for each one, then use the largest one, and hence the smallest number of independent realisations.

'Goodness of fit' of trends

The term 'goodness of fit' is used in this thesis to quantify how well a time series fits a linear trend line. The value represents the root mean square error of the time series to the trend line, normalised by the variance. This is mathematically equivalent to the square of the correlation coefficient which is calculated according to equation 2.

2.4 Wind data

Throughout this thesis, wind speed and wind stress curl data are analysed in order to attempt to explain the physical mechanisms responsible for changes in EKE. Wind speed and wind stress curl data are calculated from ERA-Interim reanalysis 10 metre zonal and meridional winds on a $0.75^\circ \times 0.75^\circ$ grid, supplied by the European Centre for Medium-Range Weather Forecasts (ECMWF). The configuration and performance of the data assimilation system is described by Dee et al. (2011). Wind speed was chosen as initial results with wind stress primarily showed the same patterns and features so wind speed was chosen for simplicity. Wind power input was also considered as part of our analysis. however, wind speed was preferred over wind power input for simplicity as it is always positive. The curl of the wind stress is calculated from monthly mean wind stress fields from ECMWF ERA-Interim re-analysis data as shown in equation 7.

$$\hat{\mathbf{k}} \cdot \nabla \times \boldsymbol{\tau} = \frac{1}{r \cos \theta} \left(\frac{\partial \tau_\theta}{\partial \phi} - \frac{\partial}{\partial \theta} (\tau_\phi \cos \theta) \right) \quad (7)$$

where $\boldsymbol{\tau}$ is the wind stress, θ is latitude, ϕ is longitude, τ_ϕ is the zonal wind stress ad τ_θ is the meridional wind stress. The curl is calculated on an Arakawa B grid (Arakawa and Lamb, 1977) as illustrated in figure 2.10.

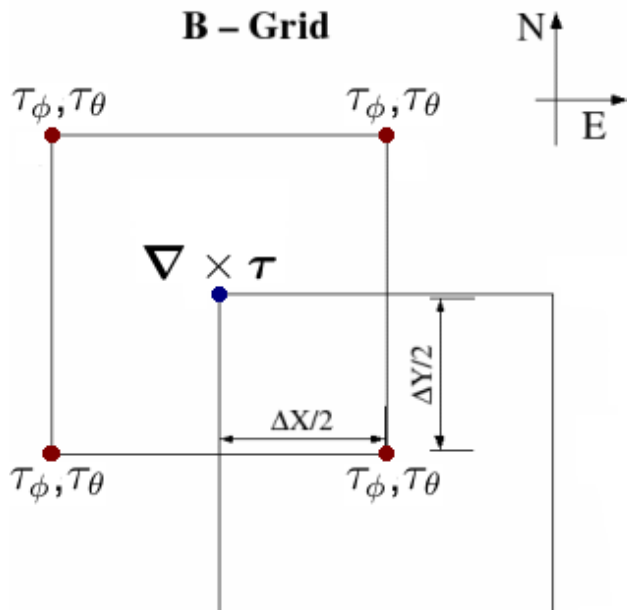


Figure 2.10: Calculation of wind stress curl using the Arakawa b-grid. τ_ϕ and τ_θ are the gridded zonal and meridional wind stresses and $\nabla \times \tau$ is the staggered wind stress curl grid point.

2.5 Climate modes

The El Niño Southern Oscillation (ENSO) monthly climate mode index (figure 2.11a) was obtained from the NOAA Climate Prediction Centre (available online at www.cpc.ncep.noaa.gov). The ENSO index is based on sea surface temperature (SST) anomalies in the El Niño 3.4 region ($5^{\circ}\text{N} - 5^{\circ}\text{S}$, $120^{\circ}\text{W} - 170^{\circ}\text{W}$) in the tropical Pacific (Bjerknes, 1969). During the early months of 1997 the tropical Pacific Ocean underwent a major transition from La Niña conditions in November 1996 to a major El Niño by the summer of 1997, with peak SST anomalies in the east Pacific in excess of 5°C (Slingo, 1998).

The Pacific Decadal Oscillation index (PDO) is defined as the leading principal component of North Pacific monthly SST variability poleward of 20°N . A notable characteristic of this index is its tendency for multi-year persistence (figure 2.11b).

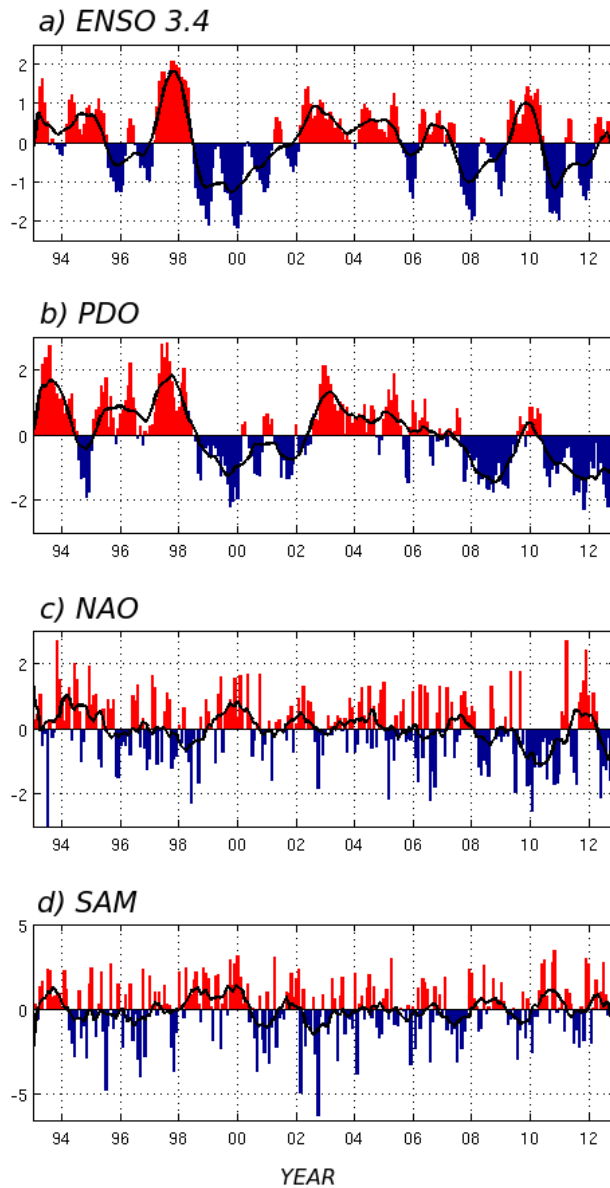


Figure 2.11: Monthly indices of major climate modes; a) El Niño Southern Oscillation (ENSO 3.4), b) Pacific Decadal Oscillation (PDO), c) North Atlantic Oscillation (NAO) and d) Southern Annular Mode (SAM). In each case red represents a positive phase, blue represents a negative phase and the black line shows the 12 month running mean.

The PDO mode of variability exhibits a robust symmetry in inter-decadal climate variability of both the northern and southern hemispheres with signature responses in East Asia, North South and Central America and Australia (Mantua and Hare, 2002).

The North Atlantic Oscillation (NAO) Index (figure 2.11c) describes a large-scale

meridional oscillation in atmospheric mass between the North Atlantic regions of the Azores high and the sub-polar low pressure system near Iceland. Most pronounced in winter, it is a major source of seasonal to inter-decadal variability in the worldwide atmospheric circulation (Hurrell and Loon, 1997). The measure for the state of the NAO is generally used as an indicator of the strength of the westerlies over the eastern North Atlantic.

The Southern Annual Mode index (SAM) is the principal mode of atmospheric variability in the Southern Hemisphere extra-tropics and high latitudes (Marshall, 2003). This mode represents the leading empirical orthogonal function in many atmospheric fields, including surface pressure, geopotential height, SST, and zonal wind (Thompson and Wallace, 2000). The variability in the SAM index (figure 2.11d) reflects a significant proportion of Southern Hemisphere climate variability including high-frequency (Baldwin, 2001) to low-frequency time scales (Kidson, 1999). Modelling studies indicate that the SAM is also likely to drive the large-scale variability of the Southern Ocean (Hall and Visbeck, 2002).

Chapter 3

The North Atlantic

3.1 Introduction

3.1.1 History

EKE in the North Atlantic was first estimated on a basin-wide scale by Wyrtki et al. (1976) who studied surface drift currents observed by merchant ships to calculate the kinetic energy of the mean flow as well as the kinetic energy of the fluctuations, interpreted as EKE. The distribution of these properties was charted for the North Atlantic based on 1° squares and for the world oceans based on 5° squares. Both distributions showed high values in the western boundary currents and in the equatorial current system and low values in the subtropical gyres. Comparing mean and eddy energies in ocean and atmosphere revealed that eddy energies in the two systems were uncorrelated. The results were consistent with the theory that eddies in the ocean are generated in areas of strong mean shear flow and are subsequently distributed over the whole ocean.

A study by Richardson (1983) measured velocities and trajectories of the near-surface currents in the North Atlantic using satellite tracked freely drifting buoys. A horizontal map of EKE was prepared on a 2° by 2° grid between latitudes 20°N and

55°N. Maximum eddy energy was found in the Gulf Stream, where the jet exhibits large amplitude meanders near 37°N 67°W. A tongue of high EKE coincided with the Gulf Stream's path eastward and around the Grand Banks into the Newfoundland Basin. A weaker tongue extended eastward across the mid-Atlantic Ridge (MAR) near 45°N. A second weak extension was identified southeastward from the Gulf Stream and crossed the mid-Atlantic Ridge between 30°N and 35°N. North and south of the Gulf Stream, EKE diminished rapidly. Lowest values were observed in the mid-gyre region and in the eastern North Atlantic and North Equatorial Current. Although the gross distribution of EKE was similar to that determined by Wyrtki et al. (1976), there were significant differences. EKE from drifters amounted to approximately twice the value measured by ship drift in the Gulf Stream and one half the ship drift values in the mid-gyre. It was suggested by Richardson (1983) that these differences are due to the horizontal averaging of mesoscale motion and the errors in navigation, both of which are problems with the ship drift technique. A similar study using satellite-tracked buoys (Krauss and Käse, 1984) concluded that the North Atlantic Current (NAC) is the main source of EKE for the northern North Atlantic, whereas the MAR is not a source of eddy energy.

In the early 1990s, regional studies of EKE in the North Atlantic included altimetric studies (Le Traon et al., 1990; Heywood et al., 1994; White and Heywood, 1995). EKE calculated from 2 years of Geosat data (Le Traon et al., 1990) compared well with estimates from surface drifters. Le Traon et al. (1990) characterised the spatial scales of mesoscale variability in terms of their wavenumber spectra and autocorrelation functions. The features of wavenumber spectra were consistent with a forcing by instability of mean currents in the high-energy regions and by fluctuating winds in the low-energy regions. There were also some indications of small-scale topographic effects east of the MAR. Spectral slopes were, however, found to be weaker than those of quasi-geostrophic theory and models, possibly due to non-geostrophic effects.

EKE in the North Atlantic subpolar gyre was studied using altimetric data by Hey-

wood et al. (1994) and White and Heywood (1995). Heywood et al. (1994) confirmed a close relationship between EKE and the topographically constrained mean currents. High EKE was observed on the flanks of topography and was higher where the slope was steeper.

3.1.2 Seasonal variability

EKE in the North Atlantic responds to the seasonal fluctuations of the intensity and curl of the local wind stress with a lag of up to a few months, for example lags of 4 months in the eastern North Atlantic (Richardson, 1983) and 2 months in the Labrador Sea (White and Heywood, 1995). Richardson (1983) identified a seasonal cycle in EKE in the North Atlantic which peaked in May-June. This seasonal cycle was also identified from current meters in the northeast Altantic by Dickson et al. (1982). If, as these previous studies suggest, the variability in the strength of the wind stress curl can modulate EKE on seasonal time-scales, we would expect both long term changes in the intensity of the wind stress curl (mechanism M4) as well as shifting wind stress curl patterns (mechanism M3) to play a significant role in EKE trends in some regions of the North Atlantic.

White and Heywood (1995) show that in regions of strong mean currents within the NAC eddies are primarily driven by baroclinic instability of the mean currents and are not seasonally varying. Outside the NAC eddies are driven primarily by wind stress and show strong seasonality. The study of the role of variable wind forcing in eddy generation in the North Atlantic was continued by Stammer and Wunsch (1999) and Stammer et al. (2001). The primary conclusion of both these studies was that significant wind impact on eddy generation (mechanism M1) is confined mainly to the northern North Atlantic (including the Labrador Sea, the Irminger Sea, and the north-eastern part of the basin). All these regions are characterized by weak stratification and low EKE. Both these factors conspire to allow the relatively small wind-induced eddy component to be detected against the background of internally-induced variabil-

ity (mechanism M6), which greatly exceeds the wind effects in the vicinity of the major open ocean frontal systems. The aforementioned regions of the northern North Atlantic are also subjected to a higher variance in the winter wind stresses than the subtropics.

The Gulf Stream region is also characterised by a seasonal cycle in EKE (Zhai et al., 2008) which peaks in summer despite the ocean being more baroclinically unstable (as measured by the baroclinic eddy growth rate) in winter. The authors argue that the summer peak is due to a reduction in eddy dissipation in summer compared with winter.

In a global study of temporal changes in EKE, Stammer and Wunsch (1999) found that over most of the subtropical oceans and along major mean fronts, seasonal variations of EKE are negligible. The regions that did show a pronounced annual cycle in eddy energy included the northern and eastern North Atlantic. White and Heywood (1995) conclude that the magnitude of the eddy field driven by baroclinic instability or wind stress can be determined by looking at the seasonality and in the region of the NAC, where a seasonal cycle is essentially absent, EKE can be used effectively as a surrogate for the mean flow implying that changes in the spatial pattern of EKE show shifting of the path of the mean currents.

3.1.3 Interannual variability

EKE interannual variability has been the subject of previous studies in different regions of the North Atlantic. Using altimetric data, White and Heywood (1995), Heywood et al. (1994) and Ducet and LeTraon (2001) have described the year to year changes in EKE for different regions of the North Atlantic revealing that the main branches of the NAC crossing the MAR are subject to interannual changes (Heywood et al., 1994). The study by Heywood et al. (1994) was extended to show that the northward and southward shifts in NAC branches crossing the MAR were related to interannual changes in the winter wind stress curl (White and Heywood, 1995) (mech-

anism M3).

The first extensive, near-global scale study of EKE interannual variability was provided by Stammer and Wunsch (1999) using TOPEX/POSEIDON altimeter data and current meter records with a focus on the North Atlantic and North Pacific Oceans. Annual changes in EKE and corresponding annual changes in the wind stress were found to be highly variable and intricate on a global scale, with few easy generalizations possible. Over the northeastern Pacific, the northern and eastern North Atlantic, as well as the tropical oceans, a strong correlation of a time-varying EKE on annual and longer periods with wind stress forcing was found and trends present in near-surface EKE were related to drifts in meteorological wind stress fields over the four year TOPEX/POSEIDON record (mechanism M3).

Stammer and Wunsch (1999) also identified an intriguing feature of the basin-wide EKE variability in the North Atlantic: a comparison of the EKE pattern from one year to another revealed that the 1996 EKE pattern was considerably weaker in the subpolar regions and stronger in the subtropics. This dipolar pattern occurred during a period where the winter NAO index became strongly negative. The authors suggested that EKE in the North Atlantic might be correlated with this atmospheric mode but were unable to demonstrate this due to the short time record.

This hypothesis was re-addressed by Penduff et al. (2004) using 7 years of TOPEX/Poseidon altimeter data and model simulations. Results showed that this subtropical-subpolar meridional contrast was reproduced realistically by the model and varied on interannual timescales. Weaker NAO events before 1993 did not significantly influence the basin-wide EKE pattern but the larger amplitude NAO events post 1993 were followed by gyre-scale EKE fluctuations with a 4-12 month lag suggesting a complex, non-linear oceanic response.

The EKE signal in the western North Atlantic is dominated by the narrow, deep-reaching and fast flowing western boundary current: the Gulf Stream. Gill et al. (1974) first suggested that the source of EKE in the western boundary regions was potential

energy generated by wind-induced Ekman pumping in the subtropical gyres resulting in eddy generation by baroclinic instability. The Gulf Stream jet exhibits substantial variability on interannual to decadal time scales (Sasaki and Schneider, 2011). The principal mode of low-frequency Gulf Stream variability is a meridional shift of the jet axis (Lee and Cornillon, 1995; Taylor and Stephens, 1998; Sasaki and Schneider, 2011). This shift lags atmospheric fluctuations related to the NAO by a few years (e.g., Taylor and Stephens (1998); Frankignoul et al. (2001)). This lagged response of the Gulf Stream jet to atmospheric forcing is attributed by Sasaki and Schneider (2011) to the westward propagation of jet undulations resulting from atmospherically-forced sea-level anomalies (SLAs) in the central North Atlantic, mechanism M2.

Previous studies have shown that altimetric EKE is very effective at identifying the major current paths and their associated changes in the North Atlantic (Heywood et al., 1994; White and Heywood, 1995; Hakkinen and Rhines, 2009). This is due to enhanced EKE associated with meandering and eddy shedding in the paths of the major currents resulting from baroclinic instability. Figure 3.1 shows the main features of the mean circulation in the northeast North Atlantic (a) and the time mean EKE for the same region (b). The regions where elevated EKE are observed correspond to the main branches of the major current systems. Highest EKE values are observed along the main path of the Gulf Stream where the bathymetry steers the Gulf Stream to the north around the Flemish cap. Further to the east, the main branches of the NAC are characterised by high EKE where the NAC flows eastward at around 50°N as well as in the Iceland basin and Rockall channel where the NAC flows northward to the Nordic Seas. A band of elevated EKE is also observed to the south at approximately 34° N in the region of the eastward flowing Azores Current. Elevated EKE is also observed in the interior of the subpolar gyre in both the Irminger basin and the Labrador Sea.

Despite these numerous previous studies of the North Atlantic, no study has yet investigated the basin-wide trends in EKE during the altimetry record. As such, no previous attempts have been made to explain the physical mechanisms responsible for

trends in EKE. In this chapter we will address the following questions:

- 1) What is the spatial distribution of trends in EKE for the North Atlantic Ocean during the altimetric record? 2) Is there evidence to indicate that local and/or remote atmospheric variability is the cause of the observed EKE trends? 3) Are there other indirect atmospheric forcings responsible for EKE trends such as shifting current paths and/or changes in the subpolar and subtropical gyres?

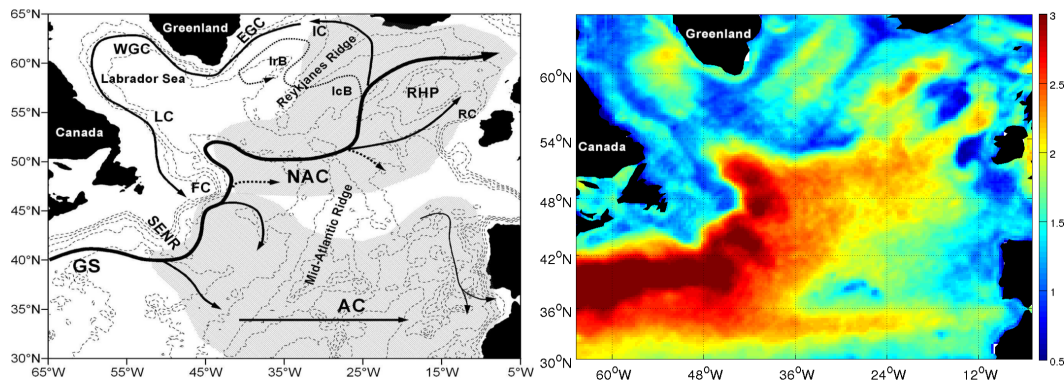


Figure 3.1: (a) Northeast North Atlantic Ocean with topography contours every 1000m and surface circulation. Abbreviations used: GS, Gulf Stream extension; NAC, North Atlantic Current; AC, Azores Current; IC, Irminger Current; WGC, West Greenland Current; EGC, East Greenland Current; LC, Labrador Current; RC, Rockall Channel; RHP, Rockall Hatton Plateau; SENR, South East Newfoundland Ridge; FC, Flemish Cap; IcB, Iceland Basin; and IrB, Irminger Basin. From Volkov (2005). (b) The log₁₀ of time mean EKE ($\text{cm}^2 \text{ s}^{-2}$) computed from altimetric sea surface height anomalies for the 18 year period 1993-2010.

3.2 Results and Discussion

3.2.1 EKE Trends

Figure 3.2 shows a distinct annual cycle in both the time series and frequency spectrum. The trendline shows that EKE has increased during the study period, but the trend is not statistically significant and the magnitude of the increase ($\sim 2\%$ of the mean) is considerably smaller than the magnitude of the high frequency variability (up to $\sim 50\%$ of the mean).

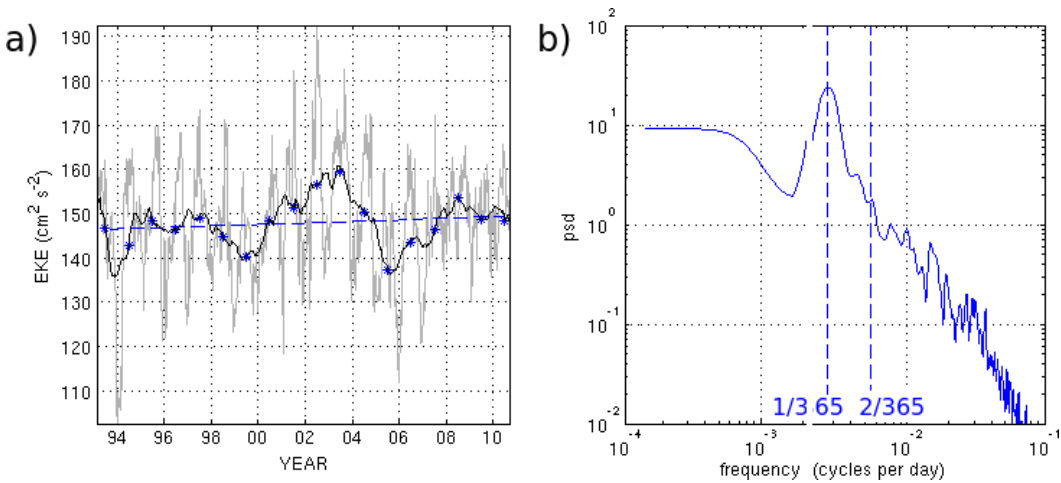


Figure 3.2: Time series of (a) area-weighted EKE in $\text{cm}^2 \text{s}^{-2}$ (grey line) averaged over the North Atlantic from Jan 1993 to Dec 2010. Included are the 12 month running mean (black line), annual means (blue stars) and the linear trend in the annual mean (blue dashed line). (b) frequency spectrum for the weekly time series in (a). Blue dashed lines indicate the first and second annual harmonic frequencies.

Both 2002 and 2003 stand out as years when the basinwide EKE is anomalously high. 1999 and 2005 stand out as years when the values are anomalously low. Annual mean EKE anomalies (figure 3.3) show the large differences in the time mean EKE from one year to another and how the spatial pattern of these differences changes from year to year. In the anomalously high EKE years, the large positive anomalies are located in the central North Atlantic downstream of the Gulf Stream. In the anomalously low EKE years, the large negative anomalies are also located in the Gulf Stream region, indicating that EKE interannual variability in the Gulf Stream region is large enough to influence the basinwide values. The magnitude of the anomalies in the Gulf Stream from one year to another exceed $600 \text{ cm}^2 \text{s}^{-2}$ ($\sim 20\%$ of the mean). The western subtropical gyre and the majority of the northeastern North Atlantic appear more negative in the earlier years and more positive in the later years whereas more central regions and the region of the Azores Current appear more positive in earlier years and more negative in the later years.

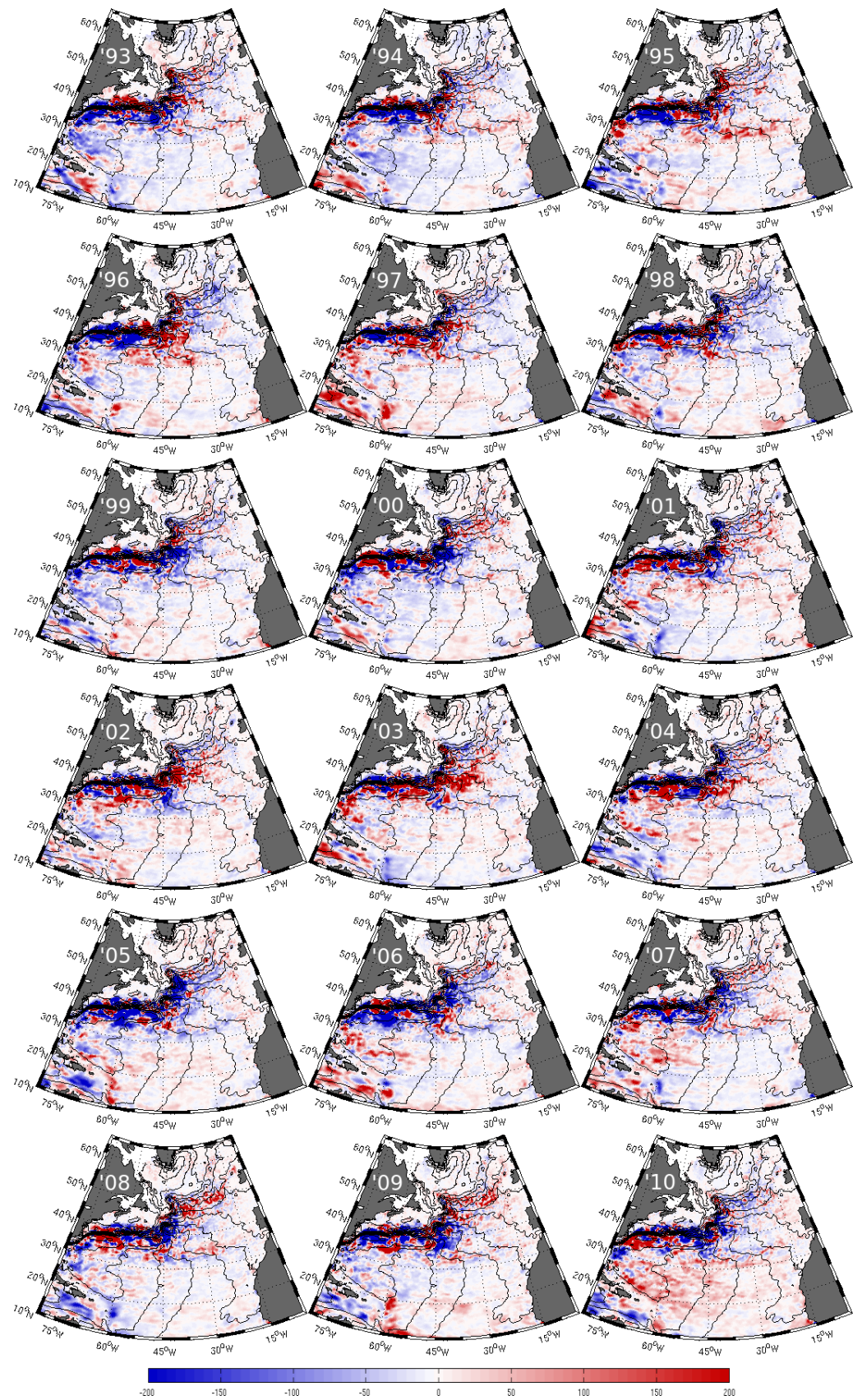


Figure 3.3: Annual EKE anomalies ($\text{cm}^2 \text{ s}^{-2}$) for the region of the North Atlantic Ocean. Contour lines represent mean dynamic topography from altimetry at 10 cm intervals.

The spatial distribution of EKE trends for the North Atlantic (figure 3.4) reveals that statistically significant positive and negative trends are widespread across the entire North Atlantic.

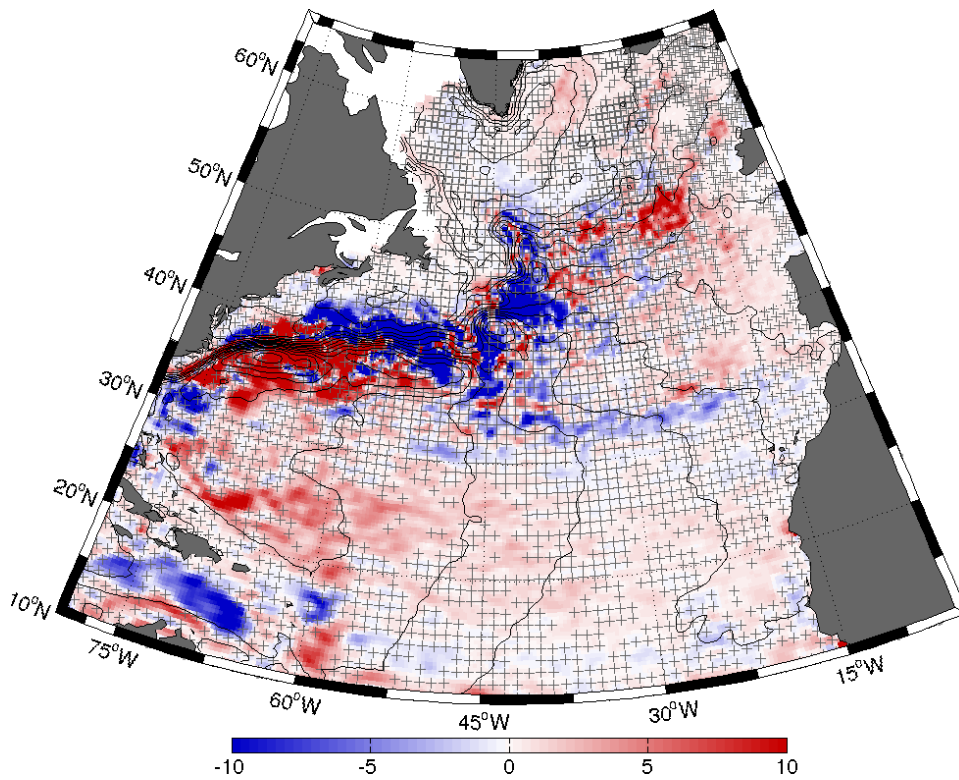


Figure 3.4: Linear trend in EKE ($\text{cm}^2 \text{ s}^{-2}$ per year) computed from altimetric sea surface height anomalies for the 18 year period 1993-2010. The hatched areas signify non-statistically significant trends at 90% confidence. Contour lines represent mean dynamic topography from altimetry at 10 cm intervals.

The largest positive trends are found in the upstream region of the Gulf Stream where trends exceed $10 \text{ cm}^2 \text{ s}^{-2}$ per year. Similar large positive trends are observed in the northeast North Atlantic and the western interior of the subtropical gyre. The largest negative trends are found in the downstream Gulf Stream region where the magnitude of the negative trends is the same as the magnitude of the positive trends in the upstream region. For our analysis we will focus on the following key features of the trend map in order to explain the mechanisms responsible for the observed trends:

- Both positive and negative statistically significant trends are found in the Gulf

Stream region where a pattern of negative trends to the north and positive trends to the south suggest the Gulf Stream jet may have shifted to the south during the study period.

- The central and western subtropics (20°N - 30°N , 40°W - 75°W) are characterised by predominantly positive statistically significant trends.
- Statistically significant negative trends are found in the central North Atlantic (35°N - 45°N , 35°W - 55°W) and the region of the Azores Current (30°N - 33°N , 15°W - 40°W).
- Positive trends characterise the majority of the northeastern North Atlantic and are located along the main routes of the NAC, including the Rockall Channel and the Iceland Basin.

A comparison of the EKE trends in the first half of the study period with the second half(figure 3.5) provides an indication of the robustness of the trends. The ratio of masked areas to non-masked areas in figure 3.5d reveals that, on a basinwide scale, 50.5% of the ocean area is characterised by trends with the same sign in both halves of the time series and 49.5% of the ocean is characterised by a change in the sign of the trend from the first half of the time series to the second. The pattern of positive trends in both the subtropical gyre and the northeast North Atlantic are generally persistent during both time periods, although a change in the trend sign does characterise a substantial proportion of the area in both these regions. This is also the case in the Gulf Stream region where a significant area has been masked in figure 3.5d. Regions where the trend appears less robust include the Azores Current and the eastern half of the subpolar gyre.

A comparison of the trends in EKE computed from the zonal eddy velocity (uEKE) and the meridional eddy velocity (vEKE) (figure 3.6) shows that the key features previously described in figure 3.4 are clearly identifiable in both the uEKE and vEKE trendmaps.

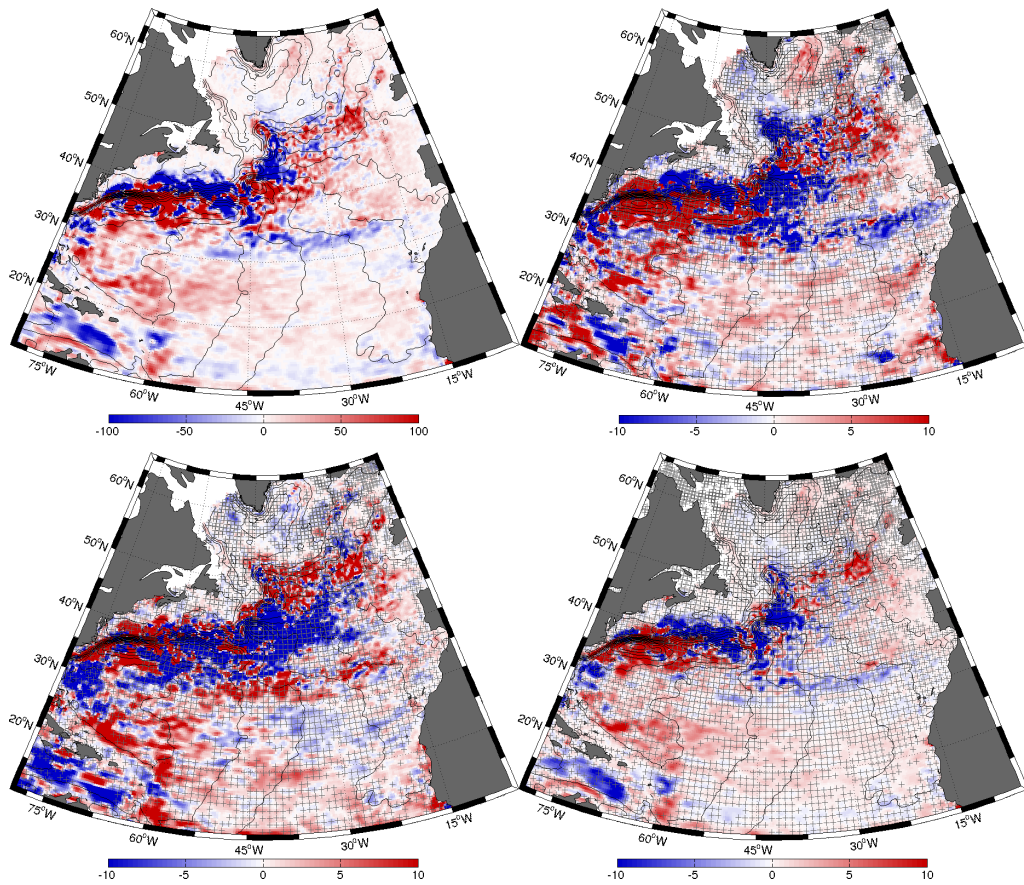


Figure 3.5: (a) Time mean EKE from 1993 to 2001 subtracted from the time mean EKE from 2002 to 2010. (b) Linear trend in EKE ($\text{cm}^2 \text{ s}^{-2}$ per year) from 1993 to 2001. (c) Linear trend in EKE ($\text{cm}^2 \text{ s}^{-2}$ per year) from 2002 to 2010. Hatching in b and c are non-statistically significant. (d) Linear trend in EKE ($\text{cm}^2 \text{ s}^{-2}$ per year) from 1993 to 2010 with an additional hatching applied to the regions where the sign of the trends in (b) and (c) are different. Contour lines represent mean dynamic topography from altimetry at 10 cm intervals.

A map of the difference between the uEKE trend and vEKE trend (figure 3.6c) reveals some small differences. For example, a notable difference is observed in the region of the Azores Current, where a more negative trend in uEKE than vEKE is apparent. This indicates that the negative EKE trend in the Azores Current may be partly caused by a decrease in the intensity of the zonal current.

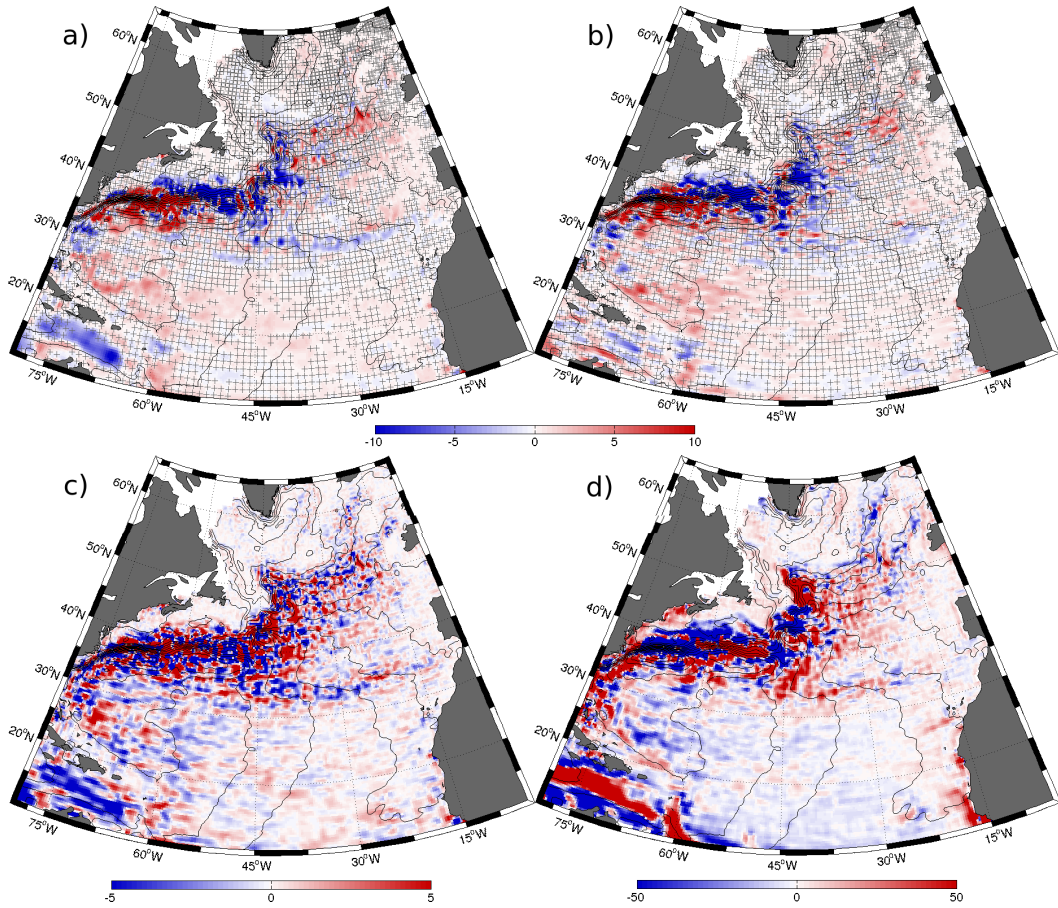


Figure 3.6: Linear trends in EKE ($\text{cm}^2 \text{s}^{-2}$ per year) computed from (a) the zonal component and (b) the meridional component of the altimetric sea surface height anomalies for the 18 year period 1993-2010. The hatched areas signify non-statistically significant trends at 90% confidence. (c) zonal EKE trend (panel a) minus meridional EKE trend (panel b) ($\text{cm}^2 \text{s}^{-2}$ per year). (d) time mean zonal EKE minus the time mean meridional EKE ($\text{cm}^2 \text{s}^{-2}$). Contour lines represent mean dynamic topography from altimetry at 10 cm intervals.

The most pronounced differences are found in the Gulf Stream where the large variability on small spatial scales and, hence, lack of any spatial structure, suggests that this is due to noise. Subtracting the vEKE temporal mean from the uEKE temporal mean (figure 3.6d) reveals that the subtropical gyre has a slightly stronger meridional component, as do the northeastern branches of the NAC in the Iceland basin and Rockall Channel. The more zonal component of the Azores Current can be identified as well as the regions where the NAC crosses the MAR. The largest differences are found in the downstream region of the Gulf Stream where the mean EKE is the largest.

Timeseries of EKE (figure 3.7) reveal the different characteristics of the regions outlined in the upper panel of figure 3.7.

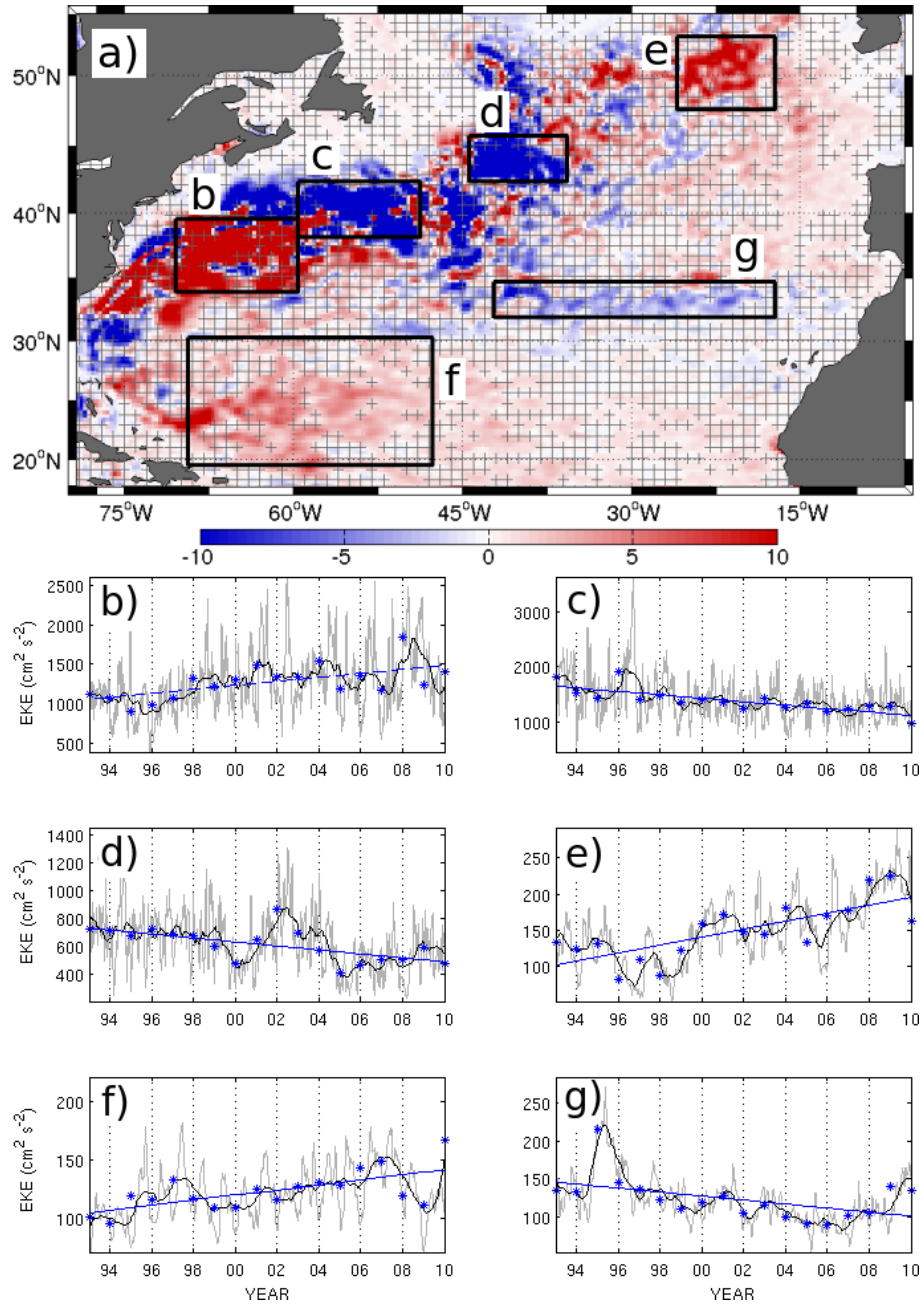


Figure 3.7: (a) EKE Trend map with boxes (b-g) to identify the regions over which the timeseries are averaged. (b-g) Timeseries of EKE for the regions displayed in the upper panel. In each case the panels show the weekly EKE (grey line) with a 12 month running mean (black line), annual means (blue stars) and linear trend in the annual means (blue line).

The mean EKE in the Gulf Stream regions (b and c) are approximately one order of magnitude higher than regions e, f and g and approximately double that of region d. Despite the differences in magnitude from one region to another, the variability in each region is fairly consistent in all the regions; approximately $\pm 50\%$ of the mean. The 'goodness of fit' value for each trend line varies from one region to the other, with the best fit in region c (0.61), decreasing in regions e (0.56), f (0.42), d (0.39) and b (0.38), with the lowest value in g (0.25). This low value in region f would inevitably be higher if the anomalously high EKE in 1995 was removed.

By examining the cross-correlations of the time series we can reveal some link between EKE variability in one region to another on annual time scales. The most notable result is the large anti-correlation ($r^2 = -0.59$) between regions b and f at one year lag (f lagging b). EKE in region g is correlated with both b ($r^2 = -0.49$ at zero lag) and f ($r^2 = 0.48$ at 1 year lag). No other significant correlations exist between the different regions. Of note is the lack of significant correlation between b and c where a change in EKE (or trend), resulting from a meridional shift in the Gulf Stream axis, should produce a negative correlation between the two regions.

3.2.2 Atmospheric Trends

The spatial pattern of the wind speed temporal mean is predominantly zonal in nature across the North Atlantic (figure 3.8a). The highest mean values are observed in a zonal band south of 25°S . High values are also observed in the mid-latitude eastern North Atlantic. In general, eastern regions are characterised by higher values than western regions except in the subpolar regions ($>50^\circ\text{N}$), where a reversal of this pattern is observed.

Statistically significant wind speed trends (figure 3.8b) are positive in the interior of the (wind-driven) subtropical gyre and are otherwise negative over virtually the entire North Atlantic basin. As much of the region where positive wind speed trends are found is also characterised by positive EKE trends, this is consistent with the

hypothesis that an increase in EKE in these regions has resulted from an increase in local wind (mechanism M1). This similarity is most notable in the central and southern subpolar gyre and in the central North Atlantic at 40°W where the Gulf Stream broadens and becomes the NAC.

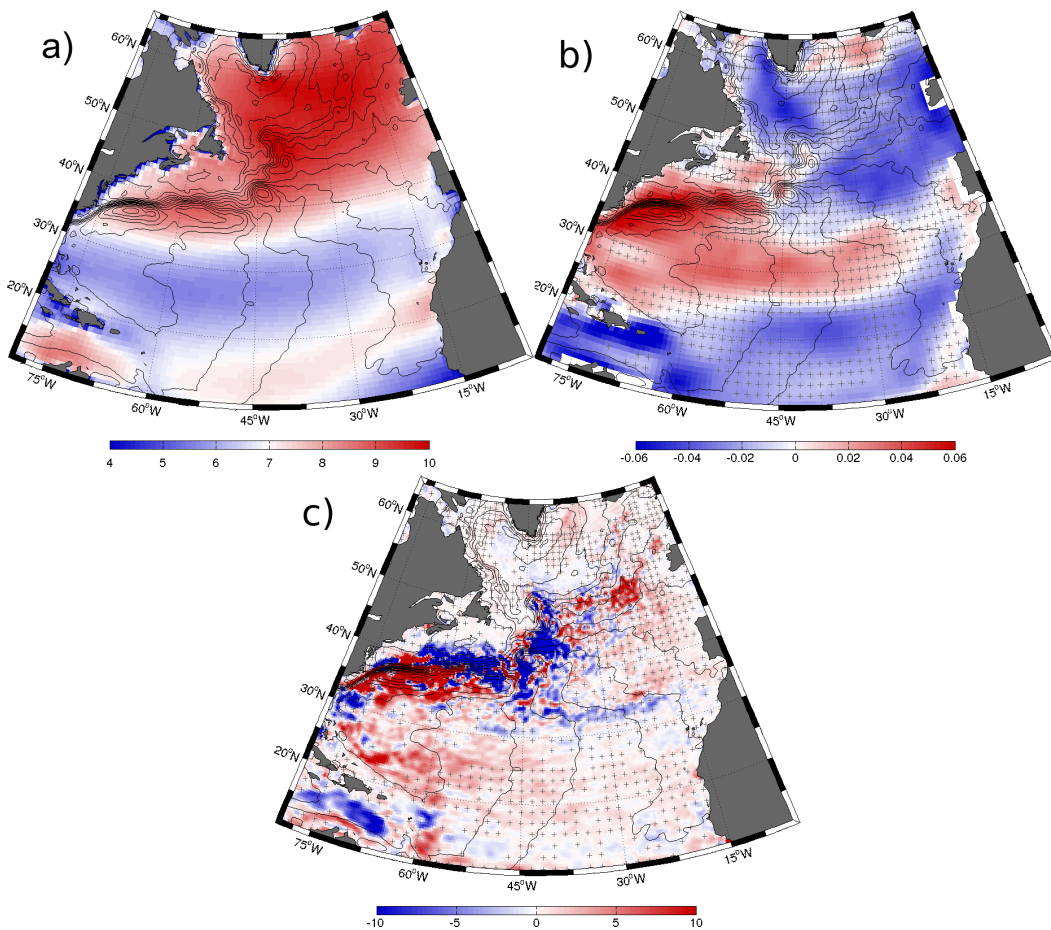


Figure 3.8: (a) Wind speed temporal mean (1993 - 2010) in $m\ s^{-1}$ from ECMWF ERA-Interim re-analysis data. (b) Linear trend in wind speed for the 18 year time period 1993 to 2010 ($m\ s^{-1}$ per year) from ECMWF ERA-Interim re-analysis data. The hatched areas signify non-statistically significant trends at 90% confidence. (c) Trend in EKE ($cm^2\ s^{-2}$ per year) from 1993 to 2010 for the regions where the trend in wind speed (panel b) is the same sign for the same time period (stipple show different signs). Black contours show mean dynamic topography at 10 cm intervals.

A clearer view of the regions where the trends in EKE and wind speed are the same sign is illustrated in figure 3.8c, where the EKE trends are shown only where EKE and wind speed trends are the same sign. This illustrates the regions where a

local relationship exists between EKE and wind speed highlighting the regions where mechanism M1 is influential. We do not expect this mechanism to have a large basin-wide influence on EKE as other mechanisms such as baroclinic instability are thought to be more dominant in large areas in the North Atlantic.

Although figure 3.8c shows large regions where the trends are the same sign, a substantial proportion of the trend map has been masked. Across the entire basin, 54.2% of the (area-weighted) area is characterised by different signs in the trends in EKE and wind speed, slightly more than half. This percentage, however, is visibly different from one region to the next. For example, south of 25°S 63.6% of the trend map has been masked in figure 3.8c. In the subtropics between 25-40°N, 80-40°W, the masked regions are only 42.8% of the total area. In the northeast North Atlantic, between 35-60°N, 80-40°W, the masked area totals 63.5%. This result indicates that a change in local wind (mechanism M1) is partially responsible for the EKE trends and the relative influence of this mechanism is highly variable from one region to another, with the subtropical North Atlantic being one large region where this mechanism is more dominant.

Statistically significant wind stress curl trends (figure 3.9b) also vary in both sign and magnitude across the North Atlantic basin. In the subpolar region, north of the zero curl isoline, wind stress curl trends are positive to the west of 40°W and negative to the east of 40°W. In the subtropics, south of the zero curl isoline, this dipolar pattern is reversed.

When investigating the significance of the wind stress curl trends and their relative influence on EKE trends it is important to consider that the mean atmospheric circulation in the North Atlantic basin is cyclonic in the subpolar region and anti-cyclonic in the subtropics. Therefore, the time mean wind stress curl is positive north of the zero wind stress curl isoline and negative to the south (figure 3.9a). Subsequently, a positive (negative) wind stress curl trend in the subtropical North Atlantic represents a decrease (increase) in the intensity of the curl. This is the opposite in the subpolar

region, where a positive trends represents an increase in curl.

Any similarity in sign between EKE trends and trends in wind stress curl magnitude is consistent with the hypothesis that an increase (decrease) in EKE in that region has resulted from a local increase (decrease) in wind stress curl intensity (mechanism M3). A direct comparison of the trends in wind stress curl with EKE trends (figure 3.9c) shows that trends in EKE and wind stress curl magnitude are predominantly the same sign in the western interior of the subtropical gyre where EKE and wind speed trends are both positive (figure 3.8c).

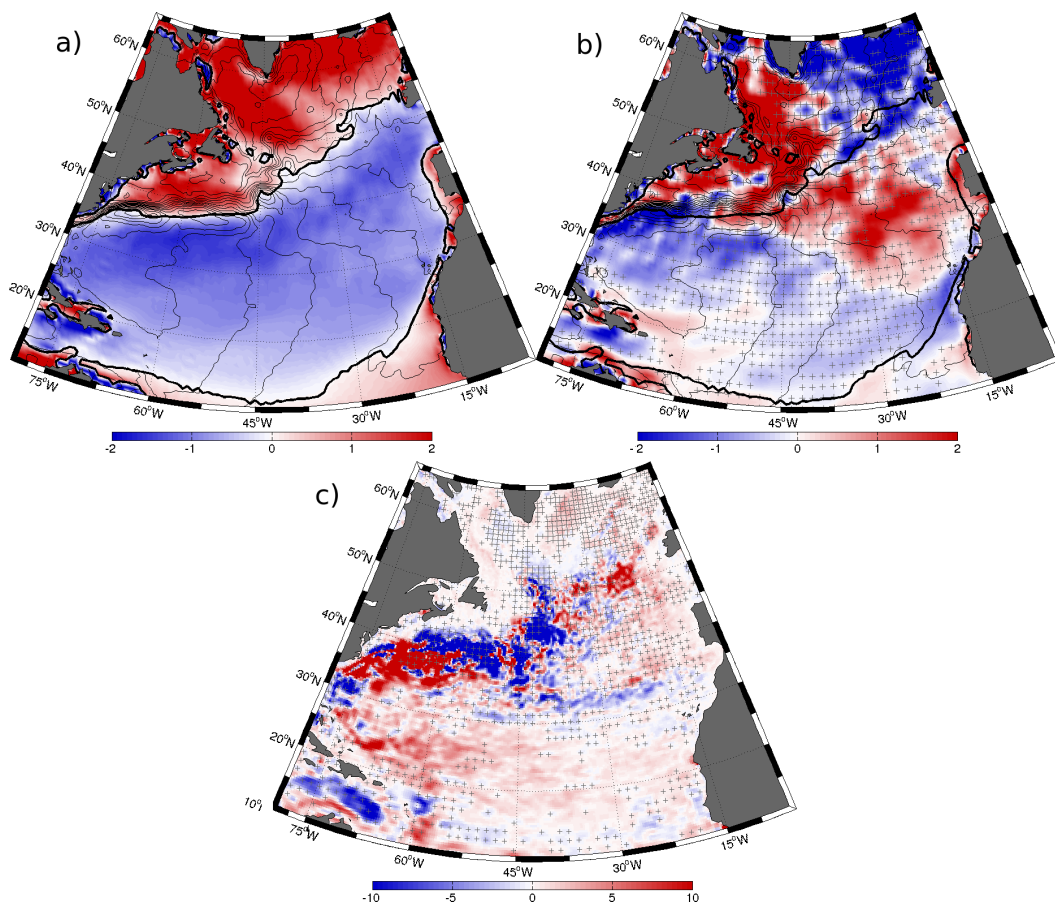


Figure 3.9: (a) Winter (DJF) wind stress curl temporal mean ($x10^{-7} \text{ N m}^{-3}$ from ECMWF ERA-Interim re-analysis data. (b) Linear trend in wind stress curl ($x10^{-8} \text{ N m}^{-3}$ per year) for the 18 year time period 1993 to 2010 from ECMWF ERA-Interim re-analysis data. The hatched areas signify non-statistically significant trends at 90% confidence. (c) Trend in EKE ($\text{cm}^2 \text{ s}^{-2}$ per year) from 1993 to 2010 for the regions where the trend in wind stress curl magnitude is the same sign for the same time period. Black contours show mean dynamic topography at 10 cm intervals.

The similarity of EKE and wind stress curl trends extends over a much larger region of the subtropics than the similarity of trends in EKE and wind speed. Large areas of the northeast North Atlantic also show similar positive trends in both EKE and wind stress curl where no similarity is found with wind speed trends. In the North Atlantic, EKE variability is dynamically linked to changes in surface circulation. For example, White and Heywood (1995) showed that the EKE in the main branches of the NAC can be used as a surrogate for the mean flow. White and Heywood (1995) also showed that the shifting of the main branches of the NAC is related to interannual differences in the winter wind stress curl pattern in the northeast North Atlantic. We can therefore hypothesise that, in some locations, trends in EKE have arisen not only from local changes in wind stress curl but also from changes in surface circulation resulting from shifting wind stress curl patterns (mechanism M4). This idea is explored further in section 4.3.4.

3.3 EKE variability and the NAO

Although the NAO index only explains approximately 30% of atmospheric variability (e.g. sea-level pressure in the North Atlantic), previous studies have shown that the North Atlantic eddy field not only responds to atmospheric fluctuations represented by the NAO but that this response exhibits a dipolar, basinwide pattern (Stammer and Wunsch, 1999; Penduff et al., 2004). With an 18 year time series we can establish if this previous hypothesis can be corroborated with a much longer time series. Here we show the correlation coefficients of annual mean EKE with the winter (DJF) NAO index at various time lags from 0 to 3 years (figure 3.10). At zero lag, statistically significant positive correlations are dominant in the northeast North Atlantic while statistically significant negative correlations are dominant in the southwest. Although other spatial patterns emerge at 1, 2 and 3 year lags, the aforementioned di-polar pattern does not persist at these lags. In order to further explore the response of EKE

to the NAO, composite maps of annual mean EKE anomalies are shown for years following strongest positive NAO winters (1994, 1995, 2000 and 2005) minus the years following the strongest negative NAO winters (1996, 1997, 1998 and 2010) (figure 3.10e).

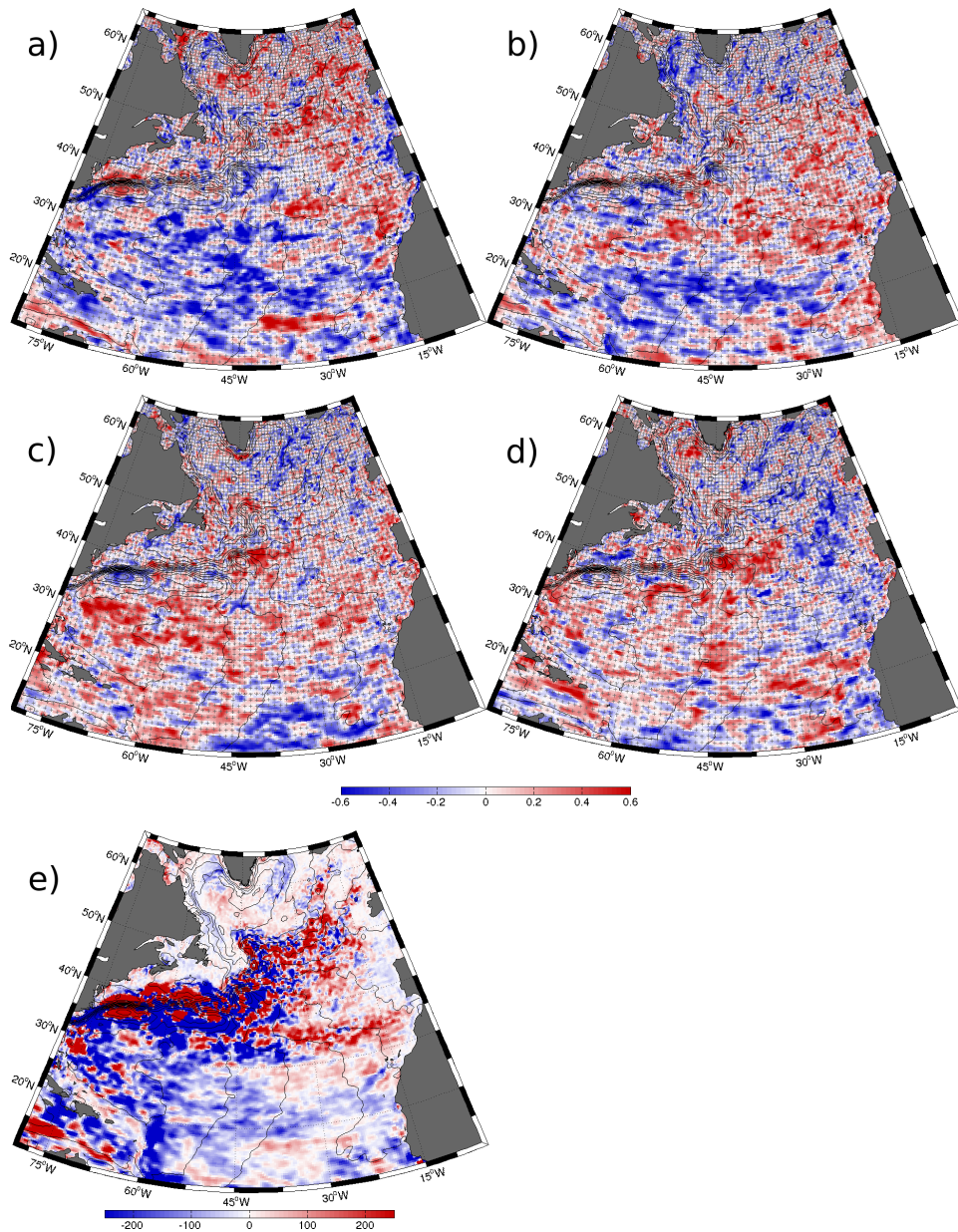


Figure 3.10: Correlation coefficients of annual mean EKE with NAO index at varying time lags; a) zero lag, b) 1 yr lag, c) 2 yr lag, d) 3 yr lag. e) EKE anomalies for the years following the strongest positive NAO winters (1993, 1994, 1995, 2000 and 2005) minus EKE for the strongest negative NAO winters (1996, 1997, 1998, 2009 and 2010). The hatched areas in a-d represent non-statistically significant correlations.

In the years following positive NAO winters, positive EKE anomalies are found in the northeast North Atlantic, however, negative anomalies are also present in this region. Notably, the positive correlation is clearly defined in the region of the Azores current. In the subtropical North Atlantic, the response is much more clearly defined than in the southwest as the western subtropics are dominated by negative anomalies. These results are consistent with the previous findings of Stammer and Wunsch (1999), Penduff et al. (2004) and Zhai and Wunsch (2013) who found that wind power input in regions of the North Atlantic, covarying with the winter NAO index, is significantly correlated with the EKE for the period from 1992 to 2011.

3.3.1 The North Atlantic subtropical Gyre

Positive statistically significant EKE trends occur in the western interior of the North Atlantic subtropical gyre where annual mean EKE in 2010 was 50% higher than in 1993. A comparison of wind speed trends and EKE trends (figure 3.8) show that in the eastern subtropical North Atlantic the spatial pattern is very similar, with statistically significant positive trends in both EKE and wind speed. Trends in the curl of the wind stress (figure 3.9) are also positive (becoming more negative) in this region. This implies that EKE trends in this region may be a direct result of strengthening local winds (mechanism M1) and/or increasing curl of the local wind stress field (mechanism M3).

EKE/NAO correlations and composite maps of EKE in positive minus negative NAO years (figure 3.10) confirm the strong relationship between EKE interannual variability and the NAO in this region. The time series of annual mean EKE in this region (figure 3.7e) has a goodness of fit value (r^2) with the trend line of 0.42. Two years in particular do not follow the trend pattern in this region: 2008 and 2009. As these outliers do not correspond to strong positive or negative NAO years this indicates that, despite both the EKE/NAO correlations and the similarity in EKE, wind speed and wind stress curl trends, a substantial amount of the variability cannot be explained by atmospheric variability. This suggests that other mechanisms, such as buoyancy

forcing (mechanism M5), may play a lesser, but still significant, role in the North Atlantic subtropical gyre.

3.3.2 The Gulf Stream

Both wind speed and wind stress curl trends are positive in the upstream region of the Gulf Stream indicating that an increase in local wind (mechanism M1) and an increase in local wind stress curl intensity (mechanism M3) have contributed significantly to the EKE trends in this region. However, both local wind and wind stress curl trends do not show similarity to EKE trends in the downstream region of the Gulf Stream.

This indicates that a mechanism other than M1 or M3 is responsible for the trends in the downstream Gulf Stream region. We suggest a change in local baroclinicity (mechanism M5) could play a significant role for the following reason: the (atmospherically forced) positive trends in the upstream region result in the tendency of the Gulf Stream jet to release more of its stored potential energy further upstream in the later years of the study period than in earlier years. Consequently, further downstream, there is less available potential energy and hence less EKE. This would implicate a change in local baroclinicity (mechanism M5) as a mechanism in the downstream region. We explore this idea by superimposing snapshots of the 40 cm SSH contour (near the $\partial h / \partial y$ maxima) for individual years (figure 3.11) and comparing the spread in each year. The greater the spread of the core of the jet in a given year, the more the jet is meandering. A more meandering jet implies a more unstable jet.

The upstream sector of the Gulf Stream paths (from 80°W to 66°W) are relatively close together in 1995-1997 and in 2007. In contrast, paths are more spatially variable in 2001-2003 and 2008-2010. The spatial distribution of annual mean EKE anomalies (figure 3.11) show that the years where the upstream jet paths are closer together correspond to years characterised by negative EKE anomalies in the upstream path. Similarly, the years where the paths are more spread out show more positive EKE anomalies.

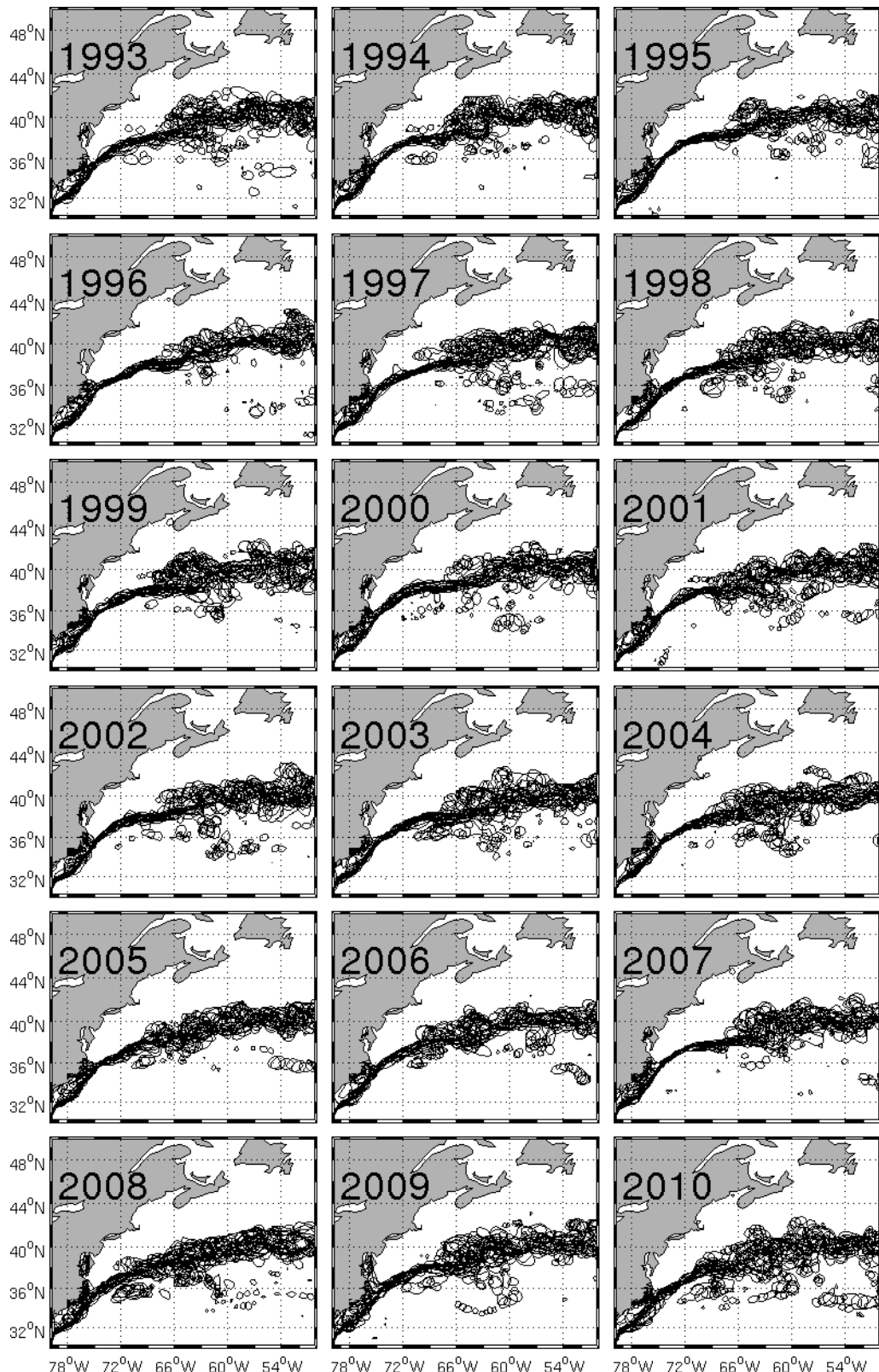


Figure 3.11: Yearly paths of the Gulf Stream and Gulf Stream Extension defined by the 40 cm contours in the weekly SSH fields. Paths are plotted every 14 days.

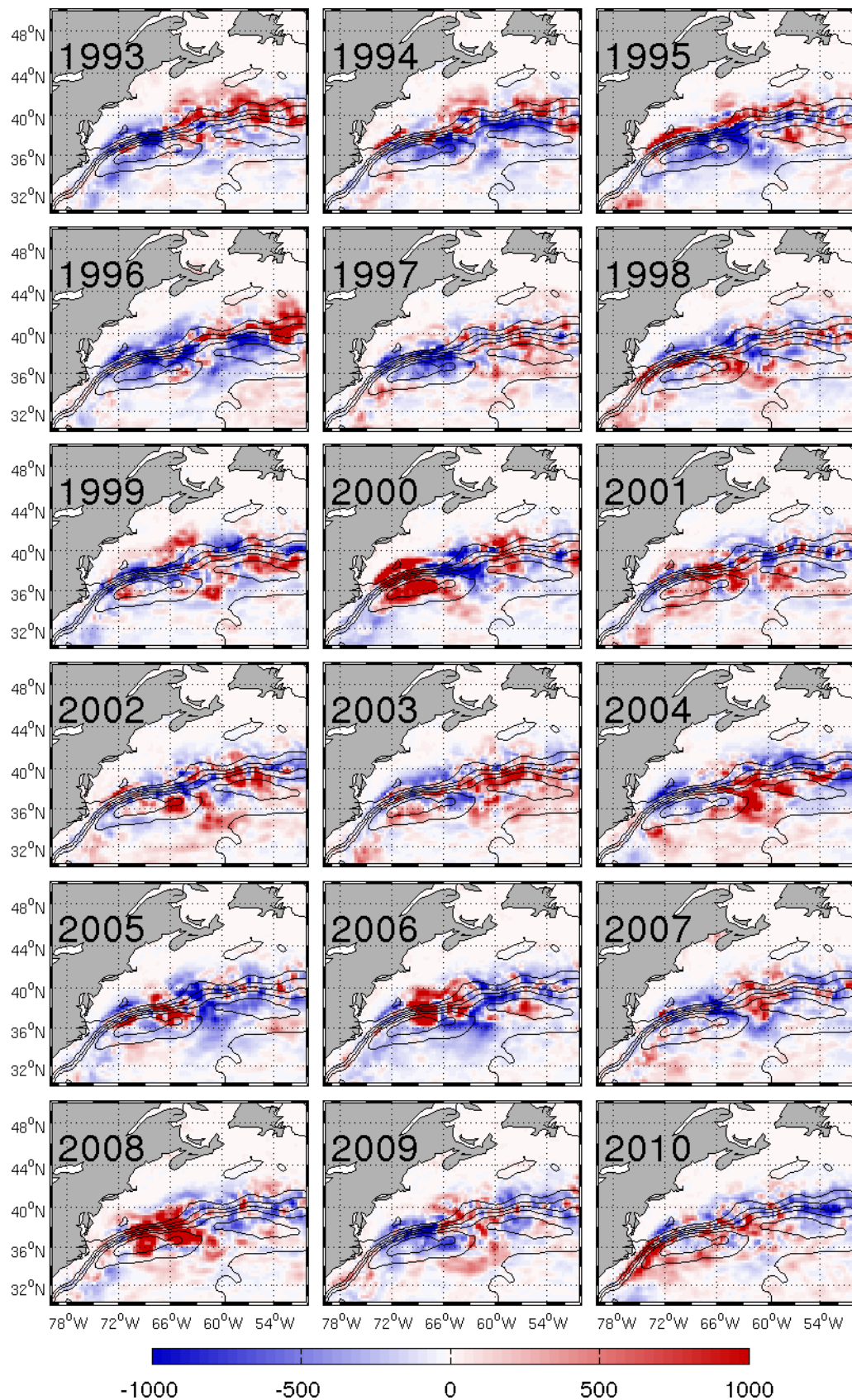


Figure 3.12: Annual mean EKE anomalies for the Gulf stream region in $\text{cm}^2 \text{s}^{-2}$. Contour lines denote mean dynamic topography at 10 cm intervals.

We therefore suggest that buoyancy effects (mechanism M5) have contributed to EKE trends in the Gulf Stream by increased baroclinic instability in the upstream region resulting in enhanced EKE, which in turn leads to decreased EKE in the downstream region due to less available potential energy and hence less baroclinic instability. As suggested by Zhai et al. (2008), the positive trend in the upstream region may be due to a decrease in the eddy dissipation rate during the study period.

Due to the variability associated with the seemingly random transient meandering of the Gulf Stream, there will inevitably be some degree of intrinsic variability (mechanism M6) in the EKE variability in this region. Although we cannot quantify the intrinsic component, we can observe that the high frequency variability in the EKE time series (figure 3.7) is relatively noisy. A combination of these observations and numerical studies of the intrinsic nature of SSH variability in the Gulf Stream (Penduff et al., 2011) lead us to conclude that this mechanism may also make a significant contribution in this region.

3.3.3 Central North Atlantic and Azores Current

The central North Atlantic (35°N - 45°N , 35°W - 55°W) and the region of the Azores Current (30°N - 33°N , 15°W - 40°W) are both characterised by negative EKE trends (figure 3.4). In the central North Atlantic, these negative trends are predominantly co-located with negative trends in both wind speed (figure 3.8c) and wind stress curl (figure 3.9c). This indicates that negative EKE trends in this location are due to a combination of both a decrease in local wind (mechanism M1) and wind stress curl deintensification (mechanism M3).

Negative EKE trends are found in the region of the North Atlantic associated with the eastward flowing Azores Current (figure 3.4). This region is characterised by a negative trend in wind speed. The trend in wind stress curl for this region is positive indicating an increase in the negative curl. In the Azores Current region, an increase in wind stress curl leads to an increase in Ekman convergence which acts to strengthen

the Azores front (Volkov and Fu, 2011). The variability in the strength of this front (or meridional temperature gradient) reflects the variability in available potential energy, the source of EKE in this region (Volkov and Fu, 2011). Trends in uEKE and vEKE confirm that the trend in the zonal component of EKE is larger than the meridional. This result, in combination with the negative trend in wind stress curl and the correlations with the NAO, are all consistent with the following conclusion of Volkov and Fu (2011). EKE in the Azores Current is significantly correlated with both the winter NAO index and with the wind stress curl over the eastern part of the subtropical North Atlantic, suggesting an adjustment of the current strength to large-scale atmospheric forcing. We therefore suggest that the decrease in wind stress curl in the region of the Azores Current during the study period has resulted in a decrease in the Ekman convergence, which has weakened the strength of the Azores current leading to the observed decrease in EKE (mechanism M3).

3.3.4 The northeast North Atlantic

EKE in the region defined in figure 3.7d is subject to large interannual variability, e.g. from $<100 \text{ cm}^2 \text{ s}^{-2}$ in 1996 to $>200 \text{ cm}^2 \text{ s}^{-2}$ in 2009 and the timeseries of annual mean EKE shows a good fit with the linear trend ($r^2=0.56$). It can be demonstrated that the trend in this region is linked to the variability in both the intensity and position of the main branches of the NAC. Previous studies have shown that altimetric EKE is very effective at identifying the main branches of the NAC and their associated changes (Heywood et al., 1994; White and Heywood, 1995; Hakkinen and Rhines, 2009). The annual changes in the position of mean SSH contours are used to clearly identify the annual mean position and strength of the NAC (figure 3.13). The annual EKE anomalies are shown to follow very closely the path of the closest SSH contours, indicating the strongest geostrophic currents. In the low EKE years (e.g. 1996, 1997, 1998), the main path of the NAC is located between 51°N and 54°N and shows relatively few meanders compared with other years.

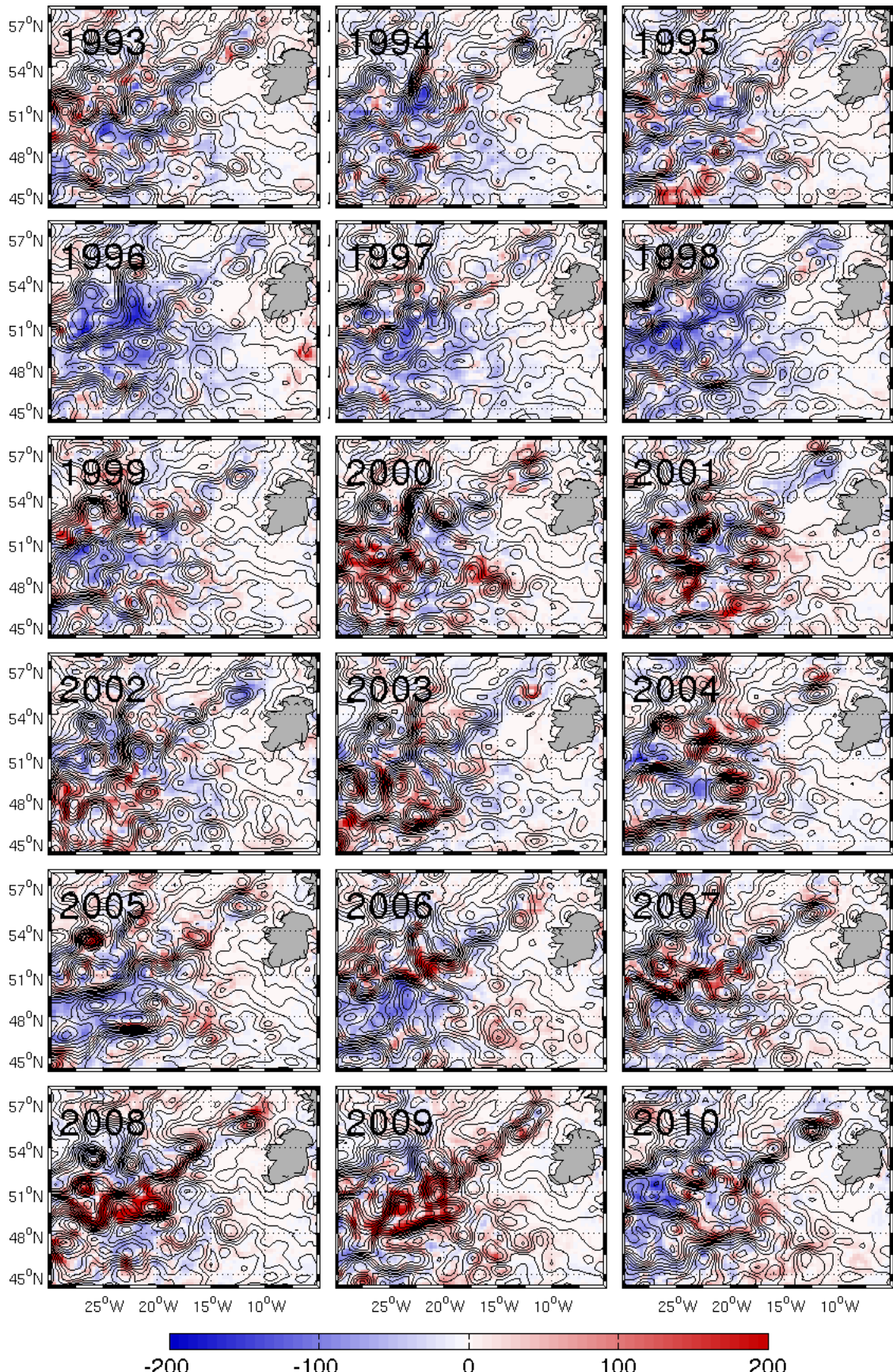


Figure 3.13: Annual mean SSH fields from altimetry for the northeast North Atlantic superimposed on annual mean EKE anomalies ($\text{cm}^2 \text{s}^{-2}$). Contour intervals are 2 cm.

In the high EKE years (e.g. 2007, 2008, 2009) the main path of the NAC is located a few degrees further south between 48°N and 52°N and is characterised by larger and more numerous meanders.

The northward and southward shifts in the current branches of the NAC have been previously found to relate to interannual differences in the winter wind stress curl pattern (eg White and Heywood (1995)). Latitudinal changes in the winter (DJF) mean position of the zero wind stress curl (figure 3.14) can be as much as 20° in the eastern North Atlantic.

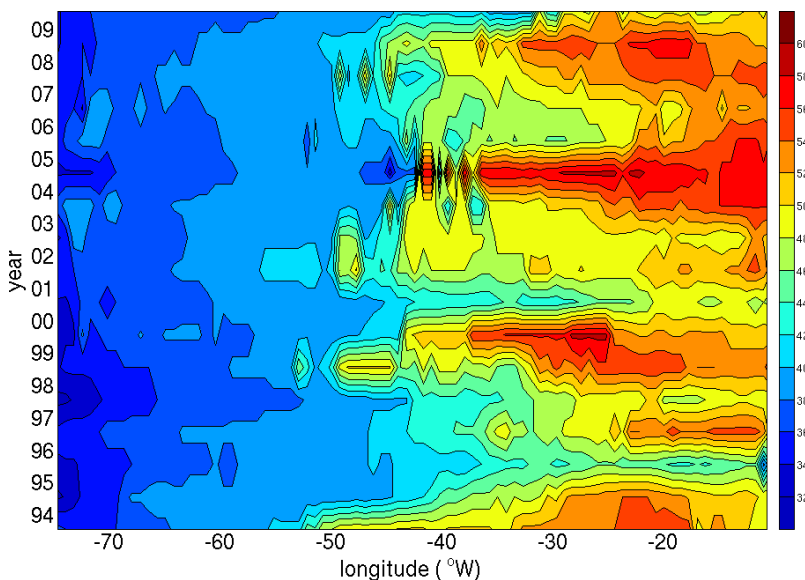


Figure 3.14: Temporal evolution in the annual winter (DJF) latitude of the zero wind stress curl for the North Atlantic from ECMWF ERA-Interim re-analysis data. Contours are in 5° increments.

The regions west of 55°W show virtually no change from year to year indicating that the zero curl isoline is much more stable in position in the west than the east. From 55°W to 45°W the annual mean wind stress curl zero line is not always well defined with multiple zero-crossings often present at any given longitude. East of 45°W the variability is significantly greater than that to the west. In this region the zero wind stress curl line is typically further north in the latter half of the time series than the first half. As the zero wind stress curl line represents the border between the subtropical

and subpolar gyres, a northward shift in the zero line signifies a northward expansion of the subtropical gyre. On interannual timescales, however, the years when annual mean EKE (figure 3.7e) is large do not always correspond to years when the latitude of the annual mean zero wind stress curl is further to the north (figure 3.14). This shows that the positive trends in EKE in the northeast North Atlantic cannot be directly attributed to either local changes in the latitudinal position of the zero curl isoline or the local (negative) trend in wind stress curl magnitude.

Another hypothesis is now explored based on the results of a study by Hakkinen and Rhines (2009). Comparing the wind stress curl during the time period between 1996 - 2000 with that from 2001 - 2005, Hakkinen and Rhines (2009) revealed that a region of positive curl extended from Cape Hatteras to the Rockall Trough from 2001 - 2005. This feature is distinctly different from the earlier period where the zero-curl line crosses nearly zonally from Labrador to British Isles, allowing the negative wind stress curl to isolate the small area of positive curl off the eastern seaboard including the Gulf Stream region. In effect, the increased meridional tilt of the wind stress curl zero line allows the formation of a positive wind curl region connecting the Gulf Stream area and the Nordic Sill region. The increasing meridional tilt of the curl allows the upper layer of the subtropical gyre to spread northeastward. The mean winter wind stress curl for the first half of the time series (1993 to 2000) (figure 3.15a) clearly shows this region of isolated negative curl. The mean winter wind stress curl for the second half of the time series (2001 to 2010) (figure 3.15c) shows the zero curl isoline extending unbroken from the Gulf Stream to eastern Europe. Corresponding EKE anomalies for each time period (figure 3.15b and d) show that EKE anomalies in the northeast North Atlantic are predominantly negative from 1993 to 2000 and predominantly positive from 2001 to 2010. Dynamically, this changing pattern of wind stress curl is as a possible forcing for surface current changes. The changing behaviour of the winter wind stress curl in the North Atlantic influences the main paths of the NAC (and subsequent EKE) via an indirect non-local mechanism. As shown

by previous studies of wind driven circulation, an increasingly meridional tilt of the wind stress curl zero line allows the northeastward expansion of the subtropical gyre (Rhines and Schopp, 1991). This gyre effect was apparent from the northeastward expansion of subtropical drifter tracks found by Hakkinen and Rhines (2009).

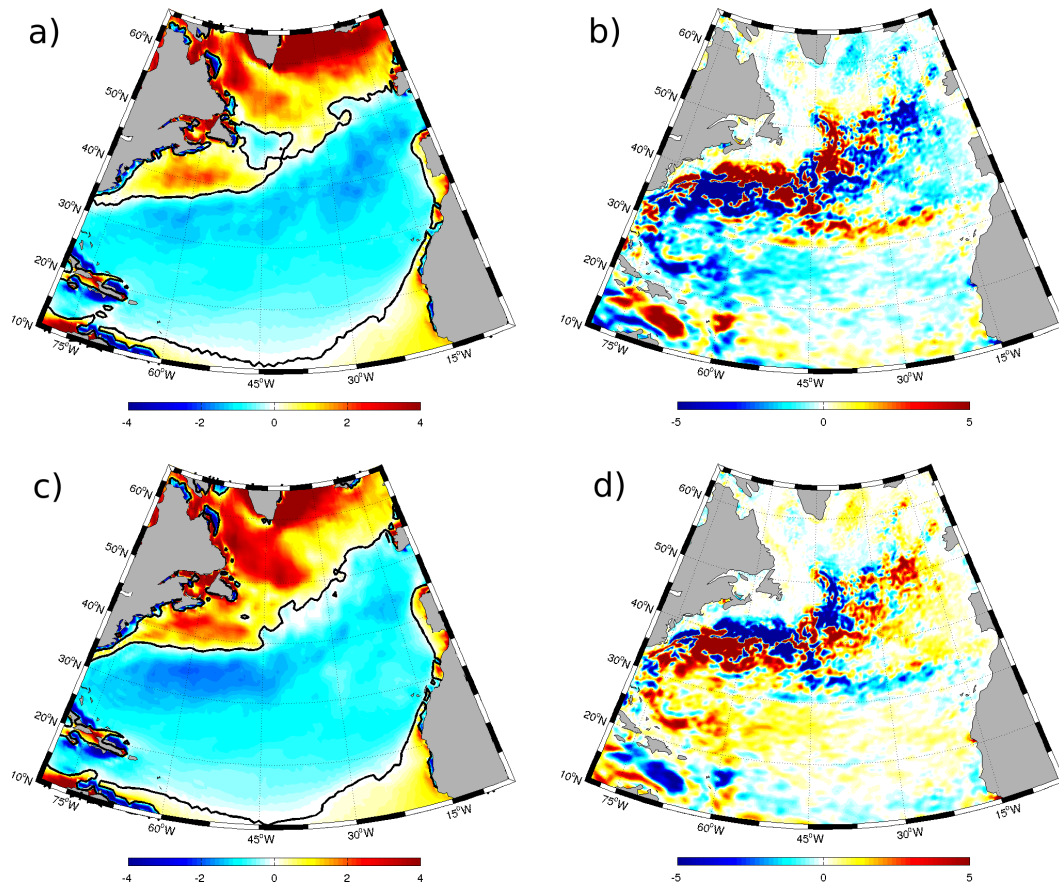


Figure 3.15: Winter (DJF) wind stress curl temporal mean ($x10^{-7} \text{ N m}^{-3}$) from (a) 1993 - 2000 and (c) 2001 - 2010 from ECMWF ERA-Interim re-analysis data. EKE anomalies ($x10^{-2} \text{ m}^2 \text{ s}^{-2}$) for (b) 1993 - 2000 and (d) 2001 - 2010.

3.4 Summary

In this chapter, the results have shown that positive and negative trends in EKE are widespread in the North Atlantic Ocean. Large-scale changes in both the wind speed (mechanism M1) and wind stress curl intensity (mechanism M4) contribute significantly to the observed trends in the subtropical gyre where EKE is strongly anti-

correlated with the NAO. Wind stress curl appears to be a more dominant mechanism than wind speed. Its influence extends across the subtropical belt to the eastern North Atlantic, implicating wind stress curl changes as a more plausible mechanism for the EKE trends in the subtropics than wind speed alone.

In the Gulf Stream region, a definitive mechanism is hard to determine as EKE is very noisy, suggesting intrinsic variability (mechanism M6) may be important here. There is, however, evidence to suggest that both wind speed and wind stress curl are significant mechanisms in the upstream region, with buoyancy effects significant further downstream.

Along the main paths of the NAC, positive EKE trends have been shown to result from changes in the position and intensity of the mean currents. The temporal transitions of these currents do not follow the NAO or the local wind stress curl at interannual time scales. Instead, temporal changes in the position and orientation of the zero wind stress curl isoline, extending across the entire North Atlantic basin, suggests mechanism M3 may be responsible for the observed positive EKE trends in the northeast North Atlantic.

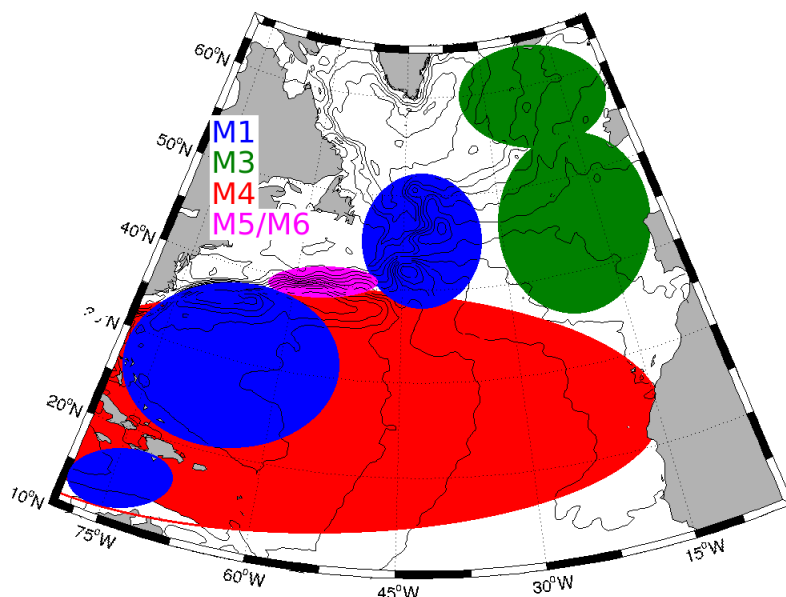


Figure 3.16: Schematic diagram to illustrate the principal mechanism responsible for the trend in EKE for each region in the North Atlantic.

In the region of the Azores Current, EKE trends are consistent with the mechanisms for EKE variability described by Volkov and Fu (2011), who suggested that a decrease in the local wind stress curl intensity (mechanism M4), which in turn results in a decrease in Ekman convergence, has weakened the Azores front resulting in the negative EKE trends in this region. A summary of the mechanisms (3.16) shows that both the wind stress curl intensity (mechanism M4) and shifting wind stress curl (mechanism M3) are the most dominant mechanisms in the North Atlantic.

Chapter 4

The North Pacific

4.1 Introduction

In the 1970s the North Pacific Experiment (NORPAX) was established to analyse the large-scale, long-range ocean-atmosphere interactions in the Pacific Ocean. This project led to the first basin-wide mapping of the dynamic topography of the Pacific Ocean and investigation of its associated variability using data from over 60,000 hydrographic stations (Wyrtki, 1975). The largest annual fluctuations were found in equatorial regions and thought to result from annual changes in the wind field. The position and meandering of currents and the presence of eddies were also found to impact the variability in dynamic height which increased from east to west across the Pacific Ocean. High EKE values were found in the North Pacific western boundary current and in the equatorial current system and low values in the sub-tropical gyres (Wyrtki et al., 1976).

The Kuroshio Extension (KE) region and North Equatorial regions were also found to exhibit the highest SSH variability in the North Pacific by Qiu (1999) using data from the TOPEX/Poseidon altimeter. The Kuroshio system oscillates between a stable and an unstable dynamical state on a quasi-decadal timescale (Qiu and Chen, 2005, 2010). During the stable state, the Kuroshio jet intensifies and has a northerly zonal

mean path. During the unstable state, the KE jet has a reduced eastward transport and a more southerly flow path. Transitions between the two dynamic states are caused by the basin-scale wind-stress curl forcing in the eastern North Pacific related to the PDO. During the positive PDO phase, the intensified Aleutian Low generates negative SSH anomalies in the eastern North Pacific through Ekman divergence. As these wind-induced negative SSH anomalies propagate to the west as baroclinic Rossby waves, they weaken the zonal KE jet and shift its path southward. This is an example of mechanism M2 (remote atmospheric) affecting changes in EKE in the North Pacific. During an unstable phase, the path length of the Kuroshio jet (defined as the 170 cm weekly SSH contour by Qiu and Chen (2010)) increases significantly resulting in increased eddy activity in the upstream KE path. Qiu and Chen (2010) found the Kuroshio to be in a stable state during October 1992 to June 1995 and January 2002 to December 2004 and in an unstable state from July 1995 to December 2001 and January 2005 to December 2008.

Another zonal band of elevated EKE exists in the western North Pacific known as the sub-tropical counter-current (STCC) region which is characterised by a seasonally modulating eastward shear of zonal flows in the upper ocean (Qiu and Chen, 2013). Dynamically, the energy source for the elevated EKE in this region is the baroclinic instability resulting from a change in the meridional potential vorticity gradient from positive in the upper 200 m ocean to negative in the subsurface layer between 200 m and 800 m (Qiu, 1999; Roemmich and Gilson, 2001; Kobashi and Kawamura, 2002; Qiu and Chen, 2013). Previous studies of eddies in the STCC region have divided this band at roughly 170°W into the western STCC (Qiu, 1999; Hwang et al., 2004; Qiu and Chen, 2010, 2013) and the eastern Hawaiian Lee Counter-current system (HLCC) region (Yoshida et al., 2011; Liu et al., 2012; Qiu and Chen, 2013).

EKE variability on interannual and longer time scales in the STCC region has been the subject of several previous studies. Qiu and Chen (2010) explored the interannual EKE signals in the STCC band. They found that the eastward horizontal shear of

the STCC was stronger in eddy-rich years than in eddy-weak years and they emphasized the role of the wind-induced Ekman convergence forcing in causing interannual changes in the eastward shear of the STCC. As the magnitude of the wind-induced Ekman convergence is controlled by the strength of the local wind stress curl, this is an example of mechanism M4 modulating the strength of the horizontal shear and subsequent EKE. The importance of the meridional Ekman convergence forcing in controlling the interannual modulations in the late winter northern STCC was also stressed by Kobashi and Kubokawa (2011). Qiu and Chen (2010) connected the EKE variability in the STCC band to the negative Western Pacific (WP) index defined by Wallace and Gutzler (1981). The correlation of EKE with the PDO index was noted by Qiu and Chen (2010) in the eastern STCC and by Yoshida et al. (2011) in the HLCC band. EKE variability in the STCC was found to be well represented by the difference in wind stress curl between a region off the Philippines (8° - 13° N, 130° - 155° E) and a region off Taiwan (22° - 25° N, 155° - 180° E) (Chang and Oey, 2012) referred to as the Philippines–Taiwan Oscillation (PTO) index. Qiu and Chen (2013) compared the decadal STCC EKE time series with PDO, WP and PTO indices. The PDO index was highly correlated with the PTO index with a lead of 3 months and both are well correlated with STCC EKE changes at a lead time of 6 and 12 months respectively. The WP index represented the low-frequency EKE changes reasonably well prior to 2007 but this correlation deteriorated after 2008. Qiu and Chen (2013) demonstrated that the EKE variability inside the sub-tropical gyre band represents one aspect of the broad-scale decadal changes embedded in the North Pacific Ocean.

In the eastern North Pacific, previous studies have focused on the regions of the Alaskan Current (Shroyer and Plueddemann, 2012) and the California Current (Kelly et al., 1998; Strub and James, 2000; Marchesiello et al., 2003; Kurian et al., 2011). This is due to the influence of eddy induced circulation, transport and mixing on the ecosystem in this region (Kurian et al., 2011). In a study of the temporal changes in eddy energy of the oceans, Stammer and Wunsch (1999) found that the northeastern

North Pacific was one region where a significant contribution of the wind field to the observed eddy energy was found. We would therefore expect mechanism M1 to have a significant influence on EKE trends in this region.

Due to extensive research studies of the North Pacific, much has been learned about the EKE spatio-temporal variability. Despite this, no study has yet investigated how the basin-wide EKE has changed during the altimetry record, or the physical mechanisms responsible for trends in EKE. In this chapter we will address the following questions; 1) What is the spatial distribution of trends in EKE for the North Pacific Ocean during the altimetric record? 2) Is there evidence to indicate that local and/or remote atmospheric variability is the cause of the observed EKE trends? 3) Does EKE variability in the North Pacific agree with the theory of a decadally modulating dynamical state? Are the EKE trends in the North Pacific a sign of changing EKE or simply resulting from the phase of low-frequency variability?

Like the North Atlantic, the spatial distribution of time-mean EKE in the North Pacific Ocean is highly inhomogeneous and varies over several orders of magnitude (figure 4.1). In the extra-tropical regions two well defined zonal bands of elevated EKE are observed. The first band centred at approximately 35°N follows the path of the Kuroshio. In this chapter, unless stated otherwise, reference to the Kuroshio Extension region refers to the region in figure 4.1 box A (32°N - 38°N, 140°E - 170°E). The second band is located within the southern half of the western North Pacific subtropical gyre between 18°N and 28°N in the STCC region (shown in figure 4.1 box B). The STCC region in this chapter is defined as the region between 18°N – 28°N, 140°E – 160°W.

In the eastern North Pacific, away from the influences of western boundary intensification and the STCC, large areas are characterised by EKE levels one or more orders of magnitude lower than, for example, the most energetic regions of the Kuroshio system. One such region defined as 32°N – 48°N, 135°W – 160°W we refer to hereafter as the eastern North Pacific (ENP) region. Elevated EKE in the otherwise low-energy

eastern North Pacific can be observed in the near-coastal regions of the California Current off the west coast of North America and the Alaskan current south of Alaska and the Aleutian Islands.

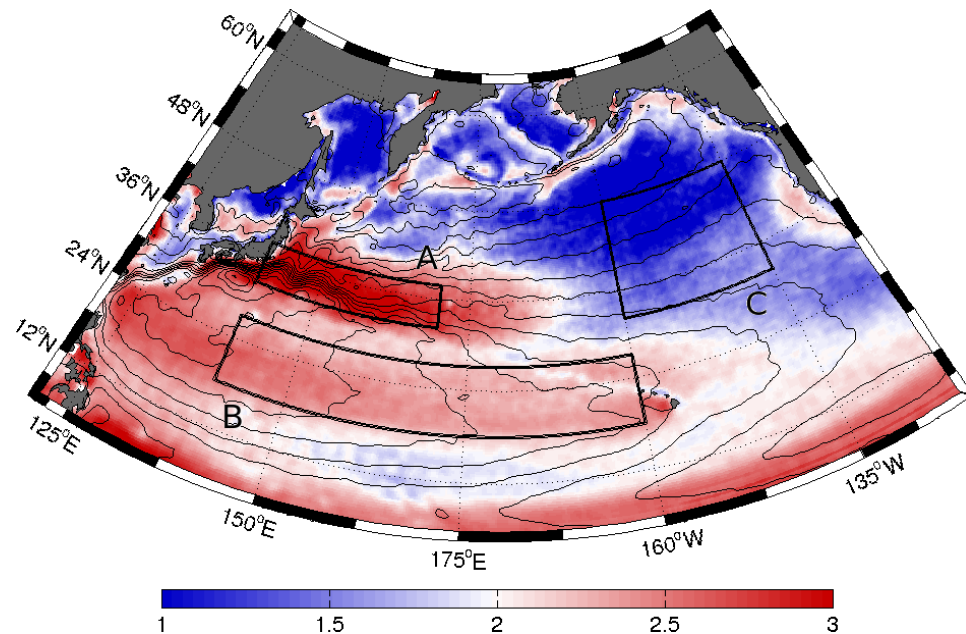


Figure 4.1: The Log_{10} of time mean EKE ($\text{cm}^2 \text{ s}^{-2}$) computed from altimetric SSH anomalies for the 18 year period 1993-2010, gridded on a $1/3^\circ$ spatial grid. Contour lines represent mean dynamic topography from altimetry at 10 cm increments.

4.2 Results and Discussion

4.2.1 EKE trends

The time series of EKE for the North Pacific (Figure 4.2a) shows that the amplitude of the high-frequency variability (grey line) is $\sim 20\%$ of the mean. The trend in the basin-wide mean EKE, averaged over the North Pacific is 1.2% per decade during the 18 year time period but the trend is not statistically significant. Spectral analysis (Figure 4.2b) reveals the dominant frequencies of variability to be at the annual and biannual frequencies. Annual mean EKE in 2003, 2004 and 2005 is notably higher than other years which inevitably has an influence on the magnitude of the trend.

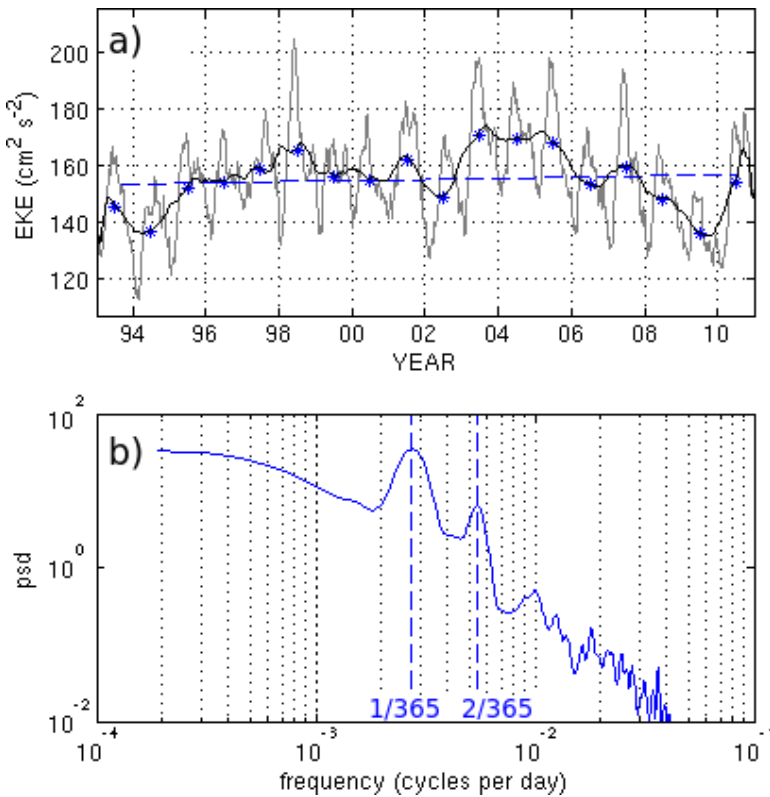


Figure 4.2: (a) Time series of weekly area-weighted EKE in $\text{cm}^2 \text{s}^{-2}$ (grey line) averaged over the North Pacific ($10^\circ\text{N} - 60^\circ\text{N}$, $125^\circ\text{E} - 120^\circ\text{W}$). Included are the 12 month running mean (black line), annual means (blue stars) and the linear trend in the annual mean (blue dashed line). (b) frequency spectrum for the weekly time series in (a).

Annual EKE anomalies for the North Pacific (Figure 4.3) show that during these anomalously high years, the positive EKE anomalies are highest in the Kuroshio region. Comparing the EKE anomalies for years corresponding to a 'stable' regime, with those years corresponding to an 'unstable' regime in the Kuroshio region reveals that a distinct pattern of variability that relates to the phase of the Kuroshio stability. Specifically, the EKE anomalies are more positive in the upstream region of the Kuroshio and more negative in the downstream region during the unstable phase with the reverse observed during the stable phase. A definition of the upstream and downstream regions as well as further analysis of the differences in the two regions can be found in section 4.2.4.

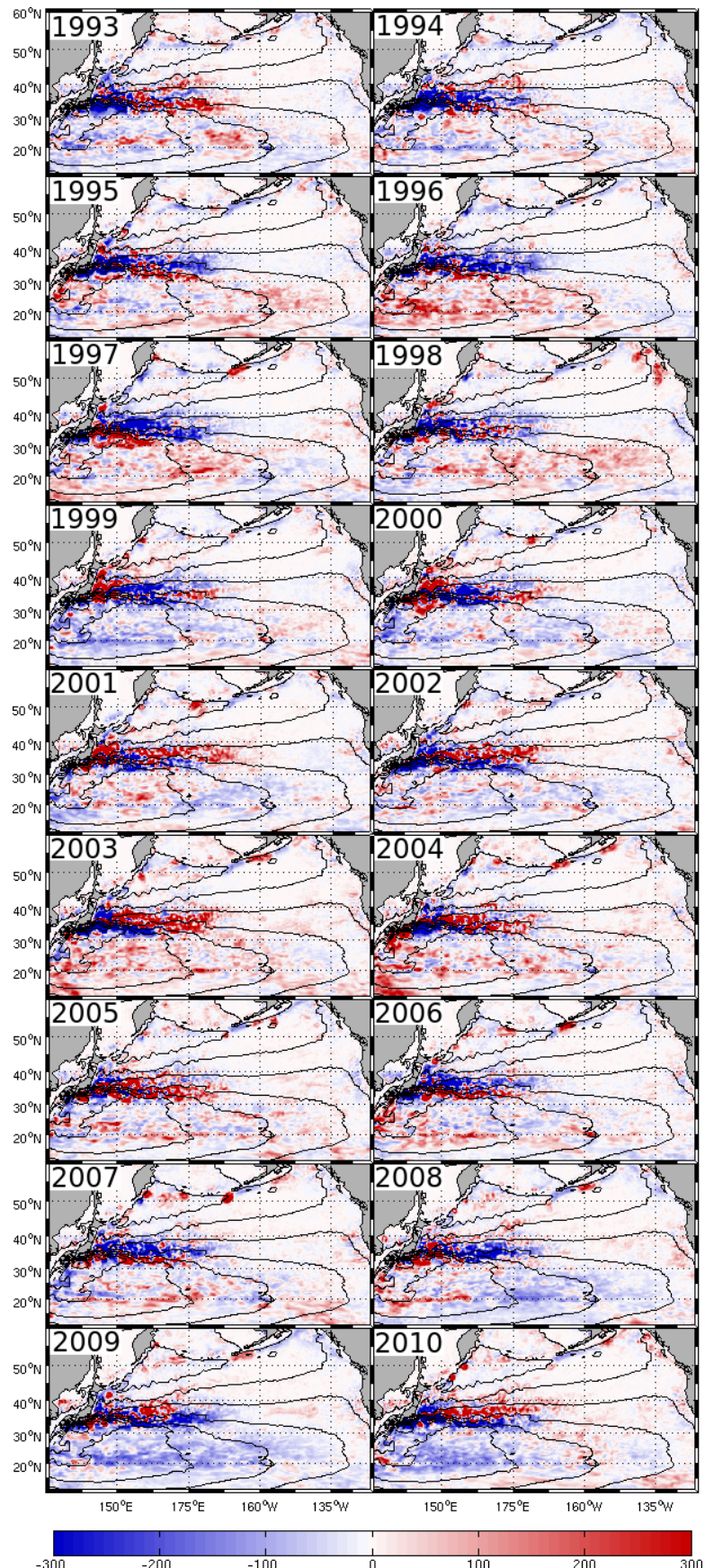


Figure 4.3: Annual EKE anomalies ($\text{cm}^2 \text{s}^{-2}$) for each year from 1993 - 2010. Black lines represent mean dynamic height contours at 20 cm intervals.

Yearly EKE anomalies also show significant interannual variability in the subtropical regions. 1996 to 1998 are years where the EKE anomalies are predominantly positive in the North Pacific sub-tropical gyre. This region is characterised by predominantly negative anomalies in 1999 to 2002 and 2008 to 2010. The same initial comparison between the EKE anomalies in years corresponding to a 'stable' regime with those years corresponding to an 'unstable' regime (Qiu and Chen, 2010) do not reveal an obvious causal link between EKE interannual variability and the two different jet stability phases in the STCC region. This is an indication that the mechanisms responsible for EKE variability and trends in the STCC are different in nature to the mechanisms responsible for EKE variability and trends in the Kuroshio region.

The spatial distribution of EKE trends for the North Pacific region (figure 4.4) reveals that statistically significant positive and negative trends are widespread across the entire North Pacific. The trend map is characterised by both large scale patterns ($>10^6 \text{ km}^2$) as well as trends on smaller spatial scales.

For our analysis we will focus on the following key features of the trend map in order to explain the mechanisms responsible for the observed trends:

- The Kuroshio Extension region is characterised primarily by positive trends. Further upstream, these positive trends are generally confined to the centre and north of the Kuroshio jet core (closest dynamic height contours). Further downstream the positive trends appear increasingly further to the north of the Kuroshio jet core. Here the positive trends are flanked to the south by negative trends.
- The subtropical North Pacific is dominated by negative EKE trends, in particular, the interior of the subtropical gyre in the STCC band where EKE trends are almost entirely negative.
- The majority of the northeast North Pacific is characterised by positive trends. These positive trends dominate the ENP region where statistically significant

trends are widespread. Trends are also positive in the upwelling region off the coast of California.

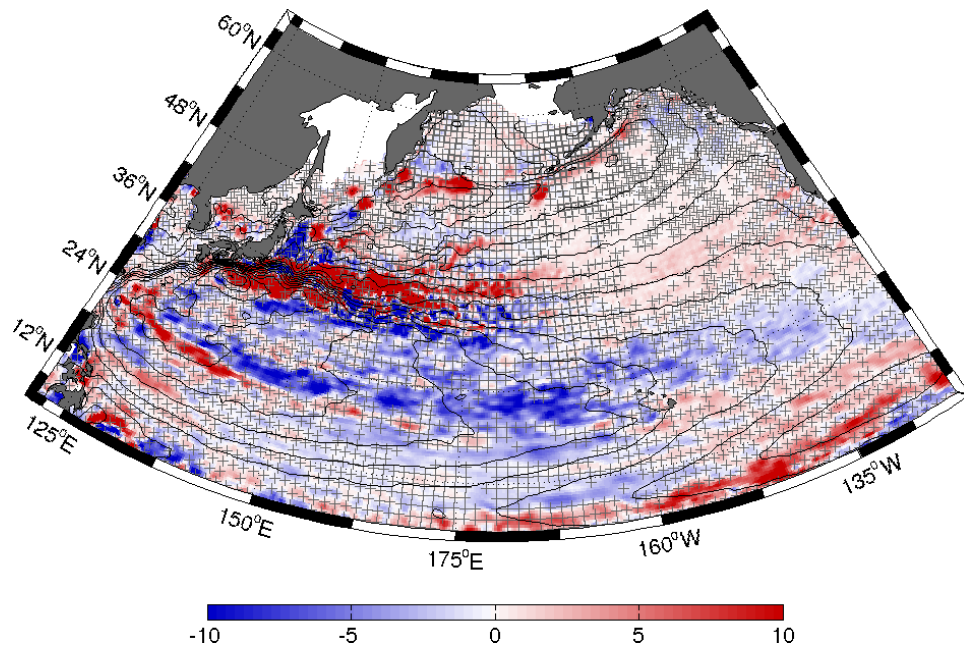


Figure 4.4: Linear trend in EKE ($\text{cm}^2 \text{ s}^{-2}$ per year) computed from altimetric sea surface height anomalies for the 18 year period 1993-2010. The hatched areas signify non-statistically significant trends at 90% confidence. Contour lines represent mean dynamic topography from altimetry at 10 cm intervals.

In addition to statistical significance, further insight into the robustness of the trends is revealed by comparing the sign of the trends in the first half of the study period (figure 4.5a) with those of the second half (figure 4.5b). This reveals that just over half (51.2%) of the area is characterised by the same sign of the trend for both time periods (figure 4.5c). Trends in the Kuroshio region display some similarity for the two time periods but also display significant differences (where a significant part of the Kuroshio region has been masked). In the STCC region, the large-scale pattern of negative trends in the subtropics is very similar in the latter time period to the earlier time period but with smaller scale regions with positive trends apparent in the earlier half. Trends in the ENP region are predominantly the same in both time periods.

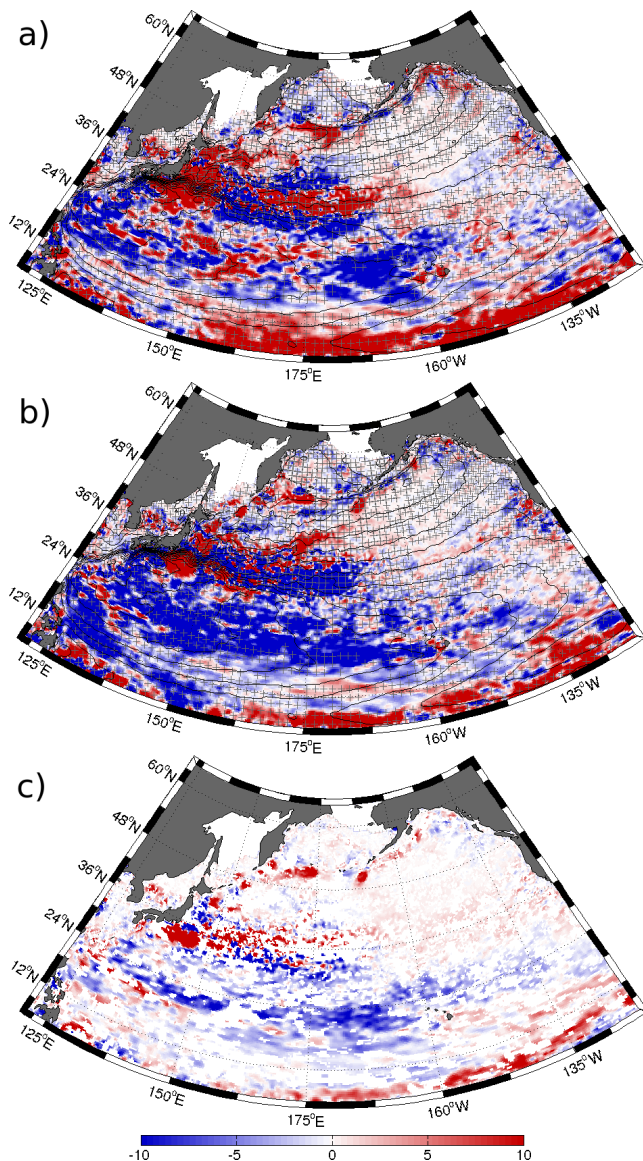


Figure 4.5: Linear trend in EKE ($\text{cm}^2 \text{ s}^{-2}$ per year) from (a) 1993 to 2001 and (b) 2002 to 2010. (c) Linear trend in EKE ($\text{cm}^2 \text{ s}^{-2}$ per year) from 1993 - 2010 with masked (white areas) regions where the sign of the trends in (a) and (b) are different. The hatched areas in (a) and (b) signify non-statistically significant trends at 90% confidence. Contour lines represent mean dynamic topography from altimetry at 10 cm intervals.

In order to compare how the magnitude of the EKE trends vary from region to region relative to the mean, figure 4.6 indicates what percentage of the mean EKE is represented by the trend (per decade). In general, there is a greater increase in the mid-latitude and subpolar regions than the subtropics across most of the central and eastern regions.

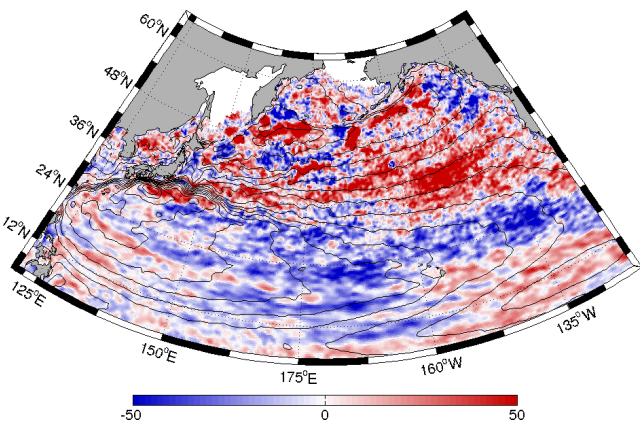


Figure 4.6: Linear trend in EKE expressed as a percentage of the mean EKE per decade. Positive values indicate percentage increase and negative values indicate percentage decrease.

Time series of EKE (figure 4.7) reveal the different characteristics of the three regions mentioned previously. EKE in the Kuroshio region (figure 4.7a) is approximately five times higher than the STCC region (figure 4.7b) which in turn is typically an order of magnitude higher than EKE in the ENP region (figure 4.7c). EKE in the STCC region has a well defined annual cycle due to the seasonal changes in horizontal velocity shear and stratification resulting in seasonally varying baroclinic instability (Qiu, 1999; Kobashi and Kawamura, 2002; Qiu and Chen, 2013). An annual cycle is less apparent in the Kuroshio region and largely absent in the ENP region.

In all three regions the trend is statistically significant. In the ENP region, annual mean EKE shows a relatively poor 'fit' ($r^2 = 0.15$) to the linear trend line, in comparison to the Kuroshio ($r^2 = 0.23$) and STCC ($r^2 = 0.22$) regions. Figure 4.7 (d), (e) and (f) show the magnitude of the correlation between annual mean EKE for each time series (Kuroshio, STCC and ENP respectively) with the PDO index at different lags. The lagged correlations in the STCC and ENP regions are similar whereas those in the Kuroshio region are not. For example, the STCC and ENP regions have a strongly positive correlation at zero and one year lag and a negative correlation at 3, 4 and 5 year lags. This dramatic shift in the sign of the correlation suggests a phase induced correlation due to the quasi-regular periodicity of both time series. The Kuroshio re-

gion is not significantly correlated except at a 5 year lag where a strong negative signal is observed.

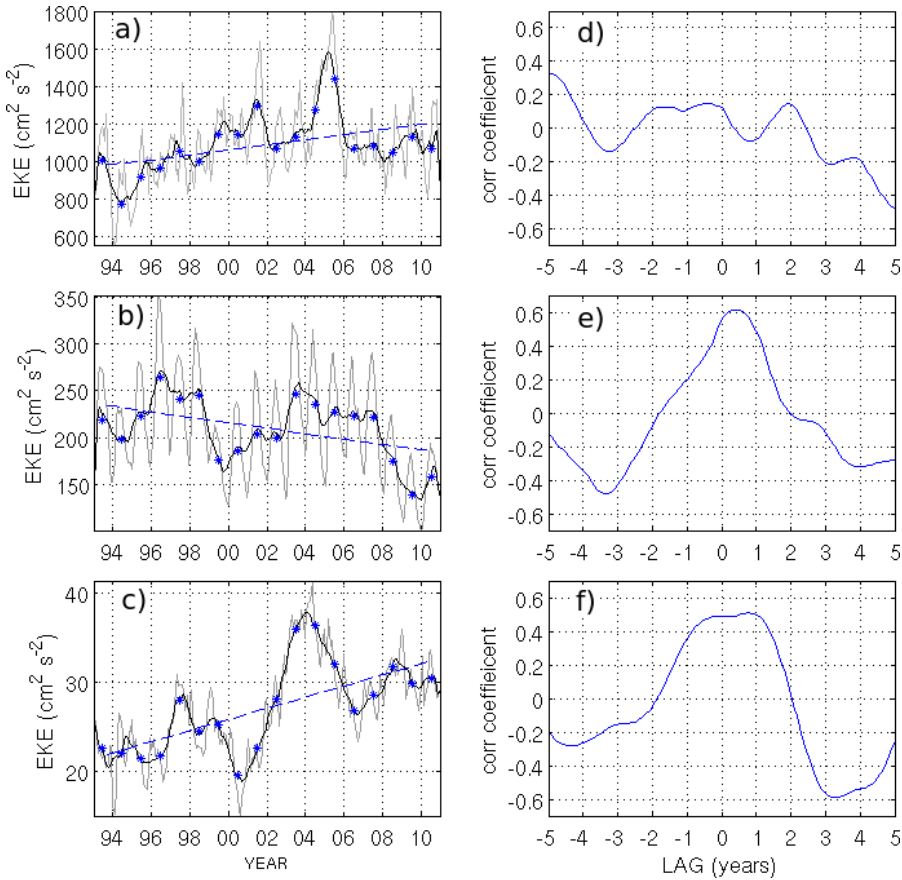


Figure 4.7: Time series of weekly EKE in $\text{cm}^2 \text{s}^{-2}$ (grey lines) averaged over the Kuroshio (a), STCC (b) and ENP (c) regions. The blue dashed line represents the linear trend in the annual means (blue stars). Correlation coefficients at varying lags between the monthly PDO index and monthly mean EKE (positive lags indicate the PDO leading EKE) for the Kuroshio (d), STCC (e) and ENP (f) regions.

4.2.2 Atmospheric trends

The wind speed climatology (figure 4.8a) reveals two basin-wide patterns in the North Pacific. Firstly, the magnitude of the wind speed is predominantly zonally uniform in nature with a band of highest wind speed in the tropics, flanked to the north by a zonal band of low wind speed roughly centred between 24°N and 36°N . Wind speed then increases in the mid-latitudes between 36°N and 50°N . Secondly, at nearly all

latitudes, wind speed in the North Pacific is higher in the eastern basin and decreases to the west.

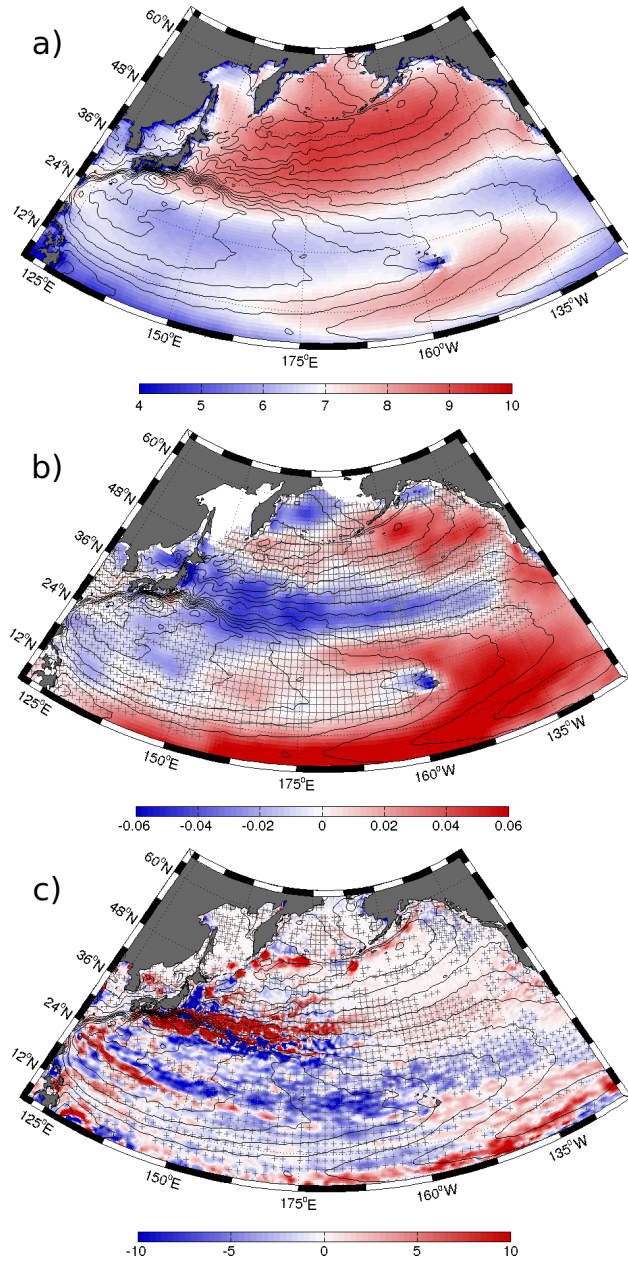


Figure 4.8: (a) Wind speed temporal mean (1993 - 2010) in $m\ s^{-1}$ from ECMWF ERA-Interim re-analysis data. (b) Linear trend in wind speed for the 18 year time period 1993 to 2010 ($m\ s^{-1}$ per year) from ECMWF ERA-Interim re-analysis data. The hatched areas signify non-statistically significant trends at 90% confidence. (c) Trend in EKE ($cm^2\ s^{-2}$ per year) from 1993 to 2010 showing only the regions where the wind speed trend and the EKE trend are the same sign (stipple shows areas where the sign is different). Black contours show mean dynamic topography at 10 cm intervals.

The basin-wide pattern of wind speed trends (figure 4.8b) reveals an east-west contrast with negative trends in the west and positive trends in the east. Negative statistically significant trends dominate in the latitudes of the Kuroshio (32°N - 38°N) as far east as 150°W . Some of the regions where positive (negative) wind speed trends are found are also characterised by positive (negative) EKE trends. This is consistent with the hypothesis that EKE trends in these regions have resulted from a change in local wind speed (mechanism M1). In particular, the negative trends in wind speed covering most of the western subtropics and the positive trends in the northeast are also co-located with EKE trends of the same sign. These regions where the trends in EKE and wind speed are the same sign are easily identified by observing the EKE trend map (figure 4.8c) with masked regions (white areas) where EKE and wind speed trends are of different signs.

Although figure 4.8c shows large regions where the trends are similar in sign, this view also reveals that a substantial proportion of the trend map (48.1%) has been masked by the stipple. This indicates that trends in wind speed can only be considered to be partially responsible for the EKE trends and the relative magnitude of this influence is variable from one area to another. For example, in the subtropical region a visibly larger amount of the trend map has been masked in figure 4.8c than the subpolar region. Importantly, the positive EKE trends in the Kuroshio region have disappeared entirely in this view indicating that the positive EKE trends in the Kuroshio region have not arisen due to an increase in local wind speed (mechanism M1).

The spatial pattern of wind stress curl climatology in the North Pacific (figure 4.9a), like the wind speed, is predominantly zonal in nature. A zonal band of negative (cyclonic) curl is centred in the subtropical belt, with positive (anti-cyclonic) curl to the north and south of this band. The exception being some coastal regions, including the Hawaiian archipelago. As well as the meridional extent of the subtropical band of negative curl being wider in the east than in the west, the magnitude of the wind stress curl is also higher to the east than to the west.

Statistically significant wind stress curl trends (figure 4.9b) also vary in both sign and magnitude across the North Pacific basin. In the tropics, wind stress curl trends are predominantly negative. Positive trends characterise the central and western subtropical regions including the interior of the subtropical gyre. North of the subtropical regions, where the wind speed trends are predominantly negative, a corresponding zonal band of negative trends in wind stress curl appears between 36°N and 48°N. Positive trends in wind stress curl can be found in the interior of the subtropical gyre where wind speed trends are negative. In the central and eastern tropical belt, where wind speed trends are strongly positive, wind stress curl trends are negative.

In order to investigate the potential role of wind stress curl changes as a forcing for EKE trends, we show in figure 4.9(c) the EKE trend map where the trend in both EKE and wind stress curl magnitude are the same sign. This view of the EKE trend map shows that approximately 50% of the trend map has been removed, indicating that half the North Pacific is characterised by similar trends in both EKE and wind stress curl.

By comparing figure 4.9(c) with figure 4.8(c) we can identify the areas where either local wind speed or local wind stress curl changes can have an influence on EKE trends. In the Kuroshio region, EKE trends do not appear to be influenced by wind speed. This indicates that the mechanism responsible for the positive trends in EKE in this region is not a local wind forcing. Wind stress curl trends do show some similarity over part of the Kuroshio region, suggesting that mechanism M4 has made some contribution to the observed EKE trends. The lack of similarity across the entire Kuroshio region indicates that this mechanism is not the dominant mechanism over the entire region and that other mechanisms must also make a significant contribution.

Negative trends in both wind speed and wind stress curl are found in the subtropical gyre where EKE trends are predominantly negative. The similarity in EKE-WSC trends extends across the entire subtropical gyre, with the notable exception of the STCC band.

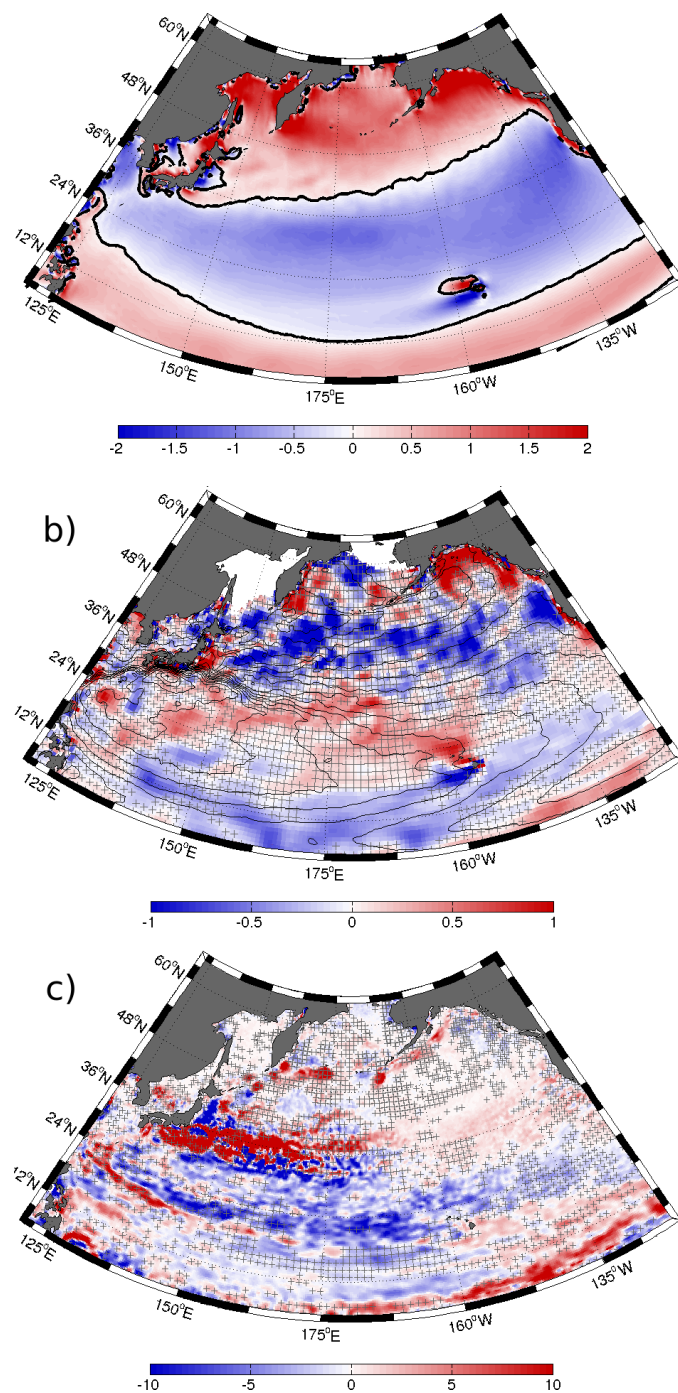


Figure 4.9: (a) Wind stress curl temporal mean ($x10^{-7} \text{ N m}^{-3}$) for the time period 1993 to 2010 from ECMWF ERA-Interim re-analysis data. (b) Linear trend in wind stress curl ($x10^{-8} \text{ N m}^{-3} \text{ per year}$) for the same time period from ECMWF ERA-Interim re-analysis data. The hatched areas signify non-statistically significant trends at 90% confidence. (c) Trend in EKE ($\text{cm}^2 \text{ s}^{-2} \text{ per year}$) from 1993 to 2010 for the regions where the trend in wind stress curl magnitude is the same sign for the same time period. Black contours show mean dynamic topography at 10 cm intervals.

This indicates that a decrease in WSC in the subtropical gyre may be responsible for a significant proportion of the negative EKE trends in this region (mechanism M4).

4.2.3 EKE and atmospheric variability

EKE variability on interannual time scales has been found to be related to changes in the dynamical state of the basin-wide circulation which, in turn, is related to the PDO index in the subtropical gyre (Qiu and Chen, 2013) and the upstream Kuroshio region (Qiu and Chen, 2005). To further investigate to what extent a relationship exists between the PDO and EKE variability at interannual time scales, figure 4.10 shows the correlation coefficients of annual mean EKE with the annual PDO index at varying lags across the entire North Pacific basin.

The most striking feature of the correlation map at zero lag (figure 4.10a) is statistically significant positive correlations which are dominant in the subtropical gyre, in agreement with Qiu and Chen (2013). The mid-latitude eastern regions are more positive and the mid-latitude central and western regions are more negative.

In general, this basin-wide pattern is persistent at one year lag (figure 4.10b). At 2 and 3 year lags (figure 4.10c and d) the pattern changes considerably. The region in the downstream Kuroshio jet is characterised by negative correlations, as is the majority of the western North Pacific. The positive signal in the subtropical gyre does not persist at these time scales. At a lag of 4 years, a significant feature of the correlation map is the strongly negative signal in the central North Pacific downstream of the Kuroshio extension.

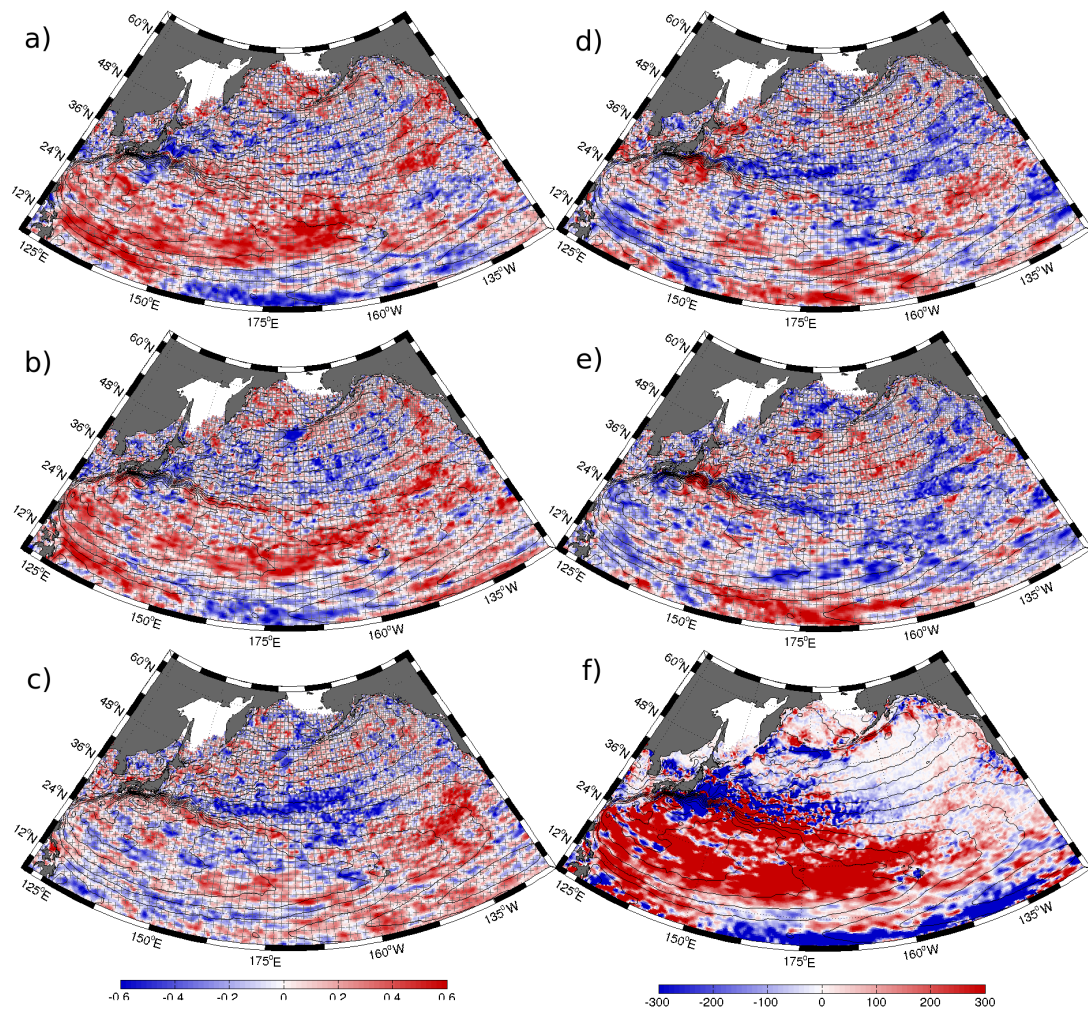


Figure 4.10: Correlation coefficients of annual mean EKE with PDO index at varying time lags from 0 to 4 years (a-e). The hatched areas represent non-statistically significant correlations at 90% confidence. (f) Composite map of EKE anomalies for the years corresponding to the strongest positive PDO years (1993, 1995, 1996, 1997, 2003 and 2005) minus the years corresponding to the strongest negative PDO years (1999, 2000, 2001, 2008, 2009 and 2010). Black contours show mean dynamic topography at 10 cm intervals.

In order to explore the relationship between basin-wide EKE variability in the North Pacific and the PDO from an additional perspective, composite maps of annual mean EKE anomalies are shown for years corresponding to the strongest positive PDO years minus the years corresponding to the strongest negative PDO years (figure 4.10f). During the positive phase of the PDO, EKE anomalies are strongly positive in

the subtropical gyre but there are also some small negative signals in the gyre interior. The Kuroshio region is characterised by small scale variability but is generally more negative to the north and more positive to the south in the downstream region. EKE anomalies in the upstream Kuroshio region are also more negative during positive PDO years.

4.2.4 The Kuroshio Extension

In the Kuroshio region, predominantly positive trends indicate an increase in the intensity of eddies within the Kuroshio jet during the study period. The absence of any corresponding positive trend in wind speed in the same location indicates that a direct, local wind forcing (mechanism M1) can be ruled out. WSC trends are positive over most of the Kuroshio region, indicating that an increase in current intensity due to WSC intensification (mechanism M4) is a plausible mechanism in this region.

In order to further explore the forcing mechanisms for the observed trends in the Kuroshio region, it is useful to consider the upstream and downstream Kuroshio regions separately. The difference in each region is clearly illustrated with composites of annual mean EKE anomalies during the positive jet stability phase (as defined in Qiu and Chen (2010)), minus the annual mean EKE anomalies during the negative jet stability phase (figure 4.11a). During the stable phase, EKE is clearly low in the upstream region and high in the downstream region. Comparing this with composites of EKE anomalies (figure 4.11b) in the same region shows that the EKE in the upstream region is low during a positive phase of the jet's stability and high during a negative phase. Surprisingly, however, the downstream region does not indicate a similar link. Despite an area of the downstream region showing negative trends, much of this region is also characterised by positive trends.

The time series of EKE in both the upstream and downstream regions of the Kuroshio (figure 4.11c and d) indicate that EKE in both regions can transition from high to low, according to the jet's stability. This is particularly evident in the down-

stream region where the years corresponding to a positive phase of the jet stability (1993 to 1995 and 2002 to 2004) correspond to high EKE years. In this region, however, the EKE during the latter stable phase (2002 to 2004) is significantly higher than the previous stable phase (1993 to 1995). The upstream and downstream regions are those defined spatially by Qiu and Chen (2005). Analysis reveals that the time series in both regions are sensitive to small changes in the boundaries but the described relation of both time series to the phase of the jet stability is not sensitive to these small changes.

This result indicates that the mechanism of remote atmospheric (mechanism M2) induced low frequency variability in the Kuroshio region described in Qiu and Chen (2005) may have a significant influence on the EKE trends in both the upstream and downstream regions, but other mechanisms are also making a significant contribution to the trends in the downstream region.

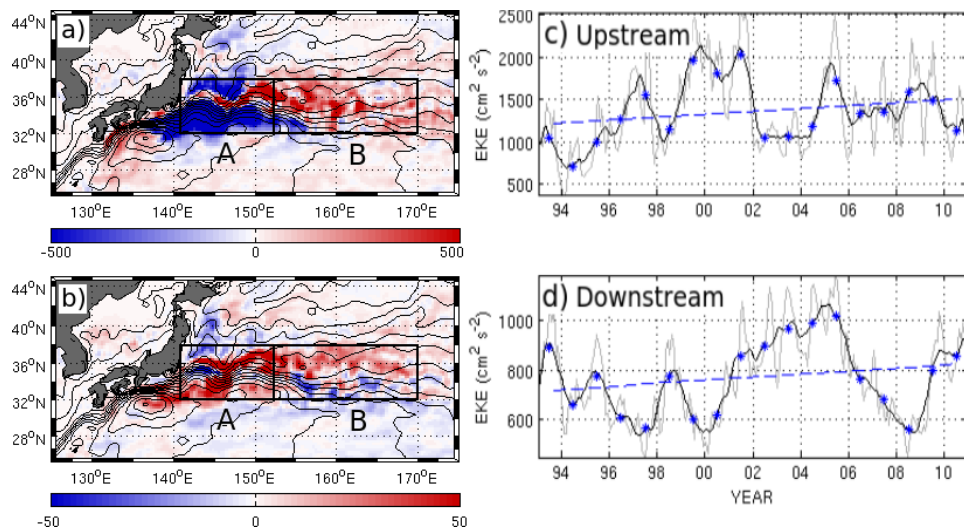


Figure 4.11: Composite of annual mean EKE anomalies for the years corresponding to (a) a positive phase of the Kuroshio jet stability (1993 - 1995 and 2002 - 2004) and (b) the negative years (1995 - 2001 and 2005 - 2010). c) Time series of EKE (grey lines) with linear trend (blue lines) in the annual means (blue stars) for the upstream ($32\text{-}38^\circ\text{N}$, $141\text{-}153^\circ\text{W}$) Kuroshio region and d) downstream ($32\text{-}38^\circ\text{N}$, $153\text{-}170^\circ\text{W}$) Kuroshio region.

Our results suggest that one or more mechanisms may be significant in the

Kuroshio region. Both EKE trends and EKE-PDO correlations are consistent with the hypothesis described by Qiu and Chen (2005) where WSC induced SSH anomalies generated in the eastern basin propagate westwards as baroclinic Rossby waves and disrupt the stability of the Kuroshio jet typically at a lag of 4 years. This implicates mechanism M2 as significant in this region. Other trends, particularly in the downstream region, may be due to intrinsic variability (Mechanism M6). This is consistent with the results of Penduff et al. (2011) who found that the intrinsic component of SSH variability at interannual time scales was as high as 70% - 80% in the Kuroshio region.

4.2.5 The STCC region

The STCC band, within the southern interior of the wind driven subtropical gyre, is dominated by negative EKE trends. As previously mentioned, this region is characterised by an eastward shear of zonal flows within the upper ocean. The STCC owes its existence to the combined forcing of surface wind stress and heat fluxes (Kobashi and Kubokawa, 2011; Qiu and Chen, 2013).

Annual mean EKE is positively correlated with the PDO in the STCC band at zero and one year lags. For both the eastern STCC and the HLCC, Qiu and Chen (2010) and Yoshida et al. (2011) found that the EKE level in their respective study regions is positively correlated with the PDO index. In particular, Yoshida et al. (2011) found that the latitude-dependent surface heat flux forcing played a more crucial role than the Ekman convergence forcing in controlling the decadal-varying eastward shear in the HLCC region. The quasi-regular decadal modulation observed in the time series of EKE in the STCC (figure 4.7b), as well as the strongly positive EKE-PDO correlations (figure 4.7e), indicate that the widespread negative trends in EKE are related to the phase of this PDO related decadal pattern. Qiu and Chen (2013) found that the modulating eddy activities are due to the decadal change in the upper-ocean eastward shear in the broad-scale STCC/HLCC band and that this observed eastward shear

change can be effectively accounted for by the decadal-varying surface heat flux forcing. Using Argo-based temperature and salinity data, Qiu and Chen (2013) also reveal that the decadal subsurface potential vorticity anomalies, adjusting to the PDO-related surface forcing, lagged behind the upper-ocean eastward shear signals and likely made minor contributions to generate the decadal-varying eddy signals in the STCC band.

We suggest that two mechanisms are responsible for the EKE trends in the subtropical North Pacific. Firstly, in the STCC band, where previous studies have indicated a strong local baroclinicity in modulating EKE at seasonal and interannual timescales, EKE trends are different in sign to trends in both wind speed and WSC. Based on these previous studies and the lack of similarity between EKE trends and trends in wind speed and wind stress curl, we suggest that the negative EKE trends in this region may be due to local baroclinicity (mechanism M5). North of the STCC, negative EKE trends are co-located with negative trends in both wind speed and WSC. Here we attribute the EKE trends to a combination of both local wind (mechanism M1) and WSC intensification (mechanism M4).

4.2.6 The eastern North Pacific

EKE trends in the ENP region are almost entirely positive. Although weak in magnitude, the majority of the trends appear as statistically significant. Figure 4.6 shows that the EKE trend, as a percentage of the mean EKE in this region, is very large in comparison with most other regions in the North Pacific. The time series of EKE in this region (figure 4.7c) reveals anomalously high EKE during 2003, 2004 and 2005. Interannual variability is high in comparison with the mean (approximately 50%) and the goodness of fit to the trend line is therefore low ($r^2 = 0.15$). The similarity between EKE trends and wind speed trends (figure 4.8c) and the similarity between EKE trends and WSC trends (figure 4.9c) indicate that local wind forcing (mechanism M1) is more dominant further to the north and WSC intensification (mechanism M4) is more dominant further south in the eastern North Pacific.

Although wind speed and WSC trends indicate that mechanisms M1 and M4 are significant in the eastern North Pacific, we suggest that another mechanism is also responsible for contributing to the positive EKE trends in the ENP region. An area of elevated EKE can be found to the east of the ENP in the upwelling region of the California Current (CC) (30°N - 45°N , 240° - 250°W) which is characterised by positive trends in EKE. The positive trends in EKE in the upwelling regions off the coast of California introduce a theory that the long-term increase in eddy activity in the ENP region may originate in this eddy rich region due to an increase in upwelling intensity during the study period which is subsequently advected into the ENP region. This hypothesis is supported by studies of long-term trends in the frequency, duration, and strength of wind-driven coastal upwelling events for the Oregon and California regions of the California Current System (García-Reyes and Largier, 2010; Iles et al., 2012). A comparison of the time series' of EKE for the ENP and California Current regions and their associated correlation coefficients (figure 4.12) indicate that this theory is a

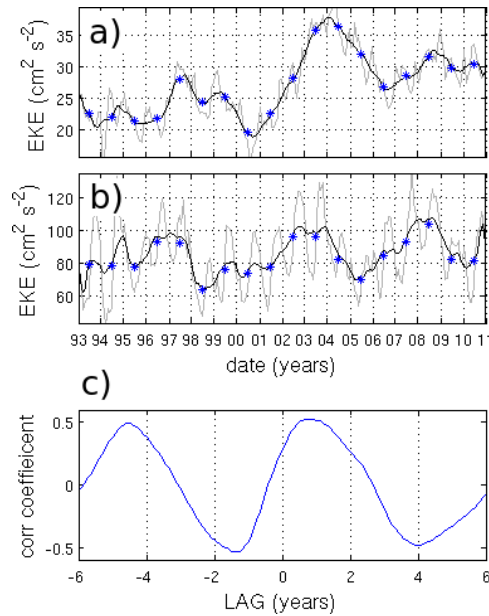


Figure 4.12: Time series of EKE (grey lines) with 12 month running mean (black lines) and annual means (blue stars) for (a) the ENP region ($30\text{-}50^{\circ}\text{N}$, $190\text{-}225^{\circ}\text{W}$), (b) California coastal upwelling region ($30\text{-}45^{\circ}\text{N}$, $240\text{-}250^{\circ}\text{W}$) and (c) Lagged correlations between annual mean EKE in both regions.

very plausible as the time series are very strongly correlated at one year lag. The size and location of the boxes were chosen to best encompass (box a) the region of statistically significant positive trends in the Eastern North Pacific shown by box C in figure 4.1 and (b) the area of elevated EKE off the coast of California also visible in figure 4.1. These results indicate that remote wind and/or local baroclinicity (mechanism M2) is a contributing mechanism in some regions of the eastern North Pacific.

4.3 Conclusions

In this chapter we have shown that basin-wide EKE has increased by 2% from 1993 to 2010 and that this trend is not statistically significant. The spatial distribution of trends is highly variable with distinct large scale patterns of both positive and negative statistically significant trends.

Our results suggest that a variety of mechanisms are responsible for the observed EKE trends in the North Pacific, the relative influence of each mechanism being spatially variable. The principal mechanism identified in regions of the North Pacific with large areas of statistically significant trends is summarised in figure 4.13

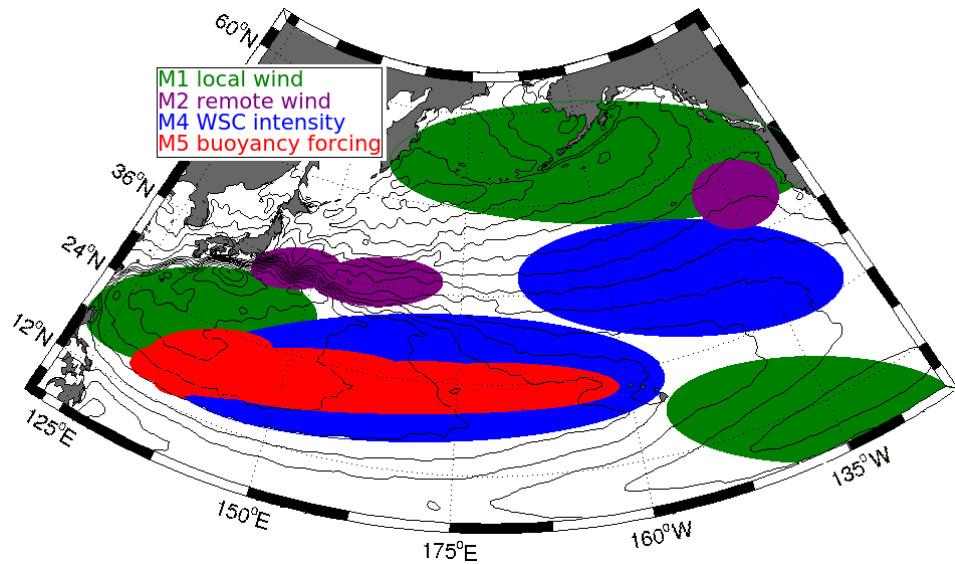


Figure 4.13: Schematic diagram to illustrate the principal mechanism responsible for the trend in EKE for different regions of the North Pacific.

A comparison of wind speed trends with EKE trends reveals large areas of the North Pacific where trends are the same sign, most notably in the northeastern North Pacific, but also reveals large areas where they are not, notably the central and eastern subtropics and the Kuroshio region. Like wind speed trends, wind stress curl trends are similar in some regions but not others. Notable similarities include parts of the Kuroshio region, the ENP region south of 40°N and the northern and eastern subtropical gyre interior. This suggests that the influence of direct atmospheric forcing (mechanism M1) and local WSC intensification (mechanism M4) in the North Pacific is highly spatially variable and only distinguishable in some regions but not others.

As found by previous studies (e.g. Qiu and Chen (2010)), our results indicate that EKE in the STCC region is highly correlated with the PDO during the 18 year study period. Our result also show that despite a similarity between EKE trends and wind stress curl trends in most of the subtropical gyre interior, much of the STCC band does not display this similarity. This strongly implies that EKE trends in the STCC region have arisen due to another mechanism. As previous studies have identified the strong influence of local baroclinicity in modulating EKE on interannual time scales, we suggest that this mechanism (mechanism M5) is the dominant mechanism for EKE

trends in this region.

In the ENP region, predominantly positive EKE trends have resulted from changes in local wind speed (mechanism M1) in the north and wind stress curl (mechanism M4) further south. Furthermore, there is strong evidence to suggest that both the EKE trends and the EKE interannual variability in this region result from non-local atmospheric effects (mechanism M2) originating in the coastal upwelling region of the California Current where eddies are generated and advected to the west.

Chapter 5

The Southern Ocean

5.1 Introduction

Mesoscale oceanic eddies play a crucial role in the dynamical balance of the Southern Ocean, contributing to the transport and mixing of tracers, as well as the redistribution of momentum, potential vorticity and energy (Ivchenko et al., 2008). The importance of the transient eddy field in the dynamics of the Southern Ocean has been demonstrated in simple theories of the current (Johnson and Bryden, 1989) and eddy-resolving quasi-geostrophic models (Wolff et al., 1991). In the Southern Ocean, eddies are the principal mechanism for the poleward transport of heat across the strongly zonal Antarctic Circumpolar Current (ACC) (Karsten and Marshall, 2002).

Seafloor bathymetry is known to play an important role in a variety of oceanic processes including intense vertical mixing (Polzin, 1997) and the dissipation of barotropic tidal energy (Munk and Wunsch, 1998). Gille et al. (2000) showed that a relationship exists between bathymetry and EKE. In regions of the ocean deeper than about 4800 m, surface EKE is greater over smooth abyssal plains than rough bathymetry, while the opposite is true in shallower waters. These findings suggest that EKE may be dissipated by rough topography in the deep ocean and shallow or very rough bathymetry may be capable of generating eddies. This is of particular relevance

in the Southern Ocean where the bathymetry is highly changeable from deep abyssal plains (e.g. Amundsen Abyssal Plain, Australian-Antarctic Basin, Crozet Basin) to shallow rough topography (e.g. Scotia Sea, Kerguelen Plateau, Campbell Plateau) along the main path of the ACC (figure 5.1).

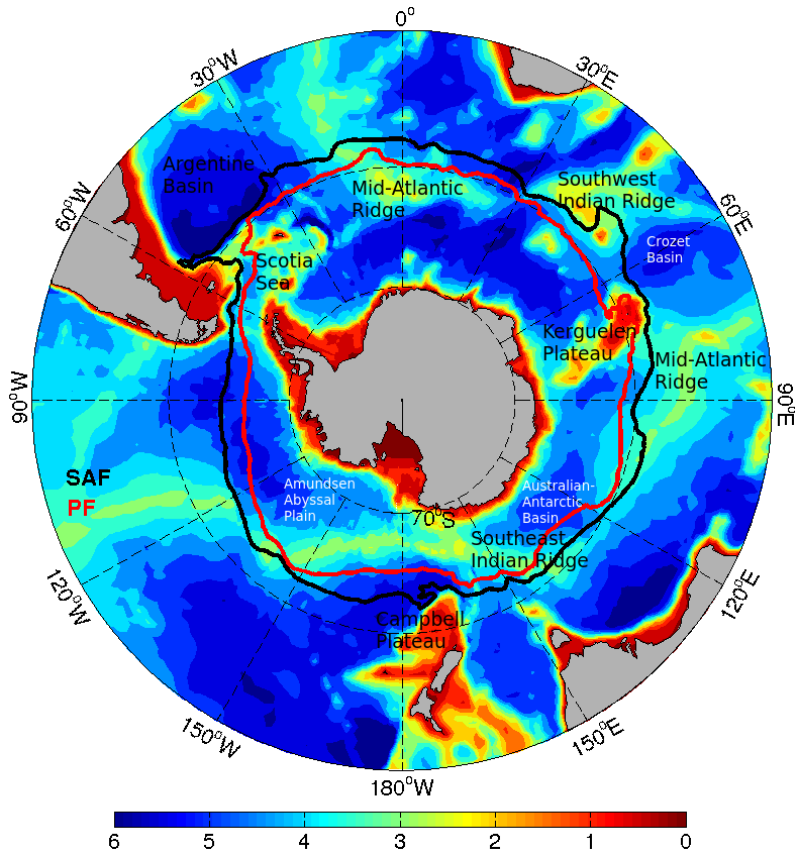


Figure 5.1: The Southern Ocean bathymetry with significant bathymetric features. Included are the Polar Front (black line) and Sub-Antarctic Front (red line) from Sallée et al. (2008). Ocean depths are in km.

Increased levels of EKE are generally found where the geostrophic currents of the ACC are strongest (i.e. where the gradient in dynamic height is largest). The meridional shifting of the ACC in response to atmospheric variability has been the subject of both observational studies (Sallée et al., 2008) and numerical simulation studies (Spence et al., 2010). Sallée et al. (2008) related the movement of the Polar Front (PF) and Subantarctic Front (SAF) to both SAM and ENSO during the period 1993–2005. They found that while the SAM is relatively symmetric, the oceanic response of the

fronts shows substantial regional differences. Around the circumpolar belt the fronts vary in latitude, exposing them to different Ekman transport anomalies induced by the SAM. Three typical scenarios were observed in response to atmospheric forcing: poleward movement of the frontal structure in the Indian Basin during positive SAM events, an equatorward movement in the central Pacific, and an intensification without substantial meridional movement in the Indo-Pacific basin. Spence et al. (2010) used a global climate model to show that the Southern Ocean responds to poleward-intensifying winds at all resolutions from coarse to eddy-permitting by a poleward migration of the ACC in the Atlantic and western half of the Indian basin. Although these previous studies show a response of the ACC to atmospheric variability, they do not seek to identify a relationship between atmospheric trends and trends in oceanic properties such as EKE or SSH associated with shifting fronts.

Previous studies have sought a causal link between EKE variability in the Southern Ocean and variability in zonal wind stress. From analysis of satellite altimetry data, Meredith and Hogg (2006) found anomalously high EKE in the Southern Ocean during the period 2000-2002. The circumpolar eastward wind stress (as quantified by the SAM) showed a significant positive peak 2-3 years earlier. They used a quasi-geostrophic model to investigate the delay between wind forcing and the eddy response and demonstrated that the lag is due to feedbacks between the mean flow, its stability and the eddies which result from instability. This implies that long term changes in the strength of the local wind (mechanism M1) may play a significant role in EKE trends in the Southern Ocean.

The role of the temporal eddy variability in the ACC in influencing Southern Ocean warming was further investigated using an eddy-resolving quasi-geostrophic model (Hogg et al., 2008), where EKE, as well as circumpolar transport and eddy heat transport to changes in wind were quantified. As found by Meredith and Hogg (2006), the modelled ocean state exhibits 'eddy saturated' behaviour on interannual time scales, where increased wind stress does not significantly change the circumpo-

lar transport but intensifies the eddy field instead. The instantaneous response of increased wind stress was increased wind-induced Ekman transport of cool water to the north. In the longer term, the enhanced eddy state was more efficient at transporting heat, leading to a warming of the ocean. The model response to long-term changes in wind forcing was also tested, including steadily increasing circumpolar wind strength over a 30 year period. The model showed a response in eddy heat flux, and a change in ocean temperature not dissimilar to observed Southern Ocean warming.

The role of eddies in modulating the Southern Ocean response to the SAM has been studied using an ocean model run at multiple resolutions from coarse to eddy resolving (Screen et al., 2009). The high-resolution versions of the model showed an increase in EKE that peaks 2–3 years after a positive anomaly in the SAM index. At all resolutions, including coarse-resolution, the model captured the instantaneous temperature response shown in the previous work by Meredith and Hogg (2006) and Hogg et al. (2008), characterized by predominant cooling south of 45°S and warming to the north. If there is a causal relationship between EKE variability and the variability in the zonal wind stress as these previous studies suggest, then we would expect long term trends in wind speed to result in trends in EKE. This response is expected to be strongest in the regions of the Southern Ocean where the correlations between EKE and the SAM are significant.

More recently, investigations into the intensification of the Southern Ocean eddy field in response to the SAM have been extended to include the response to two climate modes: SAM and ENSO (Morrow et al., 2010). They utilised 16 years of altimetry data to investigate the interannual variability of the Southern Ocean’s EKE, in response to SAM and ENSO variability. Circumpolar averages showed a peak in EKE from 2000 to 2002, 2–3 years after the peak in the SAM index, in agreement with Meredith and Hogg (2006). Although the SAM forcing was in phase around the circumpolar band, the EKE response varied regionally. This indicates that a non-local atmospheric forcing (mechanism M2) may also be significant in some regions of the

Southern Ocean. The strongest EKE was in the Pacific, with energy peaks occurring progressively later toward the east. When strong positive SAM events coincided with La Niña periods, as in 1999, anomalous meridional wind forcing was enhanced in the South Pacific Ocean. When positive SAM events coincided with El Niño periods, as in 1993, the climate modes were in opposition (a positive ENSO phase coinciding with a negative SAM phase) in the South Pacific, leading to a weak EKE response during the mid 1990s. By applying different combinations of SAM and ENSO in numerical simulations, the elevated Pacific EKE response to the SAM, as well as an additional amplification/suppression of EKE during La Niña/El Niño, was reproduced. In general, the EKE response was found to depend on the interplay between wind forcing, topography and mean flow and produced a strongly heterogeneous distribution in the Southern Ocean.

Although these previous studies have revealed that the Southern Ocean's EKE field responds to atmospheric variability represented by Southern Ocean climate modes, they do not identify and/or relate trends in EKE with long term atmospheric changes. Subsequently, until now, EKE trends in the Southern Ocean and the forcing mechanisms remain understudied. In this chapter we will investigate the spatial distribution and magnitude of the trends in EKE from 1993 to 2010 and explore the evidence to indicate the physical mechanisms responsible for the observed changes. Among the main unanswered questions relating to our current understanding of the Southern Ocean and its eddy field include the following which we will address in this chapter: Has the basin-wide EKE in the Southern Ocean increased or decreased from 1993 to 2010 and is the trend statistically significant? How has the spatial distribution of EKE in the Southern Ocean changed during the altimeter record? Is there a causal link between EKE trends in the Southern Ocean and the principal physical mechanisms including local and/or remote atmospheric changes and meridional shifting of ACC fronts? Are trends in EKE and wind consistent with the theory of an 'eddy saturated' ACC, where changes in zonal wind stress do not alter the ACC transport; Instead, the

response is dominated by eddy effects (Meredith and Hogg, 2006).

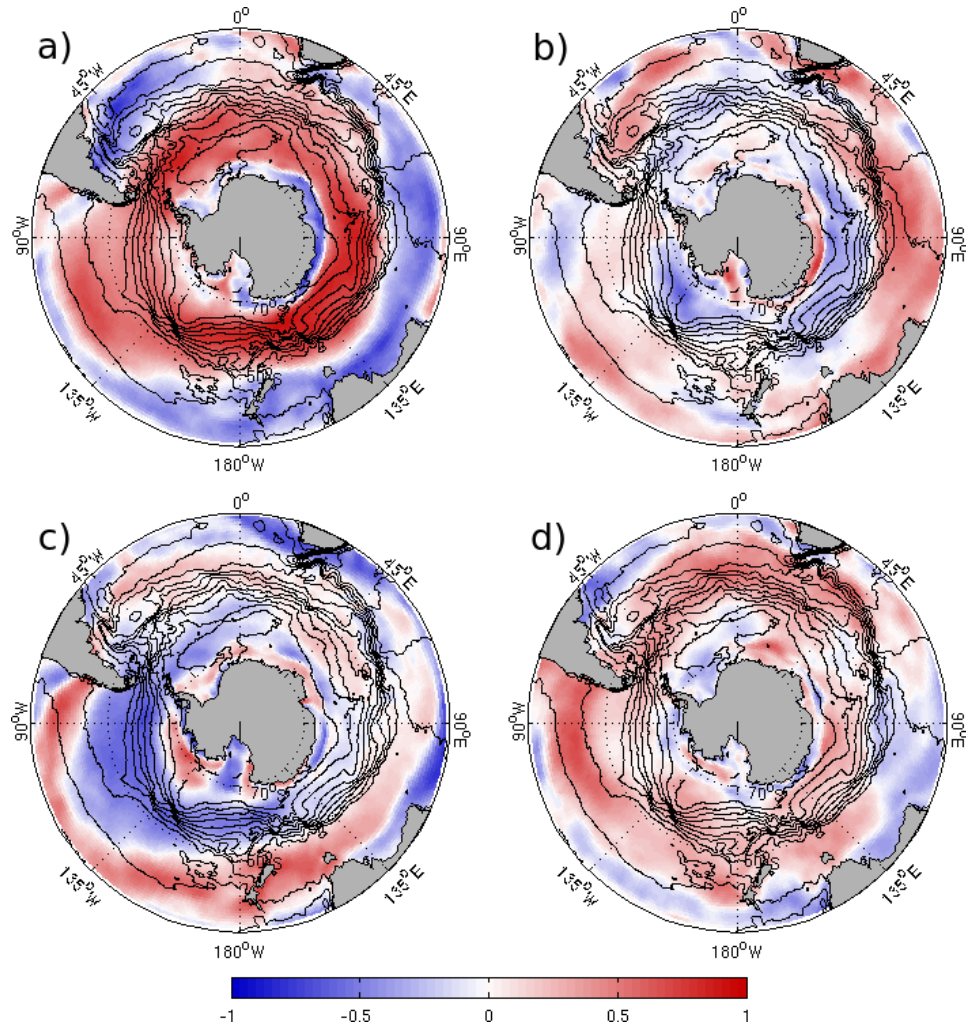


Figure 5.2: Correlation coefficients between annual mean wind speed and (a) SAM at zero lag, (b) SAM at 1 year lag, (c) ENSO at zero lag and (d) ENSO at 1 year lag. Wind speed is from ERA Interim re-analysis data. Black contours show mean dynamic topography from altimetry at 20 cm increments.

In this chapter, climate indices SAM and ENSO are used when exploring the relationship between EKE interannual variability and atmospheric variability. In order to show how well represented the wind speed in the Southern Ocean is by both SAM and ENSO indices, figure 5.2 illustrates the magnitude of the correlation between both SAM and ENSO with wind speed over the Southern Ocean. At zero lag (figure 5.2a), SAM is very strongly correlated with wind speed in a zonal band in the vicinity of the

ACC. This signal does not persist at 1 year lag (figure 5.2b). At zero lag (figure 5.2c), ENSO is very strongly anti-correlated with wind speed in the South Pacific sector of the ACC but not as spatially well defined in the other sectors as SAM.

The time-mean EKE in the Southern Ocean (figure 5.3) shows elevated EKE along the main path of the ACC. Elevated EKE is also observed in the oceans around southern Africa where the Agulhas Current retroflects and downstream of this retroflection. EKE also increases as the ACC flows through Drake Passage, after which the northern branch of the ACC, associated with the SAF, flows northward following the continental shelf of the Falkland Plateau, crossing the North Scotia Ridge.

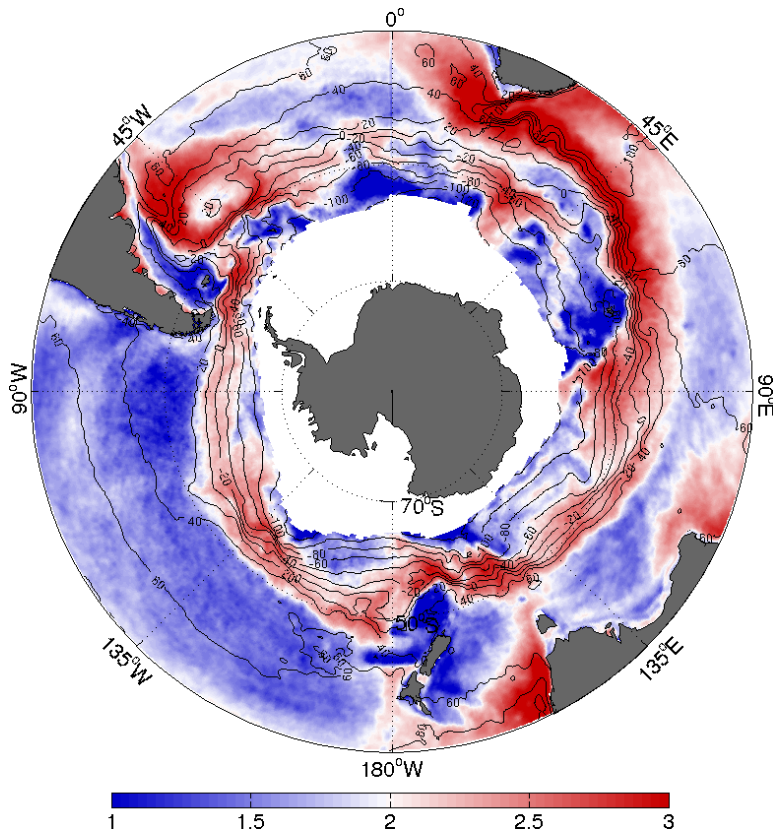


Figure 5.3: The Log_{10} of time mean EKE ($\text{cm}^2 \text{ s}^{-2}$) computed from altimetric sea surface height anomalies for the 18 year period 1993 to 2010, gridded on a $1/3^\circ$ spatial grid. Contour lines represent mean dynamic topography from altimetry at 20 cm increments. Regions where seasonal and/or permanent ice-cover is found have been removed.

This region is characterised by high levels of EKE. Evidence of enhanced EKE levels

where the ACC interacts with bathymetry are also apparent downstream of the Kerguelen Plateau and Campbell Plateau. In general terms the high EKE regions of the Southern Ocean are found either in western boundary currents (and their interaction with the ACC) in the lower latitudes, or fast, barotropic currents of the ACC flowing over shallow irregular bathymetry. The Southern Ocean is characterised by large areas of EKE one or more orders of magnitude lower than the most energetic regions. These low-EKE regions are typically in the lower latitudes north of the ACC away from the influence of western boundaries, the largest area being the abyssal plains of the South Pacific sector.

5.2 Results and Discussion

5.2.1 EKE Trends

The time series of EKE averaged over the Southern Ocean (figure 5.4) shows that the (area-weighted) mean EKE south of 30°S (excluding ice-covered regions) is $\sim 160 \text{ cm}^2 \text{ s}^{-2}$. The high frequency variability has a magnitude of $\sim 10\text{-}20 \text{ cm}^2 \text{ s}^{-2}$ which is $\sim 10\%$ of the mean. This includes an annual cycle which is observable in both the time series and frequency spectrum. The trend in the annual mean values indicates that EKE has increased on average by $\sim 8\%$ of the mean during the 18 year time period. The northern boundary of the Southern Ocean at 30°S was chosen to be consistent with previous studies (Meredith and Hogg, 2006; Morrow et al., 2010). Shifting this border 3° north and south results in a similar positive, statistically significant EKE trend.

A bootstrapping method (Efron, 1979) indicates that, unlike the basin-wide trends in the North Atlantic and North Pacific, this positive trend in the Southern Ocean is statistically significant. An r^2 value of 0.51 indicates a good fit of the trend line to the annual mean values. Anomalously low EKE in 1994 corresponds to the ERS1 ice-

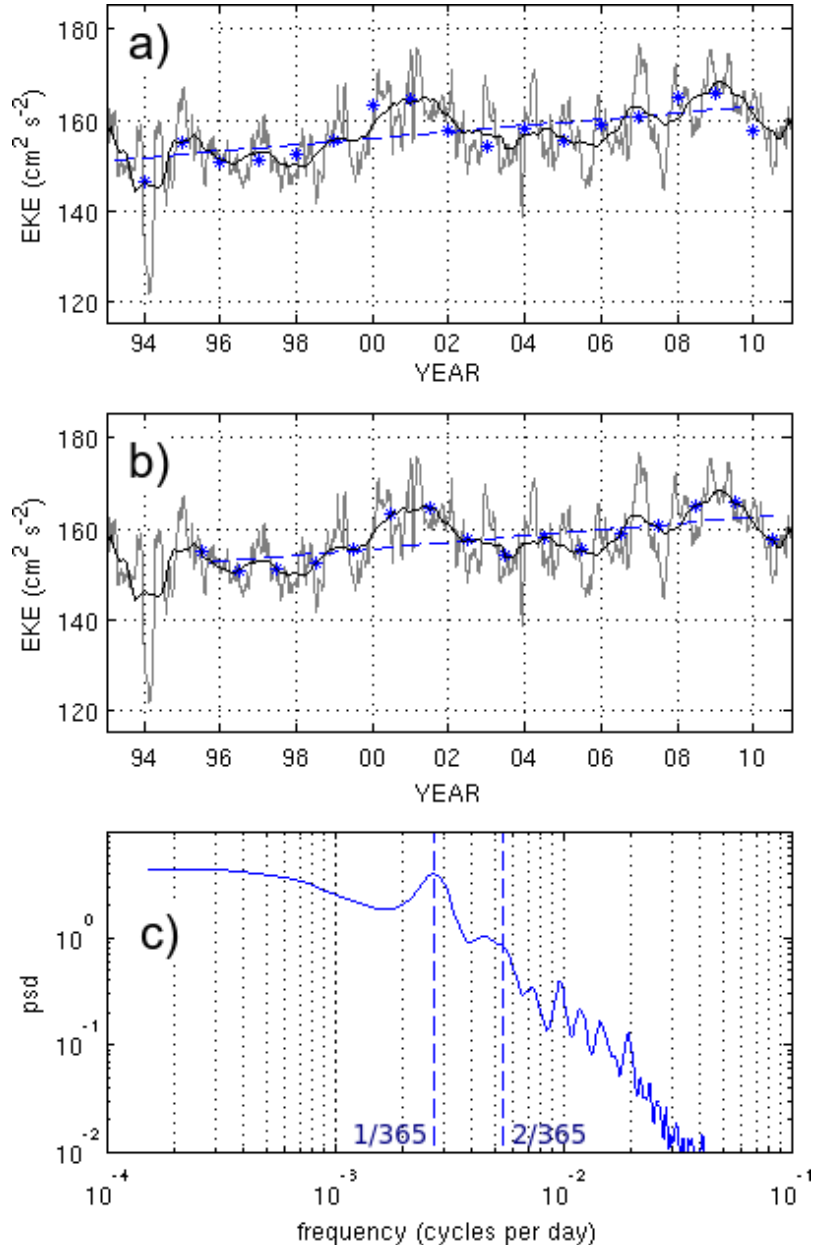


Figure 5.4: Time series of (a) area-weighted EKE in $\text{cm}^2 \text{ s}^{-2}$ (grey line) averaged over the (ice-free) Southern Ocean south of 30°S . Included are the 12 month running mean (black line), annual means (blue stars) and the linear trend in the annual mean (blue dashed line). (b) The same as (a) with the trend from 1995 - 2010. (c) frequency spectra for the time series in (a). Blue dashed lines indicate the first and second annual harmonic frequencies.

monitoring and geodetic mission during which there were no ERS data in the merged satellite product. Analysis of the TOPEX/Poseidon data alone shows that the magnitude of the trend is similar and the statistical significance is not affected. Panel (b)

further indicates that the trend and the statistical significance are not strongly influenced by the anomalous low in 1994. Two specific years that do not fit the trend line as well as other years are 2000 and 2001 when annual mean values were anomalously high. This corresponds to the anomalously high EKE years discussed by Meredith and Hogg (2006).

Maps of the annual mean EKE anomalies (figures 5.5) reveal how the spatial pattern of EKE changes from year to year from 1993 to 2010. The Agulhas retroflection stands out as the region where the magnitude of the EKE anomalies is largest in most years. In this region the magnitude of the anomalies can be as high as $500 \text{ cm}^2 \text{ s}^{-2}$, $\sim 20\%$ of the mean. The Agulhas region is also characterised by both positive and negative anomalies in every year with no distinguishable pattern from one year to another. There is no indication that the annual mean EKE anomalies in this region are any more negative in the earlier years or any more positive in the later years of the study period. Other regions do appear more negative in the earlier years and more positive in the later years. One such region is the Argentine basin. The two previously mentioned years where annual mean EKE was anomalously high (2000 and 2001) are characterised by anomalously high EKE most notably in the eastern boundary region of the southern Indian Ocean and not within the ACC.

The Southern Ocean is characterised by both positive and negative EKE trends (figure 5.6). Within the ACC most of the observed statistically significant trends are positive. There is a noticeable similarity between the location of the statistically significant positive EKE trends in the ACC and the locations where the ACC is influenced by the local bathymetry. For example, positive EKE trends are observed where the ACC passes the Kerguelen Plateau, downstream of the Campbell Plateau as well as in the Scotia Sea and Argentine Basin where the ACC flows north over the Scotia Ridge.

In both the Argentine Basin region and downstream of the Agulhas retroflection, there are regions of positive trends in the immediate vicinity of negative trends to the north, indicating that a southward shift in the main current path in these regions

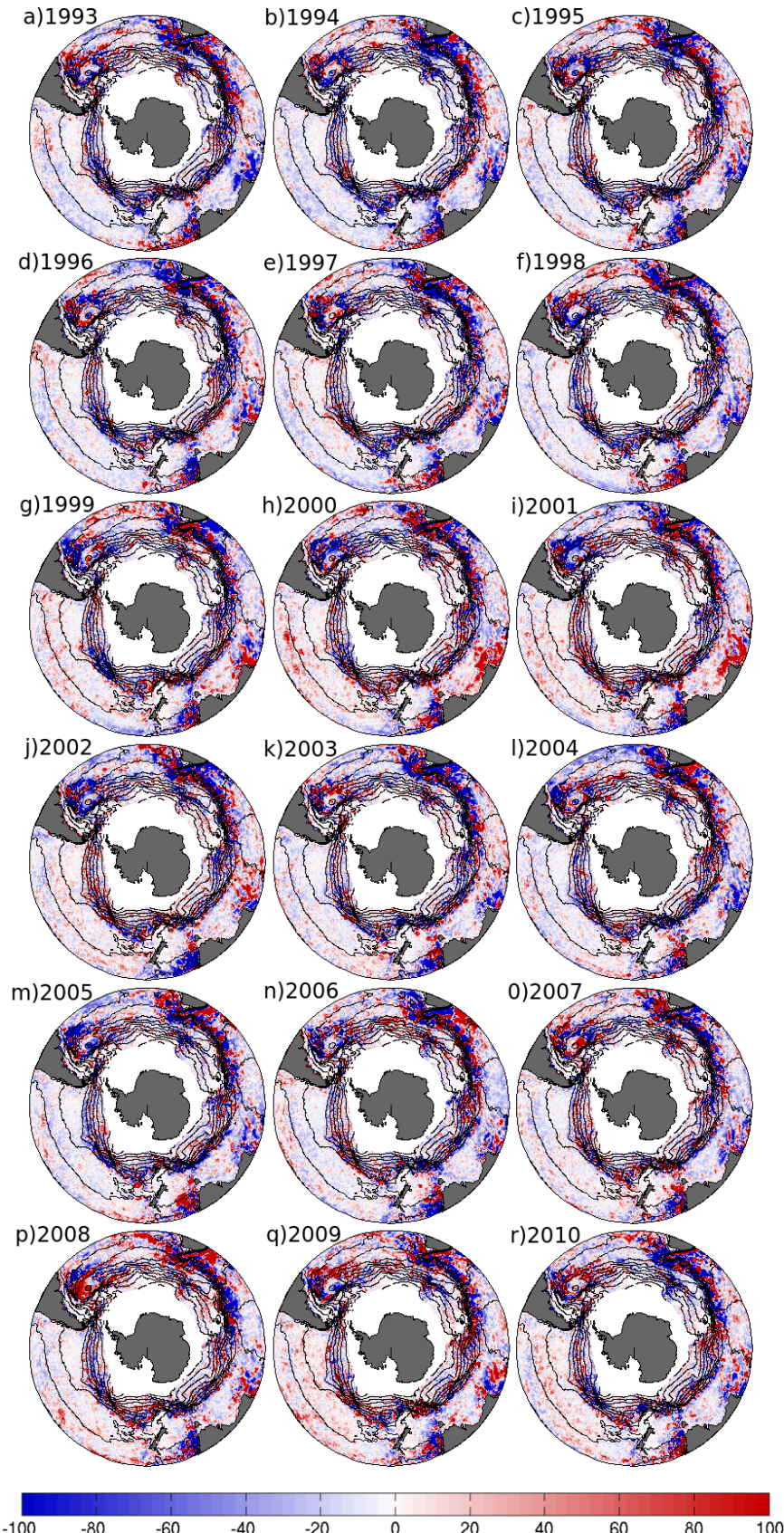


Figure 5.5: Annual EKE anomalies ($\text{cm}^2 \text{s}^{-2}$) for the region of the Southern Ocean south of 30°S . Contour lines represent mean dynamic topography from altimetry for the same time period.

may have occurred. To the north of the major paths of the ACC, where the southern branches of the Southern Hemisphere's subtropical gyres extend, larger basin-wide patterns of EKE trends can be observed. In the South Pacific, positive trends are dominant. In the southern Indian Ocean, trends are more predominantly negative. In the South Atlantic, a basin-wide pattern is much less apparent, but trends do appear slightly more negative in the west and more positive in the east. In order to identify the regions where the EKE trends are consistent in both the first and second half of the study period, figure 5.7 shows (a) the trend from 1993 to 2001, (b) the trend from 2002 to 2010 and (c) the trend from 1993 to 2010 with a mask (white areas) applied to the regions where the sign of the trend has changed in a and b.

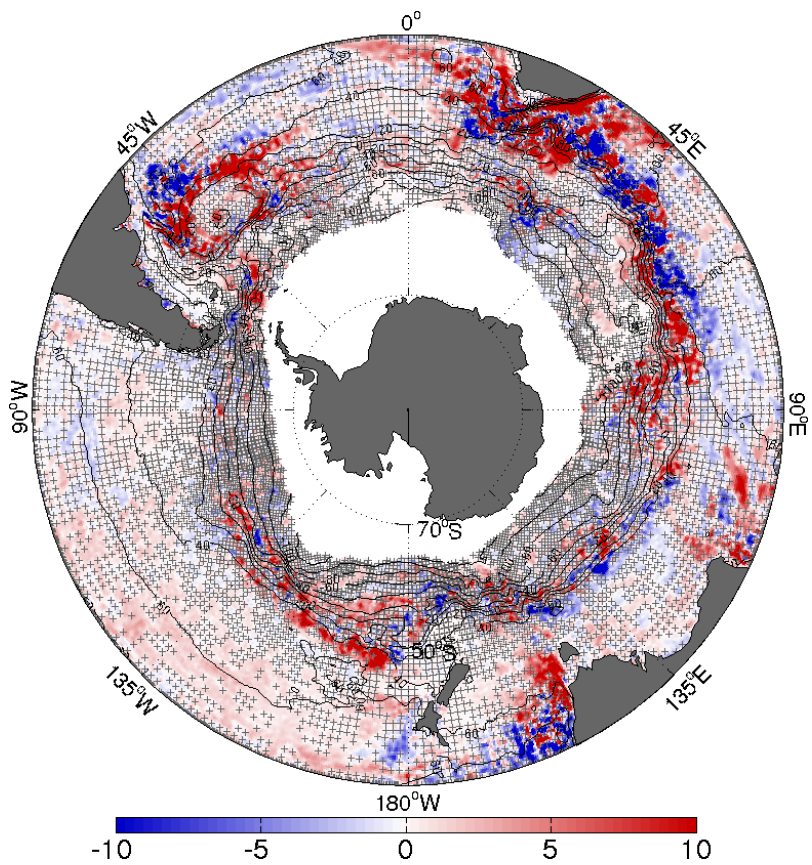


Figure 5.6: Linear trend in EKE ($\text{cm}^2 \text{ s}^{-2}$ per year) computed from altimetric sea surface height anomalies for the 18 year period 1993-2010. The hatched areas signify non-statistically significant trends at 90% confidence. Contour lines represent mean dynamic topography from altimetry at 20 cm increments.

Several notable features appear in figure 5.7c such as the consistency of the large-scale positive trend in the central South Pacific sector. The predominantly negative trends in the Indian Ocean sector, north of the ACC, also appear largely consistent in both halves of the time series. Another notable feature is the consistency in the positive trends along the main path of the ACC downstream of the Campbell Plateau, Kerguelen and in the Scotia Sea. The Agulhas region is characterised by areas where the trends appear consistent, interspersed with other areas where they are not con-

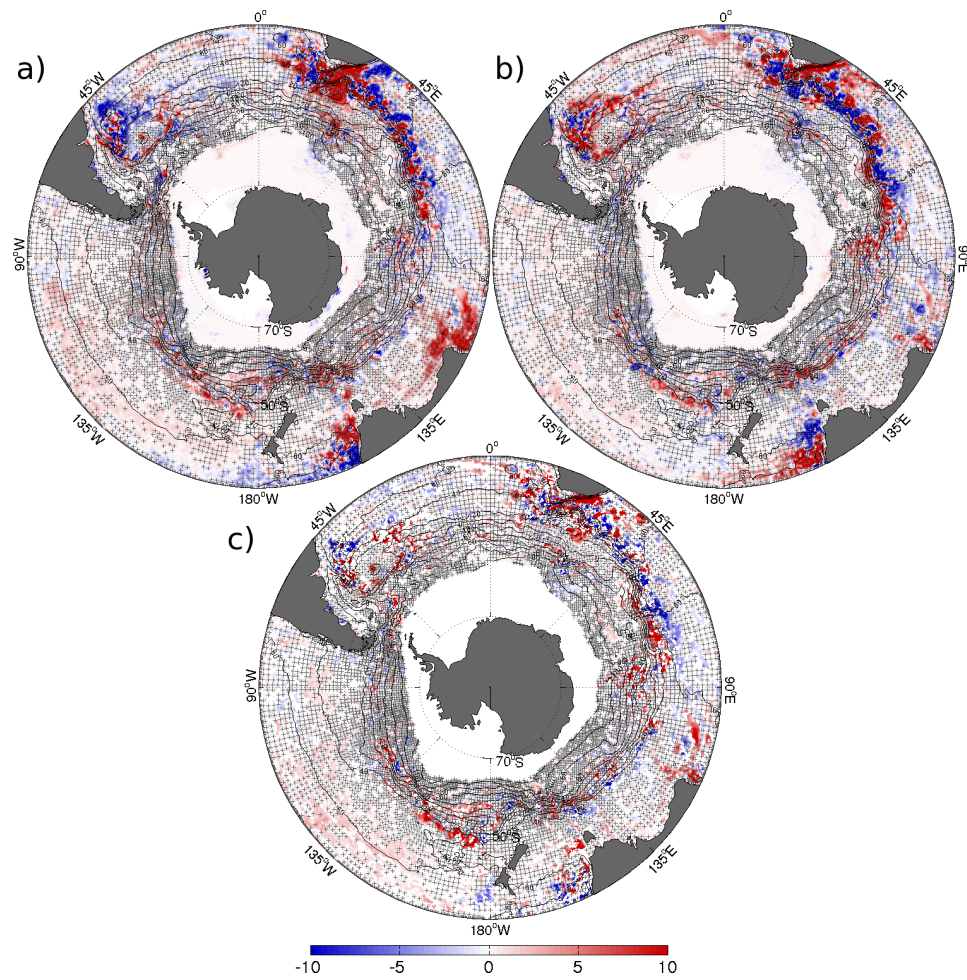


Figure 5.7: Linear trend in EKE ($\text{cm}^2 \text{ s}^{-2}$ per year) from (a) 1993 to 2001 and (b) 2002 to 2010. (c) Linear trend in EKE ($\text{cm}^2 \text{ s}^{-2}$ per year) from 1993 - 2010 with masked (white areas) regions where the sign of the trends in (a) and (b) are different. The hatched areas signify non-statistically significant trends at 90% confidence. Contour lines represent mean dynamic topography from altimetry 20 cm increments.

sistent and have no discernible pattern. In general, the regions associated with the southern hemisphere western boundary currents (Agulhas Current, Brasil Current and East Australian Current) are the regions where the lack of consistency between the trends in the two halves of the time series is most noticeable.

A comparison of the trends in EKE computed from the zonal eddy velocity (uEKE) and the meridional eddy velocity (vEKE) show that there are similarities as well as some differences between the uEKE trend and the vEKE trend (figure 5.8). Once

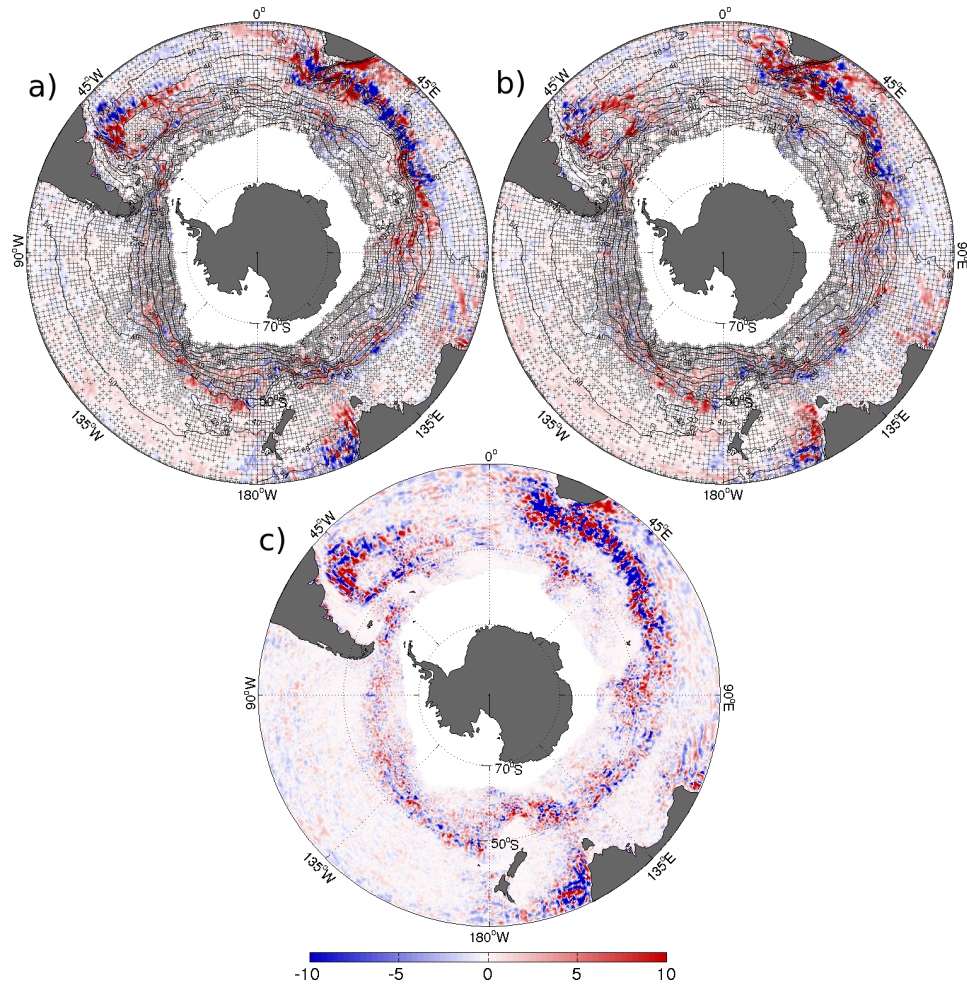


Figure 5.8: EKE trend ($\text{cm}^2 \text{ s}^{-2}$ per year) (a) computed from the zonal eddy velocity for the 18 year period 1993-2010, (b) from the meridional eddy velocity and (c) panel a minus panel b. The hatched areas in a and b signify non-statistically significant trends at 90% confidence. Contour lines represent mean dynamic topography from altimetry in 20 cm increments.

again, the basin-wide patterns of positive and negative trends to the north of the ACC in the South Pacific and Indian Ocean sectors of the Southern Ocean are distinguishable in both the uEKE and vEKE trendmaps. This indicates that the trends in these regions have resulted from an increase in eddy motions which are isotropic as opposed to an increase in either the zonal or meridional velocity components due to, for example, a shift and/or increase in the position or intensity of current paths.

Time series of annual mean EKE and trends for some of the regions of interest are shown in figure 5.9 where the upper panel shows the location where each time series is averaged over. Panel a shows the time series in the location downstream of the Campbell Plateau where the trend line has a 'goodness of fit' value ($r^2=0.70$) considerably higher than any other region. r^2 values are 0.38 and 0.37 for regions b and i respectively. Considerably lower values are found in regions k and f ($r^2=0.12$), region l ($r^2=0.15$) and region e ($r^2=0.17$). Other panels, such as e and d, visually appear as a good fit with the exception of one outlier. In regions where positive and negative trends are in close proximity to the north and south, a possible meridional shift in the position of the ACC is a plausible mechanism for such trend patterns. If this is so, we would expect to see an anti-correlation between the two time series. One such area is the regions in boxes g and h. Here the correlation coefficients for the two time series at zero lag is -0.60, indicating the time series are strongly anti-correlated. Time series for the regions d and e have a correlation of -0.23 indicating a weaker but still negative correlation.

5.2.2 Atmospheric Trends

The climatological mean wind speed in the Southern Ocean (figure 5.10a) is dominated by a near-zonal band of westerlies centred approximately between 50°S and 60°S. Unlike EKE trends, trends in wind speed (figure 5.10b) are more basin-wide, with large regions ($>10^6 \text{ km}^2$) being statistically significant. The central and eastern South Pacific sector is dominated by positive trends. Negative trends appear in the

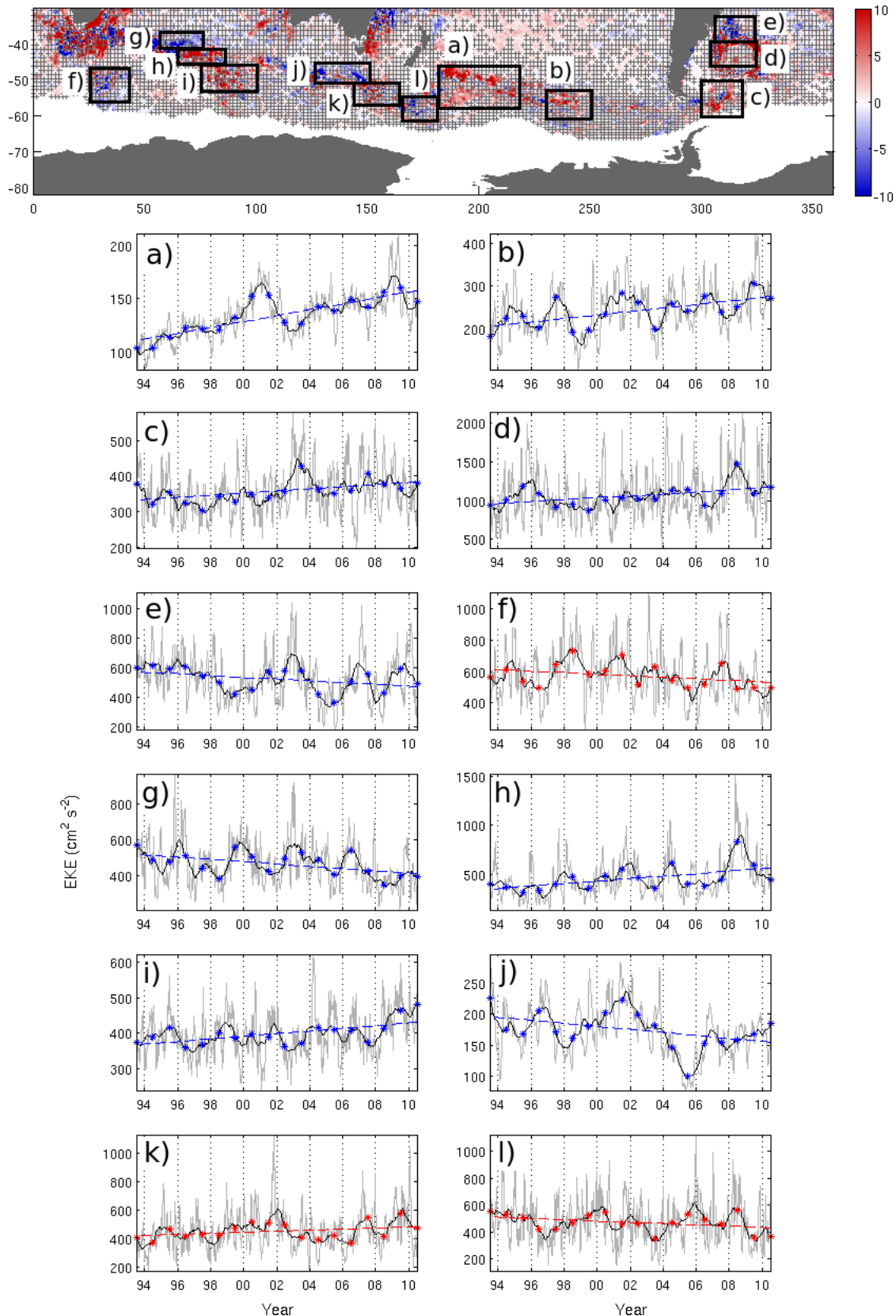


Figure 5.9: (b-m) Time series of EKE (grey lines) in $\text{cm}^2 \text{s}^{-2}$, 12 month running mean (black lines), annual means (blue stars) and trend in annual mean (blue dashed lines) where the trend is statistically significant at 90% confidence for the regions shown in the upper panel. The red stars and red trend lines indicate where the trend is not statistically significant.

western South Pacific and South Atlantic regions. In the Indian Ocean sector, trends are mostly positive in the ACC and negative to the north of the ACC. It is notable that, despite the circumpolar nature of the wind speed climatology, the wind speed trends vary considerably in different sectors.

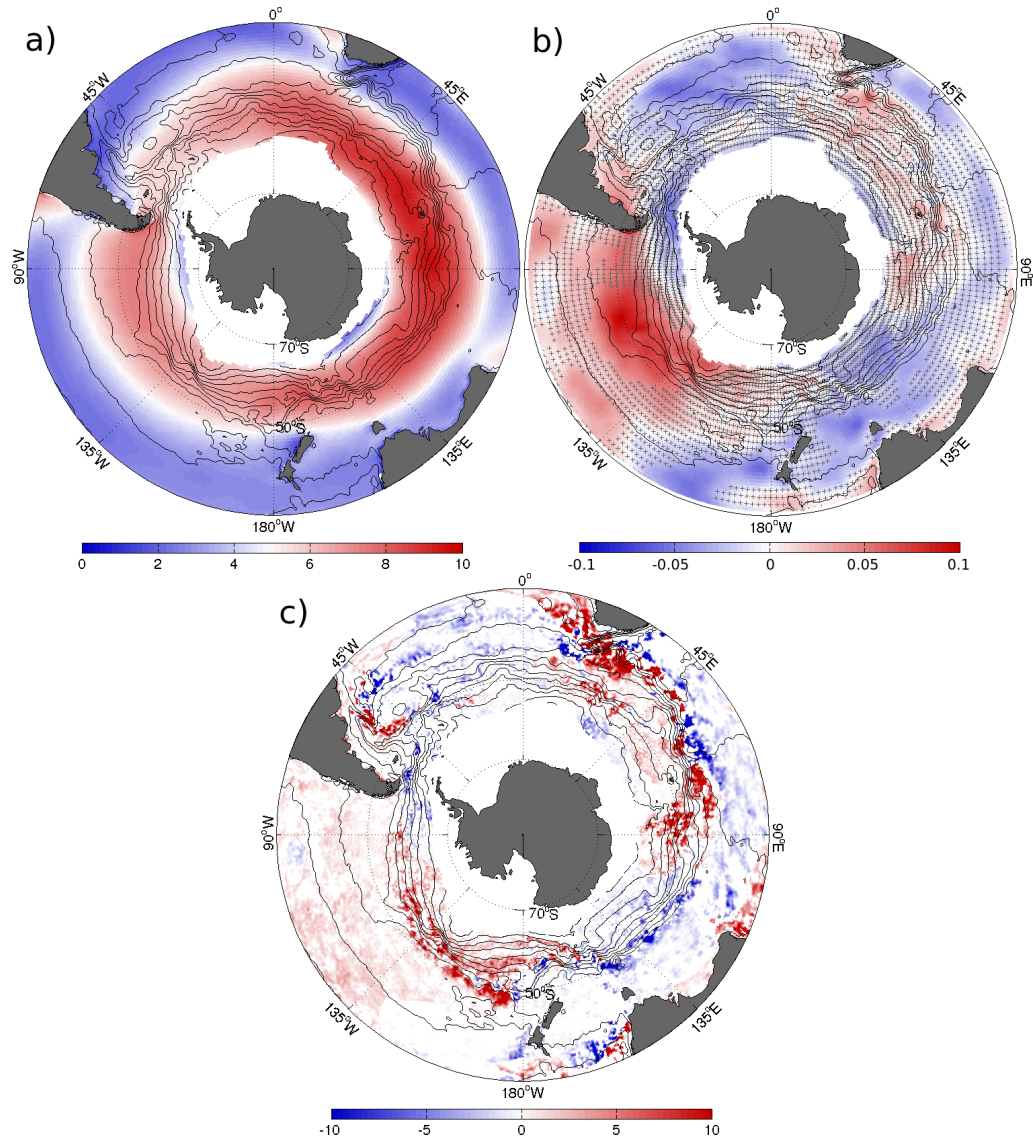


Figure 5.10: (a) Wind speed temporal mean ($1993 - 2010$) in $m s^{-1}$ from ECMWF ERA-Interim re-analysis data. (b) Linear trend in wind speed ($x10^{-1} m s^{-1}$ per year) from 1993 to 2010. The transparent areas signify non-statistically significant trends. (c) Trend in EKE ($cm^2 s^{-2}$ per year) from 1993 to 2010 showing only the regions where the trend in wind speed is the same sign. Black contours show mean dynamic topography at 20 cm increments.

A distinct similarity between the sign of the EKE trends and wind speed trends is apparent in large areas of the Southern Ocean north of the ACC. This similarity strongly implies a change in local wind forcing (mechanism M1) as a cause of the EKE trends in the South Atlantic, Indian and South Pacific sectors north of the ACC. This change in EKE, due to a direct wind forcing in these regions, may result from an increase (decrease) in wind at the ocean's surface causing an increase (decrease) in the local Ekman transport. This may result in one or more outcomes including changes in surface heat fluxes (affecting the strength of the stratification) and Ekman pumping (upwelling or downwelling) which can both effect changes in the depth and/or slope of density surfaces.

Along the main path of the ACC, many of the regions where positive EKE trends are observed correspond to regions of positive trends in wind speed including downstream of Kerguelen Plateau and downstream of Campbell Plateau. These results are consistent with the hypothesis that EKE trends in the ACC are, in some regions, caused by changes in local wind forcing (mechanism M1). This result supports the 'eddy saturation' theory where an increase in wind results in an increase in isopycnal slope. This, in turn, will lead to an increase in available potential energy, increased baroclinicity and hence an increase in eddy generation due to baroclinic instability.

The wind stress curl climatology in the Southern Ocean (figure 5.11a) is characterised by two very distinctive regions of positive curl to the north and negative curl to the south. The zero wind stress curl boundary between these two regions is generally located close to 50°S but, is zonally asymmetric, appearing further south in the western Pacific sector and further north in the Atlantic sector. In both the Atlantic and Indian sectors, wind stress curl trends (figure 5.11b) do not show the same basin-wide patterns observed in wind speed trends but instead, show variability on much smaller spatial scales. The exception to this is the South Pacific sector north of the ACC where positive statistically significant trends in wind stress curl cover a large part of this region. A comparison of the trends in wind stress curl and trends in EKE (figure 5.11c)

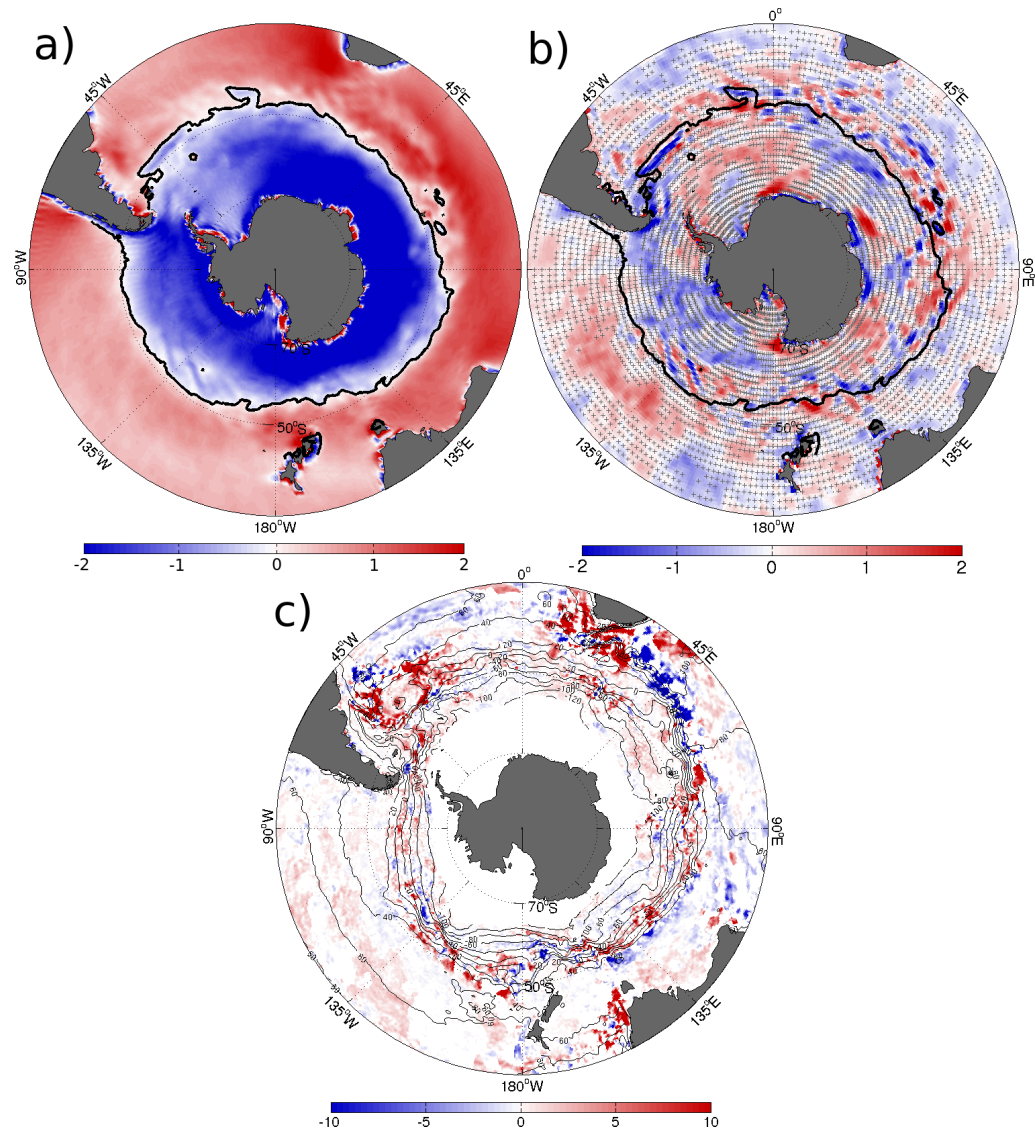


Figure 5.11: (a) Wind stress curl temporal mean ($x10^{-7} \text{ N m}^{-3}$ from 1993 to 2010 from ECMWF ERA-Interim re-analysis data. (b) Trend in wind stress curl ($x10^{-8} \text{ N m}^{-3}$ per year). Transparent areas signify non-statistically significant trends. Black contour shows zero wind stress curl line. (c) Trend in EKE ($\text{cm}^2 \text{ s}^{-2}$ per year) from 1993 to 2010 showing only the regions where the trend in wind stress curl is the same sign. Black contours show mean dynamic topography at 20 cm increments.

indicates that the influence of changing wind stress curl intensity (mechanism M4) is observable in the low-latitudes in the regions of the Southern Hemisphere gyre circulation but is largely absent within the ACC. There is also little evidence to suggest that shifting wind stress curl fields (mechanism M3) has had any significant influence on

EKE trends in the Southern Ocean. In summary, these results show that the local wind (M1) is more dominant than both wind stress curl intensity (M4) and shifting wind stress curl fields (M3) in the Southern Ocean.

5.2.3 EKE and Atmospheric Variability

As found by previous authors (Meredith and Hogg, 2006; Screen et al., 2009; Morrow et al., 2010), the correlations of EKE in the Southern Ocean with SAM at different time lags (figure 5.12) indicate that EKE variability on annual and longer time scales is correlated with this climate mode during the time period from 1993 to 2010. The correlations at a lag of 3 years show the strongest positive signal but, as found by Morrow et al. (2010), the response is highly variable from one region to another with the South Pacific sector showing the strongest positive response. Many regions of the Southern Ocean show a negative instantaneous EKE response to a positive ENSO event (figure 5.12e), most notably the South Pacific sector. At one year lag (figure 5.12f), the negative response is more prominent in the South Pacific sector and eastern Indian sector but largely absent in the South Atlantic sector.

This response is consistent with the mechanisms described by Yuan (2004); during positive ENSO phase, the South Pacific sector of the Southern Ocean experiences negative sea-surface temperature (SST) anomalies accompanied by high pressure, reduced wind stress and fewer storms due to the strengthening of atmospheric (Hadley and Ferrel) cells and subsequent northward shifting of the polar jet. This has a direct impact on the EKE in the South Pacific sector which is characterised by negative EKE anomalies during El Niño years. In the South Atlantic sector, the atmospheric response observed in the Pacific is reversed during El Niño. Atmospheric cells relax causing a poleward shift in the jet stream resulting in increased winds. The EKE response in the Indian sector to ENSO is not as apparent as the Pacific. This strong response to ENSO events in the South Pacific and weaker response in the Indian was observed by Morrow et al. (2010) who concluded that the EKE response in the South-

ern Ocean was due to the combination of both ENSO and SAM events and their phase interactions.

The relationship between EKE variability and both ENSO and SAM is further illustrated by comparing composites of annual mean EKE 3 years after the strongest positive SAM years minus the annual mean EKE 3 years after the strongest negative SAM years (figure 5.12i) and the strongest positive ENSO years minus the strongest negative ENSO years (figure 5.12j). The contrast between positive and negative SAM years is evident along the majority of the ACC where positive (negative) anomalies are prominent following positive (negative) SAM years. The strong influence of SAM on EKE is also evident in the South Pacific Sector north of the ACC. The composite maps of positive (negative) ENSO years show striking similarity to the negative (positive) SAM years. As we have already shown, both SAM and ENSO are a good representation of the zonal wind in the vicinity of the ACC. This relationship between EKE variability along the ACC and these climate modes adds more weight to the eddy saturation theory that predicts an increase in EKE within the ACC in response to an increase in zonal winds (Mechanism M1).

Our results strongly implicate local wind speed as the dominant mechanism for EKE trends within the Southern Ocean. A statistically significant positive trend in the basin-wide mean EKE is matched by a similar basin-wide positive statistically significant trend in wind speed (shown in chapter 6). Despite this similarity in basin-wide trends, only 56.2% of the area-weighted Southern Ocean is characterised by a similarity in trends. This indicates that changes in wind cannot be the only mechanism responsible for the EKE trend. It is therefore necessary to explore the potential influence of other mechanisms in this region. Intrinsic variability (mechanism M6) within the ACC may well be significant where wind speed and EKE trends do not show similarity.

Trends in zonal mean EKE for the different sectors of the Southern Ocean (figure 5.13) reveal further insight into the EKE trend patterns. In the circumpolar view,

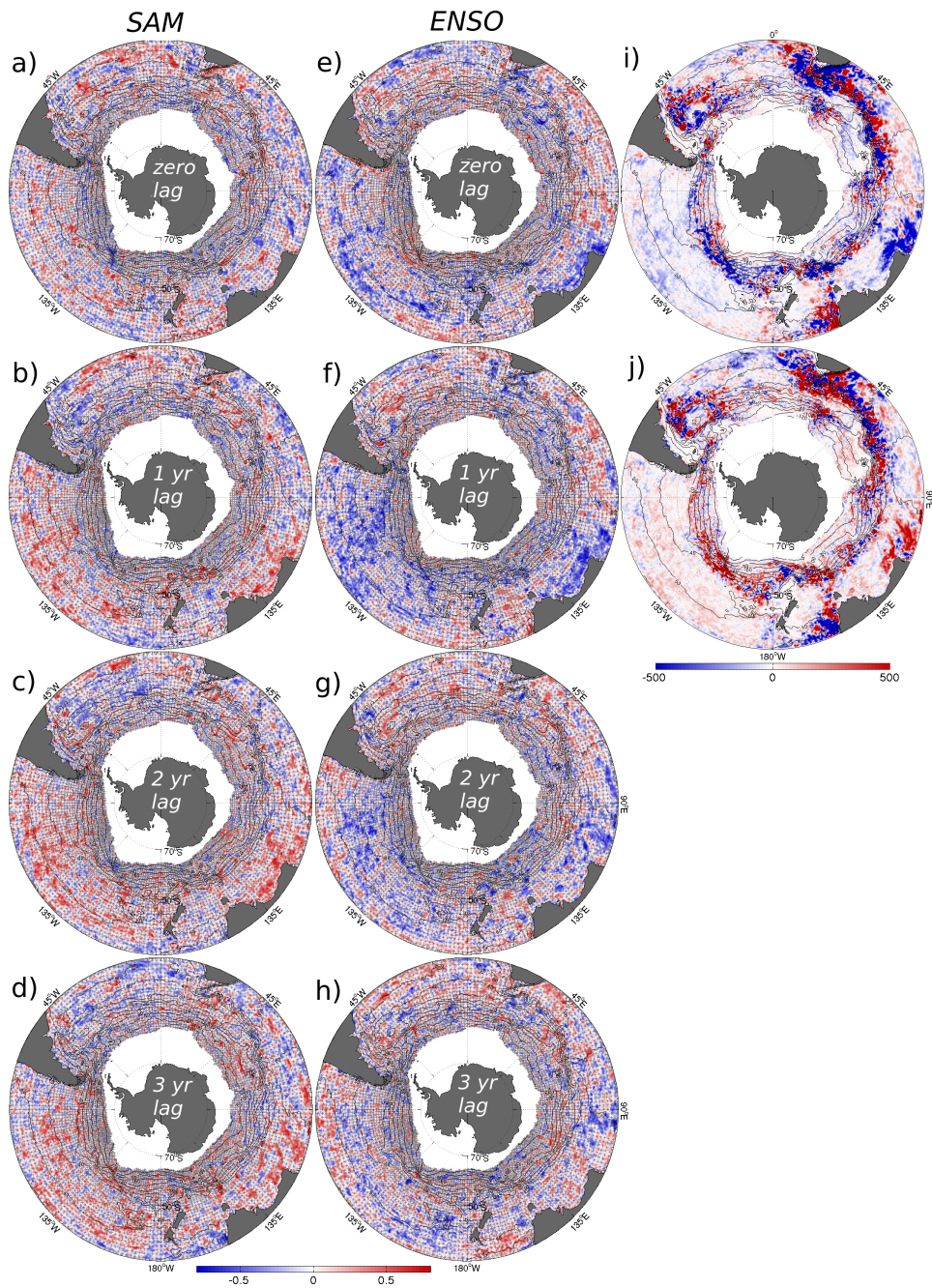


Figure 5.12: Correlation coefficients of annual mean EKE with SAM at a) zero lag, b) 1 yr lag, c) 2 yr lag, d) 3 yr lag and EKE with ENSO at e) zero lag, f) 1 yr lag, g) 2 yr lag and h) 3 yr lag. The hatched areas represent non-statistically significant correlations at 90% confidence. i) Composite of annual mean EKE anomalies for (a) the years following the strongest positive ENSO years (1992, 1994, 1997, 2002 and 2004) minus the strongest negative ENSO years (1996, 1999, 2000, 2007 and 2008) and j) composite of annual mean EKE anomalies for the years 3 years after the strongest positive SAM years (1993, 1998, 1999, 2001 and 2006) minus the years 3 years after the strongest negative SAM years (1990, 1991, 1992, 1996 and 2002). Black contours show mean dynamic topography at 20 cm increments.

trends are positive at all latitudes north of 60° S. These positive trends are largest between 40° S and 45° S, and originate in the Atlantic and Indian sectors. As previously stated, we hypothesise that a southward shift in the northern branch of the ACC in the Indian sector is the cause of the observed positive and negative trends downstream of the Agulhas region. Trends in the zonal mean EKE are consistent with this hypothesis as the very dramatic shift to negative trends at 40° S suggests. There is no other plausible mechanism for such a dramatic change in the sign of the trend in such a narrow band of latitude than a meridional shift in the axis of a high eddy energy jet or front. This hypothesis would require a corresponding sharp increase in EKE in the immediate vicinity. This large positive EKE trend is clearly visible to the south. We can therefore say with some certainty that the EKE trends in some regions within the ACC, specifically within the Indian Ocean sector, have resulted from a poleward shift in the mean currents.

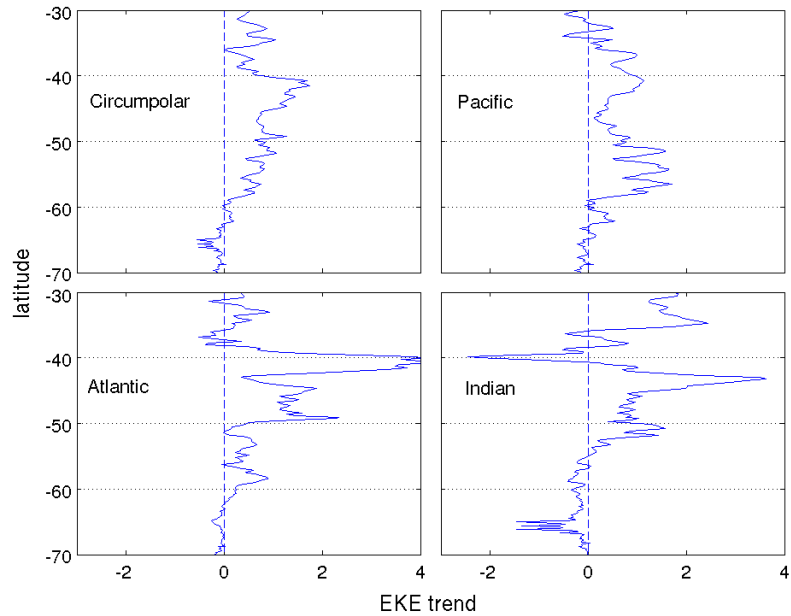


Figure 5.13: Zonal mean EKE trends ($\text{cm}^2 \text{ s}^{-2}$ per year) between 70° S and 30° S for the circumpolar, Pacific (130° E to 80° W), Atlantic (80° W to 20° E) and Indian (20° E to 120° E) sectors.

We now seek to identify a causal link between EKE variability (and subsequent

trends) and variability in the mean ACC flow. In order to identify if EKE variability and/or trends in the Southern Ocean is related to variability and trends in current velocity within the ACC, we require circumpolar mean values in current velocity and EKE. Averaging at different latitudes presents several problems as the ACC is non-zonal in many regions and is subject to meridional shifting of its main fronts (Sallée et al., 2008). In order to account for these factors, we choose to average along dynamic height contours. Trends in current speed and EKE (figure 5.14) show a striking similarity indicating the magnitude of the EKE trend along a given dh contour is very closely related to the magnitude of the trend in current velocity. There are, however, other indications that such a relationship is not always true. For instance, along the -40 cm contour, the current speed trend is negative showing speed has decreased. The EKE along this contour has increased as indicated by a positive trend.

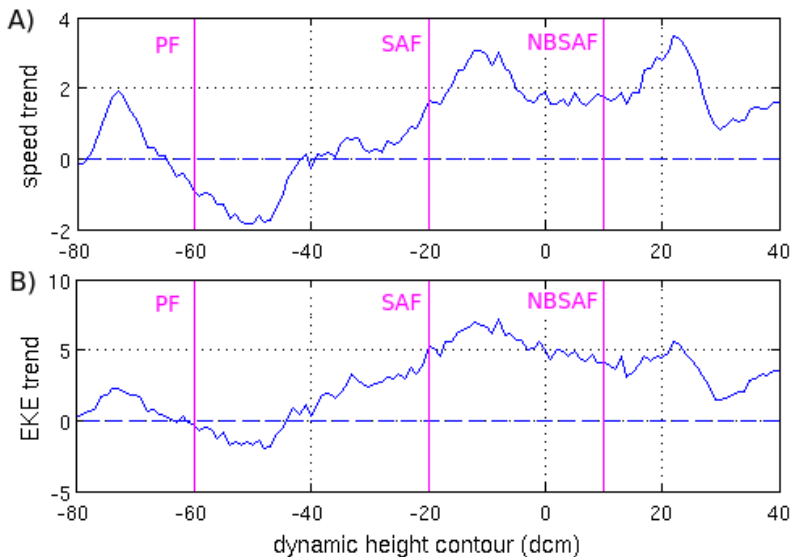


Figure 5.14: A) Trend in circumpolar mean current speed ($x10^{-4} \text{ m}^2 \text{ s}^{-2}$ per day) from altimetry, averaged along each dynamic height contour at 1 dcm intervals. B) Same as A for EKE ($x10^{-3} \text{ cm}^2 \text{ s}^{-2}$ per day). In both panels the magenta lines show the dynamic height representing the Polar Front, Sub-Antarctic Front and northern branch of the Sub-Antarctic Front. Fronts are from Sallée et al. (2008).

5.2.4 The DIMES Experiment Region

The Diapycnal and Isopycnal Mixing Experiment in the Southern Ocean (DIMES) seeks to understand the regional importance of the Southern Ocean to global circulation by measuring large-scale and small-scale mixing processes (Gille et al., 2007). In the ocean, water moves primarily along isopycnals, but it can also mix and change density between these surfaces in what is known as diapycnal mixing. This experiment, a joint effort between U.S. and U.K. scientists, began fieldwork in early 2009 by releasing a tracer in the region west of Drake passage. Subsequent fieldwork involved measuring the tracer concentrations both west of Drake Passage and in the Scotia Sea to establish the extent of mixing both horizontally and vertically. In this section, we will consider the EKE in the DIMES region to establish if the EKE during the time of the DIMES fieldwork was anomalous. This will provide the DIMES community with the opportunity to evaluate whether the mixing rates observed during the DIMES period are typical. Figure 5.15a shows that the tracer was released in a region where the time-mean EKE is relatively low in comparison to, for example, the Scotia Sea region where the time-mean EKE is typically an order of magnitude higher. As the tracer moves to the east in the ACC, both advective and diffusive processes mix and stir the tracer in both the horizontal and vertical. The horizontal mixing occurs primarily due to the meandering of the ACC currents and eddies.

The EKE trend from 1993 to 2010 (figure 5.15b) and the EKE annual anomalies for 2009 and 2010 figure 5.15c and d respectively, show that the change in EKE from 1993 to 2010 varies regionally as do the annual anomalies. For our analysis we have defined three regions shown in figure 5.15d. In 2010, EKE is anomalously low in region f and anomalously high in region g. This is significant as tracer sampling occurred in both regions during 2010. The time series of EKE from 1993 to 2010 (figure 5.15 e,f and g) show that there is no significant trend in region e and EKE during the DIMES period is typical of the previous years. In region f, there is a

negative trend in EKE but the trend is not statistically significant. The anomalously low annual mean EKE in 2010 is unprecedented in the altimetry record. In region g, the trend is both positive and statistically significant but the anomalously high EKE in 2010 is not unprecedented.

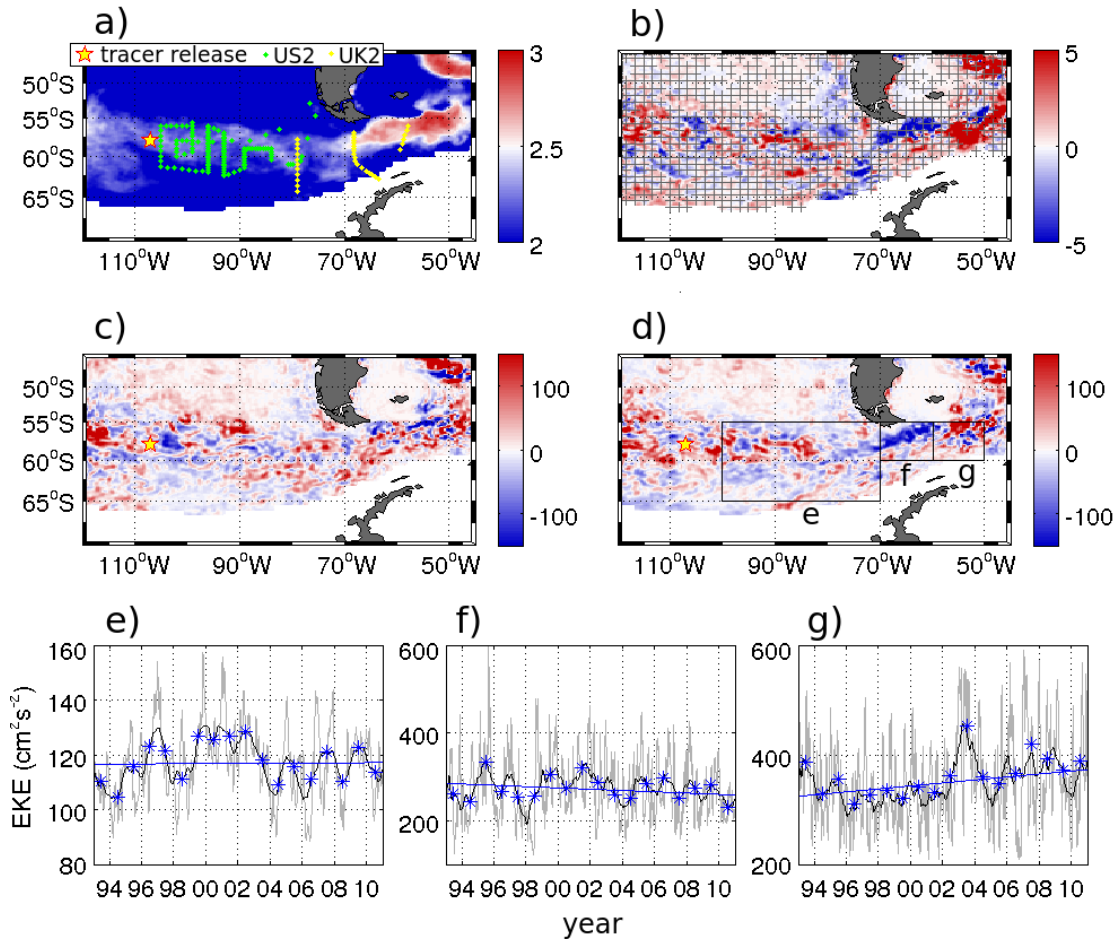


Figure 5.15: A) The DIMES region showing a) \log_{10} mean EKE ($\text{cm}^2 \text{s}^{-2}$). Included are the locations of the tracer release and the sampling stations for the US2 and UK2 cruises. B) EKE trends from 1993 - 2010 ($\text{cm}^2 \text{s}^{-2}$ per year). The hatched areas represent non-statistically significant trends at 90% confidence. c) Annual EKE anomalies ($\text{cm}^2 \text{s}^{-2}$) for 2009 and (d) 2010. Time series of weekly EKE (grey lines) including the 12 month running mean (black lines), annual means (blue stars) and trend in the annual mean (blue lines) averaged over the boxed regions shown in panel d. In panels a-d areas of seasonal and permanent ice-covered have been removed.

In summary, the mixing rates, determined by tracer sampling in 2010 during the

UK2 cruise, are likely to be typical of the last 18 years in the region west of Drake Passage. In Drake Passage, observed mixing rates in 2010 may be lower than average in region f where EKE was anomalously low and the trend is negative and higher than average in region g where EKE was anomalously high and the trend is positive and statistically significant.

5.3 Summary

In this chapter we have shown that a positive statistically significant trend exists in the basin-wide EKE in the Southern Ocean. The dominant mechanism in this region is local wind speed (M1) although it is difficult to distinguish between this mechanism and non-local winds (M2) due to the primarily zonally symmetric nature of the mean wind fields. For example, an increase in wind in a region of the ACC may result in an increase in EKE further downstream where the wind has also increased but is not influencing the EKE locally. The similarity between EKE trends and wind speed trends, as well as the correlations between EKE and SAM, indicate that the influence of this mechanism is strongest in the South Pacific sector of the Southern Ocean. Our results indicate that the primary mechanisms responsible for the EKE trends are consistent with the mechanisms of EKE variability proposed by Meredith and Hogg (2006), Hogg et al. (2008), Morrow et al. (2010) and are in agreement with the eddy saturation theory from the same studies.

Time series of EKE and a comparison of trends in the zonal and basin-wide mean EKE indicate that the meridional shifting of the ACC, in response to atmospheric variability, is primarily responsible for the observed trends in part of the western Indian Ocean sector of the ACC. This is consistent with the results of Sallée et al. (2008) but our results show no evidence to implicate shifting fronts as a mechanism in the other sectors of the ACC. In the Southern Ocean, changes in wind speed (mechanism M1) appear to have a stronger influence on EKE than changes in wind stress curl.

Chapter 6

Summary and Global Perspective

6.1 Introduction

In this thesis the results chapters have focussed regionally on the North Atlantic, the North Pacific and the Southern Ocean. In this chapter we will summarise the results of this thesis by presenting a synthesis of the key results from chapters 3, 4 and 5 in a global context. The data set for this chapter has been extended to include the years 2011 and 2012. This longer time series provides us with the opportunity to obtain more statistically robust trends and correlations.

In this chapter we will address the following questions:

- 1) Do statistically significant trends exist in the near-global mean and/or hemispheric mean EKE?
- 2) Can any global generalisations be deduced regarding the mechanisms responsible for the observed trends?
- 3) Do the EKE trends in the 20 year time series corroborate or contradict the results of previous studies of shorter time periods (Stammer and Wunsch, 1999; Stammer et al., 2006)?

Finally we will discuss the limitations of this study and how this work can be progressed in the future.

6.2 Results and Discussion

6.2.1 Global EKE trends

The time series of EKE (figure 6.1a) shows that near-global EKE has increased by 0.3% of the mean from 1993 to 2012 but there is no statistically significant trend in the near-global EKE. In the northern hemisphere, EKE has decreased by 5.1% of the mean from 1993 to 2012 but the negative trend is not statistically significant. In the southern hemisphere, EKE has increased by 3.5% of the mean from 1993 to 2012 and this trend is statistically significant.

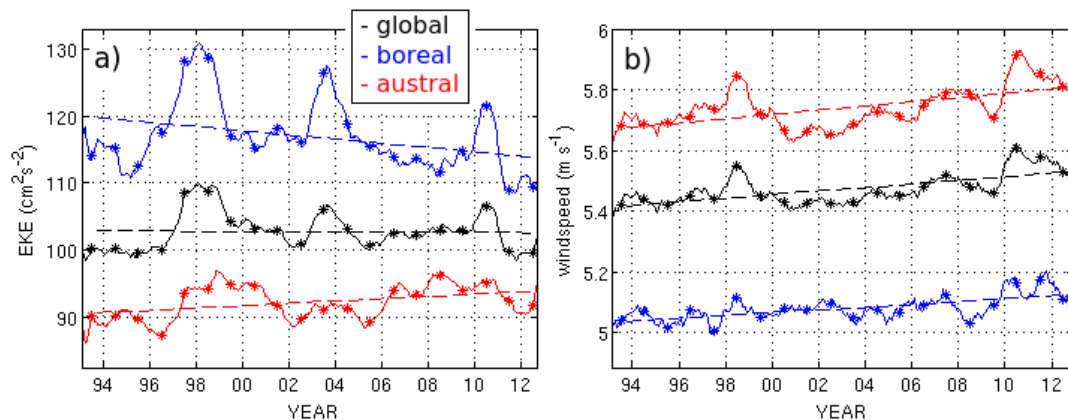


Figure 6.1: (a) Time series of near-global (black solid line), northern hemisphere (blue solid line) and southern hemisphere (red solid line) de-seasoned EKE ($\text{cm}^2 \text{ s}^{-2}$). Included are the annual means (stars) and the linear trend in the annual mean (dashed lines). (b) The same as panel a) but for wind speed for the same geographical locations.

The corresponding trends in wind speed for the same regions (figure 6.1b) are both positive and statistically significant for the near-global and hemispheric means. The correlation coefficients of near-global and hemispheric mean EKE with mean wind speed for the same region indicate that EKE-wind correlations are low on a global scale ($r=0.21$) and in the northern hemisphere ($r=-0.19$). In the southern hemisphere the correlation is larger ($r=0.49$), therefore, the global mean wind speed is not strongly correlated with global mean EKE but the relationship is stronger in the southern hemi-

sphere than in the northern hemisphere.

There are three very distinct peaks in the northern hemisphere mean EKE corresponding to the years 1997/1998, 2003 and 2010. These peaks do not correspond in time to similar peaks in the southern hemisphere mean EKE, but are large enough to influence the near-global mean EKE which is characterised by peaks corresponding to the same three time periods. The peaks in both 1998 and 2010 correspond to periods of anomalously high wind speed (figure 6.1b) but the peak in 2003 does not.

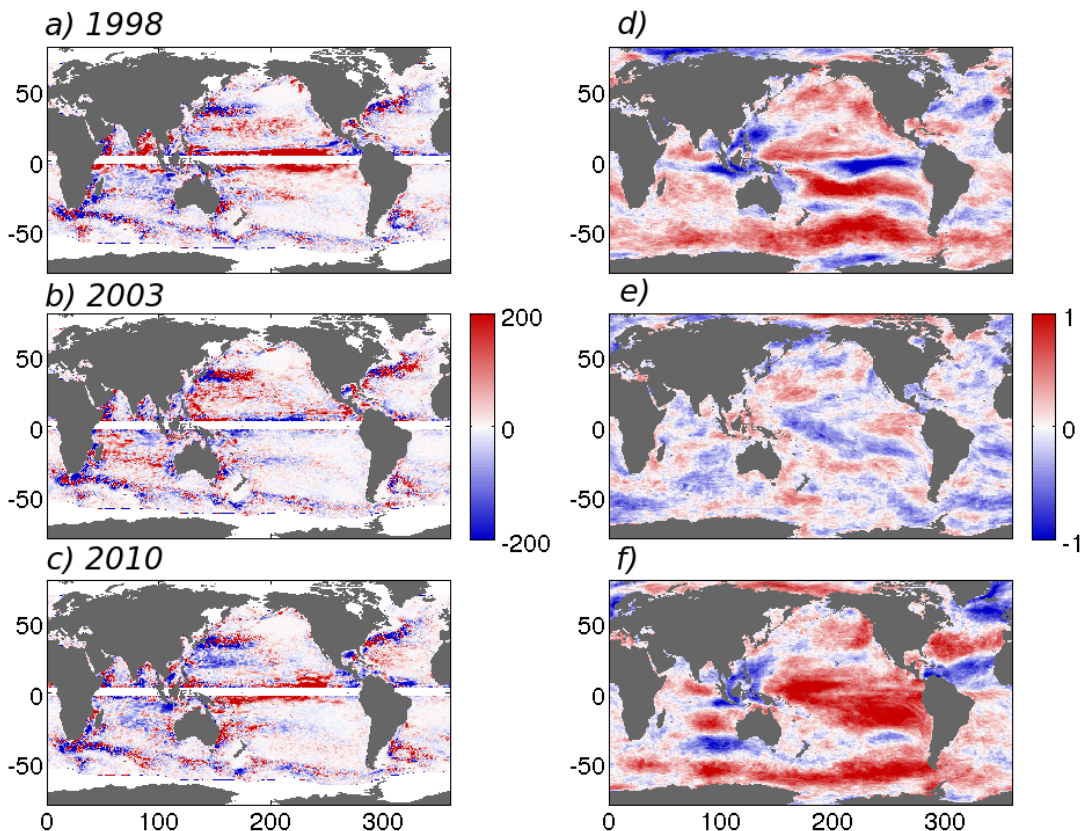


Figure 6.2: Annual EKE anomalies ($\text{cm}^2 \text{ s}^{-2}$) and corresponding annual wind speed anomalies for the years 1998 (a and d), 2003 (b and e) and 2010 (c and f).

The global distribution of annual mean EKE and wind speed anomalies for these time periods (figure 6.2) reveal that the origin of the anomalies for the three different time periods are not the same. The first peak in 1997/1998 corresponds to a period of time which is well documented as one of the strongest ENSO events in recent

decades. The EKE anomalies during this period are significantly high in the tropical Pacific. Anomalously high EKE is also apparent in the tropical Indian Ocean and the subtropical Pacific. The second and third peaks, however, do not correspond to significant ENSO events and the geographical origin of the anomalously high basin-wide mean EKE is different in all three periods. Both the time-mean EKE and the EKE interannual variability (9.3% of the mean) are larger in the northern hemisphere than the southern hemisphere (4.3% of the mean), whereas the time-mean wind speed and the wind speed interannual variability (2.2% of the mean) are larger in the southern hemisphere than the northern hemisphere (2.0% of the mean).

On a regional basis, statistically significant trends are found in all of the major ocean basins (figure 6.3b). Predominantly positive trends characterise the North and South Atlantic subtropical gyres, the south east Indian Ocean and in the Southern Ocean where the main branches of the ACC interact with the bathymetry. In contrast, the North and South Pacific subtropical gyres are characterised by predominantly negative trends, as well as the central North Atlantic. Interesting is the contrast between the decrease in EKE in the North and South Pacific subtropical gyres and the increase in EKE in the subtropical gyres of the North and South Atlantic. A stark contrast is also observed between the Gulf Stream region, where EKE has increased to the south and decreased to the north and the Kuroshio region, where EKE has increased to the north and decreased to the south. When the magnitude of the trend map is expressed as a percentage of the mean EKE (figure 6.3c), the largest positive trends appear in the mid-latitudes of the North and South Pacific basins and the northeast North Atlantic. The largest negative trends are in the subtropical gyres of the North and South Pacific.

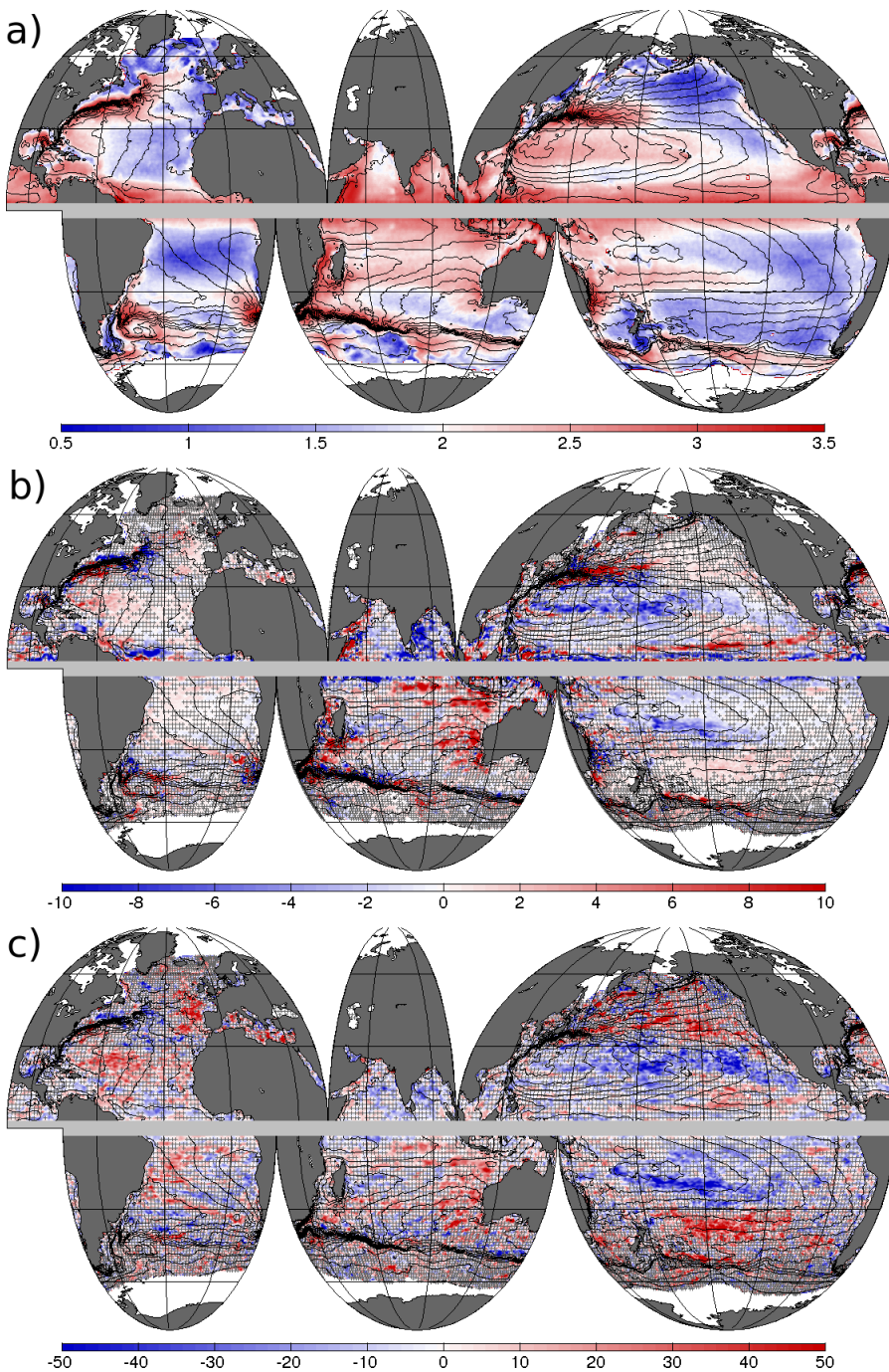


Figure 6.3: a) The Log_{10} of time mean EKE ($\text{cm}^2 \text{s}^{-2}$) computed from altimetric sea surface height anomalies for the 20 year period 1993 to 2012, gridded on a $1/3^\circ$ spatial grid. b) Linear trend in EKE ($\text{cm}^2 \text{s}^{-2}$ per year) computed from altimetric sea surface height anomalies for the 18 year period 1993-2012. b) Linear trend in EKE expressed as a percentage of the mean EKE (a) per decade. Positive values indicate percentage increase and negative values indicate percentage decrease. In panels b and c the hatched areas signify non-statistically significant trends at 90% confidence. Contour lines represent mean dynamic topography from altimetry at 10 cm intervals.

A comparison between the global trends in EKE and the global trends in κ from Stammer et al. (2006) (figure 6.4) shows some small differences but the large basin-wide patterns discussed in previous chapters show strong similarity. Stammer et al. (2006) defined κ as 'slope variance', the product of the EKE and the sin of the latitude (to avoid the problem of the vanishing coriolis parameter near the equator). The only variable in κ is therefore EKE so temporal changes in κ will result only from changes in EKE.

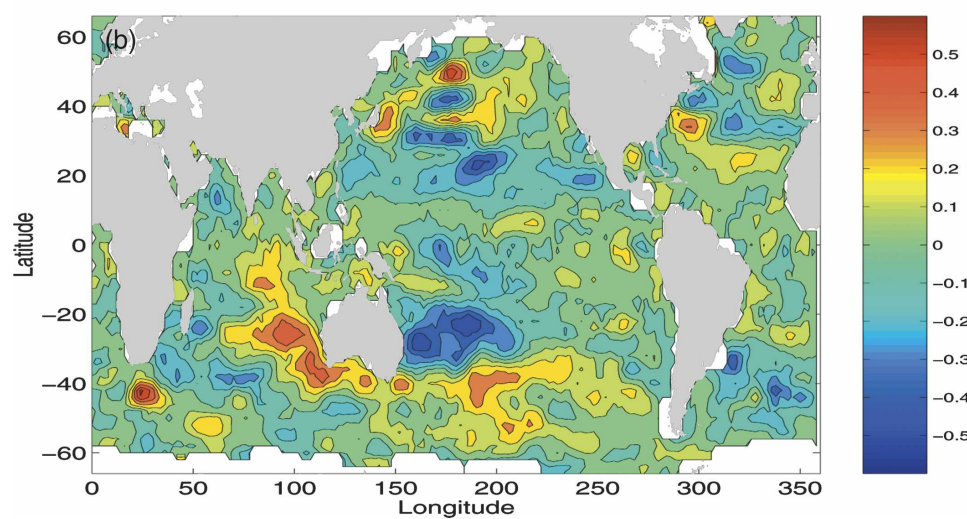


Figure 6.4: Long-term (1993–2003) fractional changes in κ (slope variance), estimated by fitting at each grid location a least squares line to estimates from individual years, from Stammer (2006).

6.2.2 Atmospheric trends

The trend in the global mean wind speed from 1993 to 2012 is both positive and statistically significant 6.1b). The geographical distribution (figure 6.5b) shows large regional differences, with predominantly positive and statistically significant trends in the tropics. The global mean trend is clearly influenced by the large positive increase in the tropical Pacific.

On a global scale, the similarity in the sign of EKE and wind speed trends (figure 6.5c) covers 48.3% of the area-weighted ocean between 60°S and 60°N. This simi-

larity is slightly higher in the northern hemisphere (48.8%) than the southern hemisphere (47.8%). There is, however, a notable contrast between the tropical/subtropical ($<30^{\circ}\text{N/S}$) to subpolar ($>30^{\circ}\text{N/S}$) regions in both hemispheres. In the northern hemisphere, the ratio is larger (49.5%) in the region south of 30°N than in the region north of 30°N (47.4%). In the southern hemisphere, the opposite is true with only 41.7% of the area being similar north of 30°S and 54.0% south of 30°S . These statistics indicate that the influence of the local wind (mechanism M1) varies with latitude. This influence is strongest in the latitudes of the Southern Ocean.

The similarity in the sign of the EKE and wind stress curl trends (figure 6.6c) covers 45.5% of the near-global ocean, slightly lower than that of wind speed. This similarity is again higher in the northern hemisphere (46.0%) than the southern hemisphere (45.1%). In the northern hemisphere, the area is larger in the subtropics and tropics (47.9%) than the subpolar (44.1%).

In summary, more of the global ocean between 60°N and 60°S is characterised by a similarity in EKE and wind speed trends than EKE and wind stress curl trends. Although this implies that local wind forcing (mechanism M1) is more dominant than wind stress curl intensification (mechanism M4), this global perspective has the potential to smooth out, for example, a relatively strong influence of M4 in the South Pacific coupled with a relatively weak influence in the South Atlantic. Our results suggest that in the northern hemisphere oceans, the influence of local wind forcing (mechanism M1) on the EKE trends is significantly more apparent in the tropics and subtropics than the subpolar regions. In the southern hemisphere the opposite is true and the contrast is even greater.

The influence of shifting wind stress curl fields (mechanism M3) on EKE trends has been discussed in previous chapters on a regional basis. A global view of the changes in the zero wind stress curl from the first decade to the second (figure 6.7) reveals that the zero wind stress curl isolines are generally stable in position from one decade to the other. In the mid-latitudes of the northern hemisphere some significant

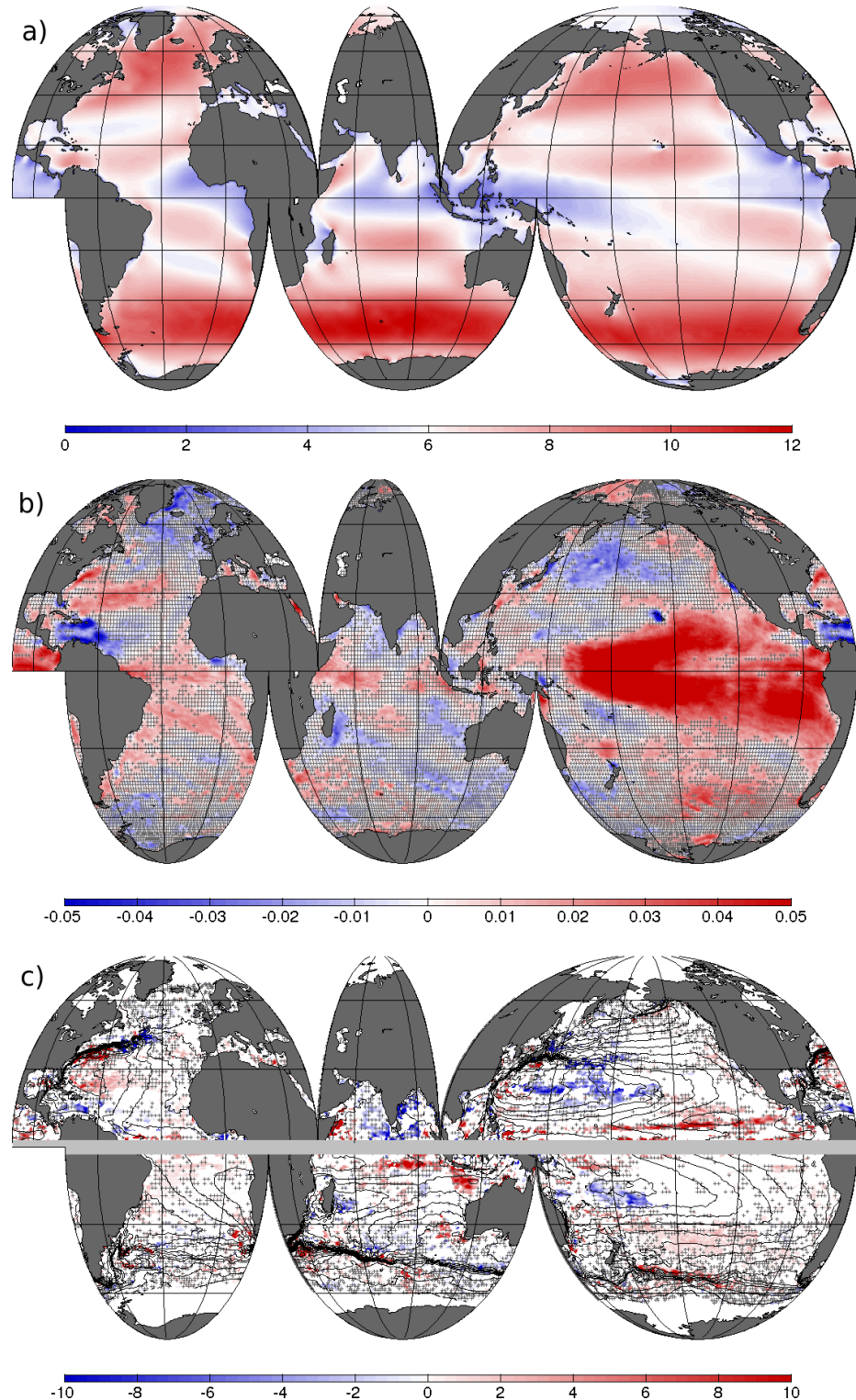


Figure 6.5: (a) Wind speed temporal mean (1993 - 2012) in $m s^{-1}$ from ECMWF ERA-Interim re-analysis data. (b) Linear trend in wind speed for the 20 year time period 1993 to 2012 ($m s^{-1}$ per year) from ECMWF ERA-Interim re-analysis data. The hatched areas signify non-statistically significant trends at 90% confidence. (c) Trend in EKE ($cm^2 s^{-2}$ per year) from 1993 to 2012 showing only the regions where the wind speed trend and the EKE trend are the same sign. Black contours show mean dynamic topography at 10 cm intervals.

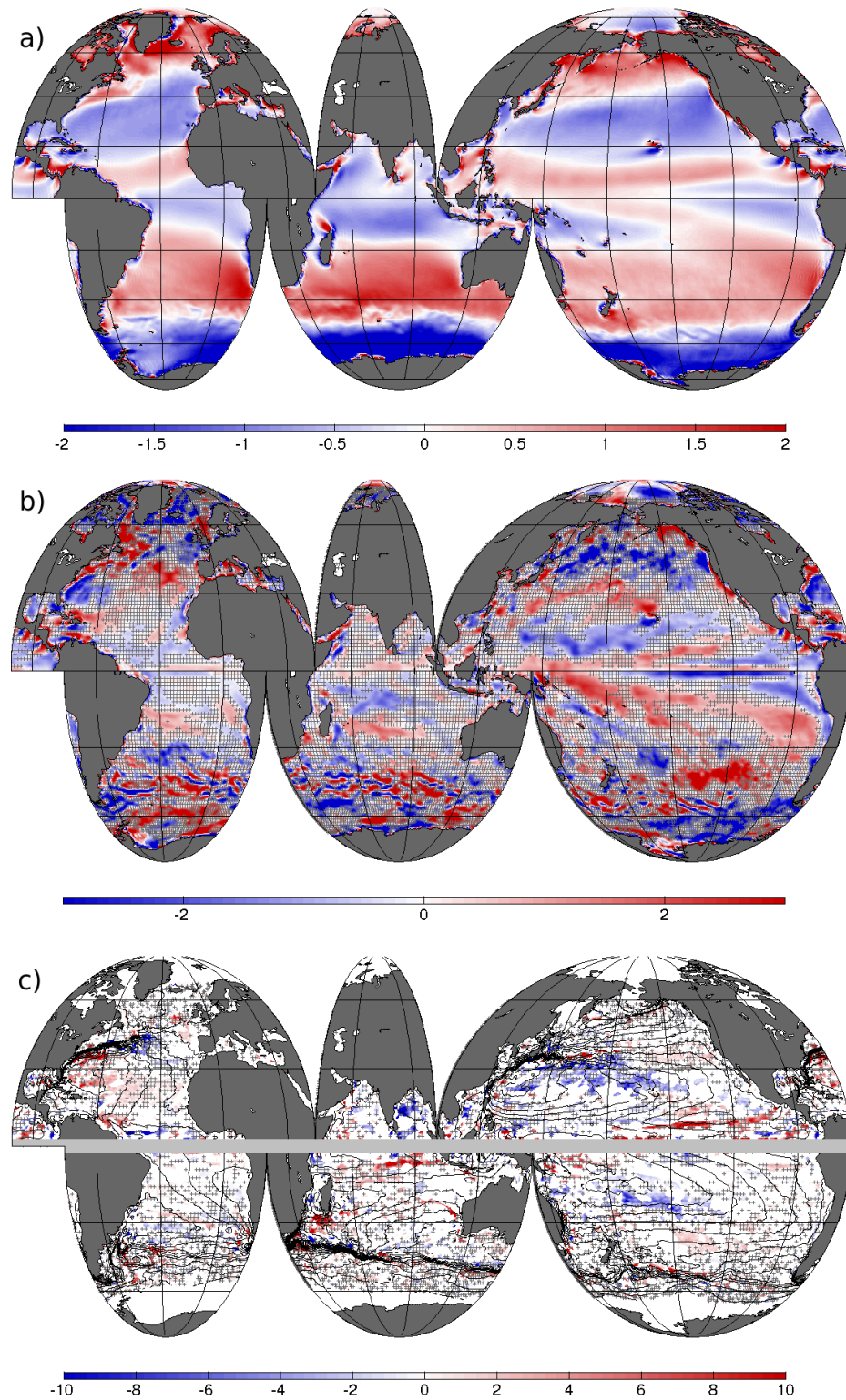


Figure 6.6: (a) Wind stress curl temporal mean ($\times 10^{-7} \text{ N m}^{-3}$) for the time period 1993 to 2012 from ECMWF ERA-Interim re-analysis data. (b) Linear trend in wind stress curl ($\times 10^{-8} \text{ N m}^{-3}$ per year) for the same time period from ECMWF ERA-Interim re-analysis data. The hatched areas signify non-statistically significant trends at 90% confidence. (c) Trend in EKE ($\text{cm}^2 \text{ s}^{-2}$ per year) from 1993 to 2012 for the regions where the trend in wind stress curl magnitude is the same sign for the same time period. Black contours show mean dynamic topography at 10 cm intervals.

changes are observed. The zero curl line is further to the north in the second decade in the northeast North Atlantic and North Pacific. The difference, however, is very small and it is not clear if this small difference is significant.

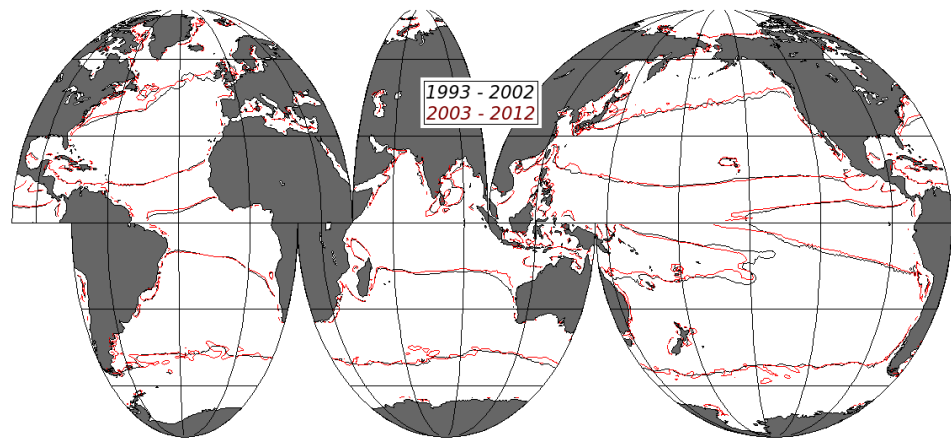


Figure 6.7: Position of the zero wind stress curl isolines for the decadal mean wind stress curl from 1993 to 2002 (black contours) and 2003 to 2012 (red contours).

Comparing the trends in the zonal mean of both wind speed and EKE at different latitudes (figure 6.8) reveals that the trend in wind speed is positive at all latitudes south of 32°N and negative at all latitudes north of 32°N . The trend in EKE does not show a similar pattern but, instead, undergoes several rapid changes over only a few degrees. The large peaks in the EKE trend at $\sim 38^{\circ}\text{N}$ and $\sim 50^{\circ}\text{N}$ do not correspond to similar peaks in wind speed trends. The only generalisation possible from the zonal mean trends is that EKE trends in the Southern Ocean (south of 25°S) are predominantly positive and wind speed trends are entirely positive.

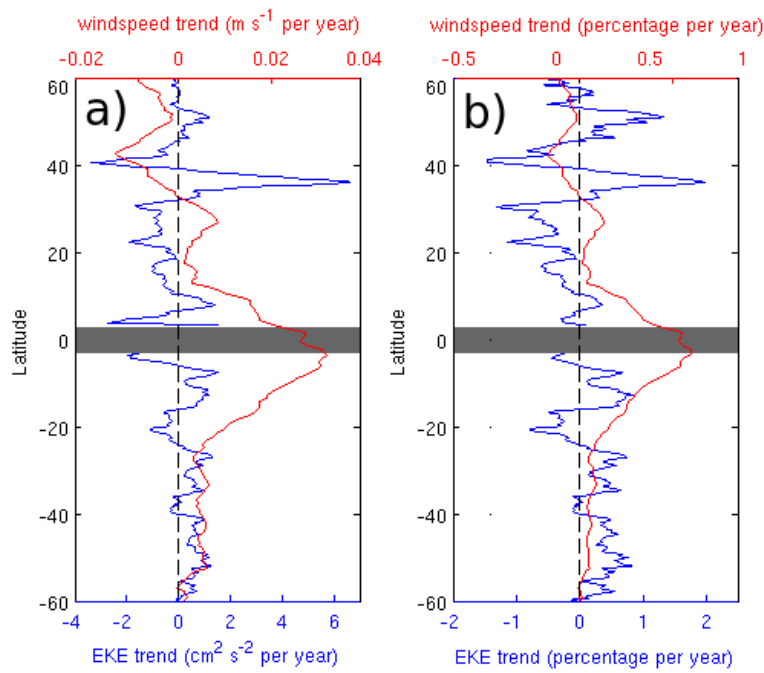


Figure 6.8: a) Comparison of the trend in the zonal mean EKE ($\text{cm}^2 \text{s}^{-2}$ per year) from 1993 to 2012 (blue line) and the trend in the zonal mean wind speed (m s^{-1} per year) for the same period (red line). b) Same as (a) but expressed as a percentage of the zonal mean per year.

6.2.3 EKE variability and climate modes

As discussed in previous chapters, regional studies have shown that EKE variability is correlated with different climate modes. We now present in figure 6.9 a global perspective on the correlations between EKE interannual variability and the climate mode which best represents the large-scale patterns of atmospheric variability in each basin. In the North Atlantic, the correlation of annual mean EKE with the NAO index has a distinct dipolar pattern with a significant positive correlation to the north and east and a more negative pattern to the south and west. In the subtropical North Pacific, a strong positive correlation is observed between annual mean EKE and the PDO index. Although previous studies have shown that EKE is correlated with PDO in the STCC, here we demonstrate that over the entire basin, other than some small regions, the positive correlations are confined to the gyre interior with predominantly negative

correlations in the central and eastern tropics and the subpolar regions in the North Pacific.

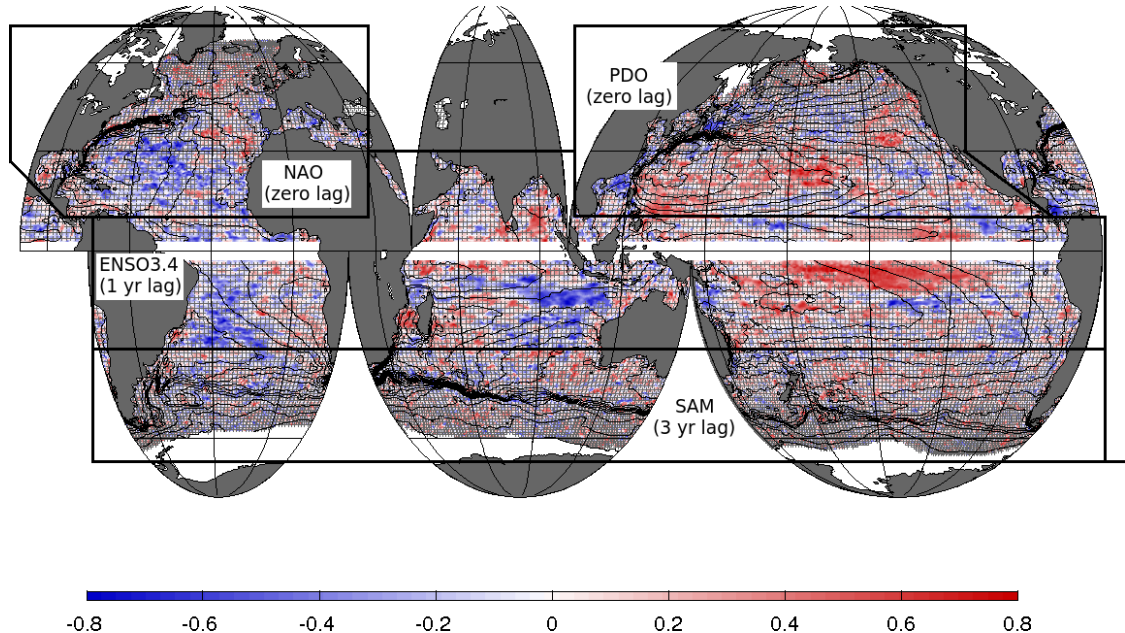


Figure 6.9: Correlation coefficients of (annual mean) EKE with various climate modes. Hatched area represents non-statistically significant correlations.

Previous studies (Meredith and Hogg, 2006; Morrow et al., 2010) found that the positive EKE response to an increase in the SAM index peaks at a lag of 2 to 3 years. Here we show that the Southern Ocean's response is highly variable on small spatial scales. In general, the response is strongest in the Pacific sector.

Another notable feature of the correlation map is the influence of ENSO, not only in the tropical Pacific but also in the South Atlantic and Indian basins. A strong anti-correlation between EKE and ENSO (at 1 year lag) is evident in the southeast Indian Ocean and the western South Atlantic subtropical gyre. Both these regions are characterised by positive EKE trends, much of which appears as statistically significant (figure 6.3c).

Most scientific research on ENSO has focused on the Pacific Ocean Basin where early studies (Bjerknes, 1969; Wyrtki et al., 1976) identified the core of the physical processes underlying the phenomenon occurs. The global influence of ENSO was

later well established during the Tropical Ocean Global Atmosphere (TOGA) decade. The heat sources and sinks associated with the displacements of deep atmospheric convection in the tropical Pacific force atmospheric planetary waves associated with global teleconnections (Trenberth and Hoar, 1996). A negative correlation between the Indian summer monsoon and ENSO has been explained to some extent by the modulation of the Walker circulation (Slingo, 1998). During warm Pacific events, the ascending branch of the Walker circulation shifts eastward in response to the anomalous warming in the central and eastern Pacific, resulting in subsidence and reduced rainfall over the Indo-West Pacific region.

In the Indian Ocean, the largest negative correlations appear in the region associated with the highest volume transport from the Pacific to the Indian basin via the Indonesian Archipelago (Sebille et al., 2014), known as Indonesian Throughflow Transport. The Indonesian Throughflow has been studied for many years, culminating in fieldwork in the early 2000s known as the International Nusantara Stratification and Transport (INSTANT) experiment (Sprintall et al., 2004). The INSTANT campaign led to an increase in the understanding of the variability of Indonesian Throughflow and the dynamics that drive that variability. Previous work has shown that ENSO influences the magnitude of the Indonesian Throughflow on interannual time scales (Meyers, 1996; Du and Qu, 2010; Yuan et al., 2011). Changes in the tropical Pacific trade winds on both interannual and longer term decadal time scales generate planetary waves that pass through the Indonesian Seas (Wijffels and Meyers, 2004; Schwarzkopf and Böning, 2011). Based on the assumption that an increase (decrease) in Indonesian Throughflow volume transport results in an increase (decrease) in EKE where the volume transport anomalies occur, our results, in combination with previous work, suggest a non-local atmospheric forcing (mechanism M2) influences EKE in this region of the Indian Ocean.

In the South Atlantic Ocean, the South Atlantic subtropical dipole mode (SASD) is the dominant mode of coupled ocean-atmosphere variability and is characterised

by a dipole pattern of SST anomalies oriented northeast-southwest and a monopole structure in sea level pressure (SLP) (Venegas et al., 1997). The positive phase of the SASD is induced by the strengthening and poleward shift of South Atlantic subtropical high (Haarsma, R. J. et al., 2005; Morioka et al., 2011). A causal link between SST anomalies in the tropical Pacific linked to ENSO and the SASD has recently been established by Rodrigues et al. (2015) using both observational data and idealised model experiments. This study shows that negative SASD events are associated with central Pacific El Niño 34 events by triggering the Pacific-South America wave train (PSA). The PSA causes a weakening and meridional shift of the South Atlantic subtropical high (SASH), which then generates the negative SASD events. On the other hand, a strengthening of the SASH related to central La Niña teleconnections causes positive SASD events. Our results corroborate the findings of Rodrigues et al. (2015) and imply that a non-local atmospheric forcing (mechanism M2), originating in the central Pacific, has a significant influence on EKE in the subtropical South Atlantic.

6.3 Conclusions and Future work

The goal of this thesis was to establish if there has been any significant trends in EKE, both globally and regionally, during the altimetry record and to identify, where possible, the principal mechanisms for the observed trends. This study was made possible due to the near-global, quasi-synoptic data from altimetry and atmospheric reanalysis data. As the altimetry time series is ever increasing in length, we have had the opportunity to shed new light on the dynamical changes and causes of EKE variability, as well as to corroborate or counter previous hypotheses derived from shorter time periods. In the future, longer time series will provide clearer insight into the statistical robustness of both the EKE trends and the relationship between EKE variability and the different major modes of climate variability. More specifically, it will be possible to investigate whether the trends are due to a changing ocean or simply phase-induced

trends in low-frequency intrinsic variability.

On a global scale, the most significant result is that EKE has increased in the southern hemisphere and decreased in the northern hemisphere. The statistically significant positive trend in the southern hemisphere is coupled with a statistically significant positive trend in wind speed, whereas the hemispheric mean trends in wind speed and EKE are opposite signs in the northern hemisphere. We can conclude that, based on this result, local and/or remote wind forcing (mechanisms M1 and M2) are more dominant in the southern hemisphere (primarily south of 30°S) than in the northern hemisphere.

In the North Atlantic, our results confirm that the relationship of EKE variability to the NAO, suggested by Stammer and Wunsch (1999) and later confirmed by Penduff et al. (2004), is evident in the basinwide correlations of EKE with the NAO during the altimetry record. Our results also show that the subtropical gyre is the region where the influence of the local wind (mechanism M1) and wind stress curl intensification (mechanism M4) is greatest in the subtropical North Atlantic. The influence of the local wind forcing in the sub-polar northeast Atlantic suggested by Stammer and Wunsch (1999) is not evident in the 18 year trends. Instead, the influence of shifting wind stress curl patterns (mechanism M3) suggested first by Heywood et al. (1994) and later by Hakkinen and Rhines (2009) is more significant in this region.

In the North Pacific, different mechanisms are responsible for the observed EKE trends with the relative influence of each mechanism varying regionally. Like the North Atlantic, a significant contribution is made by local wind speed (M1) and/or wind stress curl intensification (M4) in the subtropics. Unlike the North Atlantic, the North Pacific subtropical gyre is home to the density-driven STCC. As found by previous studies (e.g. Qiu and Chen (2010)), EKE in the STCC region is highly correlated with the PDO during the 18 year study period. Our results also show that, despite a similarity between EKE trends and wind stress curl trends in most of the subtropical gyre interior, much of the STCC band does not display this similarity. This strongly

implies that EKE trends in the STCC region have arisen due to another mechanism. As previous studies have identified the strong influence of local baroclinicity in modulating EKE on interannual time scales, it is likely that this mechanism (mechanism M5) is dominant for EKE trends in this region.

In the Southern Ocean, our results revealed a positive, statistically significant trend in the basin-wide EKE, including statistically significant positive trends in the ACC. This is of particular importance for studies of global climate change, as an increase in EKE in the ACC may facilitate an increase in meridional heat transport which has the potential to warm the Ocean around Antarctica. We suggest that the dominant mechanism in this region is local wind speed (M1) although it is difficult to distinguish between this mechanism and non-local winds (M2) due to the primarily zonally symmetric nature of the mean wind fields. The similarity between EKE trends and wind speed trends as well as the correlations between EKE and SAM indicate that the influence of this mechanism is strongest in the South Pacific sector of the Southern Ocean. Our results indicate that the primary mechanisms responsible for the EKE trends are consistent with the mechanisms of EKE variability proposed by Meredith and Hogg (2006), Hogg et al. (2008) and Morrow et al. (2010) and are in agreement with the eddy saturation theory from the same studies.

6.4 Outlook

Despite the contribution this study has made to our understanding of the mechanisms responsible for EKE trends, it will conclude by raising some new questions including the following:

- 1) Why has EKE increased in the southern hemisphere and decreased in the northern hemisphere, despite an increase in wind speed in both hemispheres? Does this suggest that the EKE trends in the northern hemisphere are predominantly caused by low-frequency intrinsic variability (mechanism M6) that the 20 year altimetry record

is not substantial enough to resolve?

2) What is the global significance of changes in local baroclinicity (mechanism M5) on EKE trends? Does an increase in the strength of the stratification result in an increase in EKE due to an increase in baroclinic shear and/or baroclinic instability or a decrease in EKE due to the increase in the growth rate of baroclinic eddies?

3) Could EKE trends be influenced by long term changes in factors influencing eddy dissipation? This thesis has focussed solely on the mechanisms responsible for eddy generation. If seasonal changes in the rate of eddy dissipation can force the seasonal modulation of EKE in the Gulf Stream (Zhai and Wunsch, 2013), long term changes in the rate of eddy dissipation may also play a significant role in EKE trends.

In the future, our understanding of the relationship between EKE and local baroclinicity can be greatly improved by studying the global changes in the hydrographic (temperature and salinity) properties of the upper 2000 m of the ocean using data from ARGO floats. With the continued advancement in computer technology, advancement in numerical studies of EKE changes in response to varying forcings will inevitably contribute significantly to our understanding of these dynamical processes. Finally, the altimeter time series is ever increasing and with this lengthening period will come the opportunity to acquire more statistically robust trends and correlations as well as an opportunity to better understand the characteristics of the low-frequency variability.

Bibliography

- Arakawa, A. and V. R. Lamb, 1977: Computational design of the basic dynamical processes of the UCLA general circulation model. *Methods in computational physics*, **17**, 173 – 265.
- Aristegui, J., P. Sang, and S. Hern, 1994: Island-induced eddies in the Canary Islands. *Deep Sea Research Part I: Oceanographic Research Papers*, **41 (10)**.
- Baldwin, M. P., 2001: Annular modes in global daily surface pressure. *Geophysical Research Letters*, **28 (21)**, 4115–4118.
- Berloff, P., W. Dewar, S. Kravtsov, and J. McWilliams, 2007: Ocean eddy dynamics in a coupled ocean–atmosphere model. *Journal of Physical Oceanography*, **37 (5)**, 1103–1121.
- Bjerknes, J., 1969: Atmospheric teleconnections from the equatorial pacific. *Monthly Weather Review*, **97 (3)**, 163–172.
- Boland, E. J. D., 2013: Jets , Mixing , and Topography in the Southern Ocean. Ph.D. thesis, University of Cambridge.
- Chang, Y.-L. and L.-Y. Oey, 2012: The Philippines–Taiwan Oscillation: Monsoon like interannual oscillation of the subtropical–tropical western North Pacific wind system and its impact on the ocean. *Journal of Climate*, **25 (5)**, 1597–1618.
- Chelton, D. B. and M. G. Schlax, 2003: The Accuracies of smoothed sea surface height fields constructed from tandem satellite altimeter datasets. *Journal of Atmospheric and Oceanic Technology*, **20 (9)**, 1276–1302.
- Chelton, D. B., M. G. Schlax, and R. M. Samelson, 2011: Global observations of nonlinear mesoscale eddies. *Progress in Oceanography*, **91 (2)**, 167–216.
- Chelton, D. B., M. G. Schlax, R. M. Samelson, and R. a. de Szoeke, 2007: Global observations of large oceanic eddies. *Geophysical Research Letters*, **34 (15)**, L15 606.
- Cheney, R. E. and J. G. Marsh, 1981: Seasat altimeter observations of dynamic topography in the Gulf Stream Region. *Journal of Geophysical Research*, **86 (C1)**, 473–483.
- Cheney, R. E. and J. G. Marsh, 1983: Global mesoscale variability from collinear tracks of Seasat altimeter data. *Journal of Geophysical Research*, **88 (C7)**, 4343–4354.

- Dee, D. P., et al., 2011: The ERA-Interim reanalysis: configuration and performance of the data assimilation system. *Quarterly Journal of the Royal Meteorological Society*, **137** (656), 553–597.
- Dickson, R., W. J. Gould, P. A. Gurbutt, and P. D. Killworth, 1982: A seasonal signal in ocean currents to abyssal depths. *Nature, London*, **295**, 193 – 198.
- Dijkstra, H. A. and M. Ghil, 2005: Lowfrequency variability of the largescale ocean circulation: A dynamical systems approach. *Reviews of Geophysics*, **43** (3), 1–38.
- Douglas, B. C. and P. D. Gaborski, 1979: Observation of sea surface topography with Geos 3 altimeter data. *Journal of Geophysical Research*, **84** (B8), 3893–3896.
- Du, Y. and T. Qu, 2010: Three inflow pathways of the Indonesian throughflow as seen from the simple ocean data assimilation. *Dynamics of Atmospheres and Oceans*, **50** (2), 233–256.
- Ducet, N. and P. Y. LeTraon, 2001: A comparison of surface eddy kinetic energy and Reynolds stresses in the Gulf Stream and the Kuroshio Current systems from merged TOPEX/Poseidon and ERS-1/2 altimetric data. *Journal of Geophysical Research*, **106** (C8), 16,603–16,622.
- Ducet, N., P. Y. LeTraon, and G. Reverdin, 2000: Global high-resolution mapping of ocean circulation from TOPEX/Posseidon and ERS-1 and -2. *Journal of Geophysical Research*, **105** (C8), 19,477 – 19,498.
- Efron, B., 1979: Bootstrap methods: another look at the jackknife. *The Annals of Statistics*, 1–26.
- Ferrari, R. and C. Wunsch, 2009: Ocean circulation kinetic energy: reservoirs, sources, and sinks. *Annual Review of Fluid Mechanics*, **41** (1), 253–282.
- Frankignoul, C., G. DeCoëtlogon, T. M. Joyce, and S. Dong, 2001: Gulf Stream variability and ocean – atmosphere interactions. *Journal of Physical Oceanography*, **31** (12), 3516–3529.
- Frankignoul, C. and P. Müller, 1979: Quasi-geostrophic response of an infinite β -plane ocean to stochastic forcing by the atmosphere. *Journal of Physical Oceanography*, **9** (1), 104 – 127.
- Fu, L.-L. and A. Cazenave, 2000: Satellite altimetry and earth sciences: a handbook of techniques and applications (Vol. 69). Access Online via Elsevier pp.
- Fu, L.-L., D. Chelton, P.-Y. Le Traon, and R. Morrow, 2010: Eddy dynamics from satellite altimetry. *Oceanography*, **23** (4), 14–25.
- García-Reyes, M. and J. Largier, 2010: Observations of increased wind-driven coastal upwelling off central California. *Journal of Geophysical Research*, **115** (C4), C04 011.

- Gill, A. E., J. S. A. Green, and A. J. Simmons, 1974: Energy partition in the large-scale ocean circulation and the production of mid-ocean eddies. *Deep Sea Research and Oceanographic Abstracts*, **21** (7), 499–528.
- Gille, S. T., K. Speer, J. R. Ledwell, and A. C. Naveira Garabato, 2007: Mixing and Stirring in the Southern Ocean. *Eos, Transactions American Geophysical Union*, **88** (39), 382–383.
- Gille, S. T., M. M. Yale, and D. T. Sandwell, 2000: Global correlation of mesoscale ocean variability with seafloor roughness from satellite altimetry. *Geophysical Research Letters*, **27** (9), 1251–1254.
- Haarsma, R. J., C. W. E. J., Hazeleger, C. Severijns, A. R. Piola, and F. Molteni, 2005: Dominant modes of variability in the South Atlantic : A study with a hierarchy of ocean – atmosphere models. *Journal of Climate*, **18** (11), 1719–1735.
- Hakkinen, S. and P. B. Rhines, 2009: Shifting surface currents in the northern North Atlantic Ocean. *Journal of Geophysical Research*, **114** (C4), C04 005, doi:10.1029/2008JC004883.
- Hall, A. and M. Visbeck, 2002: Synchronous variability in the southern hemisphere atmosphere , sea ice , and ocean resulting from the annular mode. *Journal of Climate*, **15** (21), 3043–3057.
- Heywood, K. J., E. L. McDonagh, and M. A. White, 1994: Eddy kinetic energy of the North Atlantic subpolar gyre from satellite altimetry. *Journal of Geophysical Research*, **99** (C11), 22,525–22,539.
- Hogg, A. and J. R. Blundell, 2006: Interdecadal variability of the Southern Ocean. *Journal of Physical Oceanography*, **36** (8), 1626–1645.
- Hogg, A. M. C., M. P. Meredith, J. R. Blundell, and C. Wilson, 2008: Eddy heat flux in the Southern Ocean: Response to variable wind forcing. *Journal of Climate*, **21** (4), 608–620, doi:10.1175/2007JCLI1925.1.
- Holland, W. R., 1978: The role of mesoscale eddies in the general circulation of the ocean-numerical experiments using a wind-driven quasi-geostrophic model. *Journal of Physical Oceanography*, **8** (3), 363 – 392.
- Huang, N. E., C. D. Leitao, and C. Parra, 1978: Large-scale Gulf Stream frontal study using Geos 3 radar altimeter data. *Journal of Geophysical Research*, **83** (C9), 4673–4682.
- Hurrell, J. W. and H. V. Loon, 1997: Decadal variations in climate associated with the North Atlantic Oscillation. *Climatic Change at High Elevation Sites*, 69–94.
- Hwang, C., C.-R. Wu, and R. Kao, 2004: TOPEX/Poseidon observations of mesoscale eddies over the Subtropical Countercurrent: Kinematic characteristics of an anti-cyclonic eddy and a cyclonic eddy. *Journal of Geophysical Research*, **109** (C8), C08 013.

- Iles, A. C., T. C. Gouhier, B. a. Menge, J. S. Stewart, A. J. Haupt, and M. C. Lynch, 2012: Climate-driven trends and ecological implications of event-scale upwelling in the California Current System. *Global Change Biology*, **18** (2), 783–796.
- Ivchenko, V. O., S. Danilov, and D. Olbers, 2008: Eddies in numerical models of the Southern Ocean. *Ocean Modeling in an Eddying Regime*, 177–198.
- Jia, Y., P. H. R. Calil, E. P. Chassignet, E. J. Metzger, J. T. Potemra, K. J. Richards, and a. J. Wallcraft, 2011: Generation of mesoscale eddies in the lee of the Hawaiian Islands. *Journal of Geophysical Research: Oceans (1978–2012)*, **116** (C11).
- Johnson, G. C. and H. L. Bryden, 1989: On the size of the Antarctic Circumpolar Current. *Deep Sea Research Part A. Oceanographic Research Papers*, **36** (1), 39–53.
- Karsten, R. H. and J. Marshall, 2002: Constructing the residual circulation of the ACC from observations. *Journal of Physical Oceanography*, **32** (12), 3315–3327.
- Kelly, K. A., R. C. Beardsley, R. Limeburner, J. D. Paduan, and T. K. Chereskin, 1998: Variability of the near-surface eddy kinetic energy in the California Current based on altimetric , drifter , and moored current data. *Journal of Geophysical Research: Oceans (1978-2012)*, **103** (C6), 13 067–13 083.
- Kidson, J. W., 1999: Principal modes of southern hemisphere low-frequency variability obtained from NCEP – NCAR reanalyses. *Journal of Climate*, **12** (9), 2808–2830.
- Kobashi, F. and H. Kawamura, 2002: Seasonal variation and instability nature of the North Pacific Subtropical Countercurrent and the Hawaiian Lee Countercurrent. *Journal of Geophysical Research: Oceans (1978-2012)*, **107** (C11), 6–1, doi:10.1029/2001JC001225.
- Kobashi, F. and A. Kubokawa, 2011: Review on North Pacific subtropical countercurrents and subtropical fronts: role of mode waters in ocean circulation and climate. *Journal of Oceanography*, **68** (1), 21–43.
- Krauss, W. and R. H. Käse, 1984: Mean circulation and eddy kinetic energy in the eastern North Atlantic. *Journal of Geophysical Research*, **89** (C3), 3407 – 3415.
- Kurian, J., F. Colas, X. Capet, J. C. McWilliams, and D. B. Chelton, 2011: Eddy properties in the California Current System. *Journal of Geophysical Research: Oceans (1978-2012)*, **116** (C8), C08 027.
- Le Traon, P.-Y., M. C. Rouquet, and C. Boissier, 1990: Spatial scales of mesoscale variability in the North Atlantic as deduced from Geosat data. *Journal of Geophysical Research*, **95** (C11), 20 267–20 285.
- Lee, T. and P. Cornillon, 1995: Temporal variation of meandering intensity and domain-wide lateral oscillations of the Gulf Stream. *Journal of Geophysical Research*, **100** (C7), 13 603 – 13 613.

- Liu, Y., C. Dong, Y. Guan, D. Chen, J. McWilliams, and F. Nencioli, 2012: Eddy analysis in the subtropical zonal band of the North Pacific Ocean. *Deep Sea Research Part I: Oceanographic Research Papers*, **68**, 54–67.
- Mantua, N. J. and S. R. Hare, 2002: The Pacific decadal oscillation. *Journal of Oceanography*, **58** (1), 35–44.
- Marchesiello, P., a. C. McWilliams, and A. Shchepetkin, 2003: Equilibrium structure and dynamics of the California Current system. *Journal of Physical Oceanography*, **33** (4), 753 – 783.
- Marshall, G. J., 2003: Trends in the Southern Annular Mode from observations and reanalyses. *Journal of Climate*, **16** (24), 4134–4143.
- Mather, R. S., C. Rizos, and R. Coleman, 1979: Remote sensing of surface ocean circulation with satellite altimetry. *Science*, **205** (4401), 11–17.
- Menard, Y., 1983: Observations of eddy fields in the northwest Atlantic and northwest Pacific by Seasat altimeter data. *Journal of Geophysical Research*, **88** (C3), 1853–1866.
- Meredith, M. P. and A. M. Hogg, 2006: Circumpolar response of Southern Ocean eddy activity to a change in the Southern Annular Mode. *Geophysical Research Letters*, **33** (16), L16 608.
- Meyers, G., 1996: Variation of Indonesian throughflow and the El Nino Southern Oscillation. *Journal of Geophysical Research*, **101**, 12,255–12,263.
- Morioka, Y., T. Tozuka, and T. Yamagata, 2011: On the growth and decay of the subtropical dipole mode in the South Atlantic. *Journal of Climate*, **24** (21), 5538–5554.
- Morrow, R., R. Coleman, J. Church, and D. Chelton, 1994: Surface eddy momentum flux and velocity variances in the Southern Ocean from Geosat altimetry. *Journal of Physical Oceanography*, **24** (10), 2050 – 2071.
- Morrow, R., M. L. Ward, A. M. Hogg, and S. Pasquet, 2010: Eddy response to Southern Ocean climate modes. *Journal of Geophysical Research*, **115** (C10), C10 030.
- Müller, P. and C. Frankignoul, 1981: Direct atmospheric forcing of geostrophic eddies. *Journal of Physical Oceanography*, **11** (3), 287–308.
- Munk, W. and C. Wunsch, 1998: Abyssal recipes II: energetics of tidal and wind mixing. *Deep Sea Research Part I*, **45** (12), 1977–2010.
- Munk, W. H., 1950: On the wind driven ocean circulation. *Journal of Meteorology*, **7** (2), 79–93.
- Penduff, T., B. Barnier, W. K. Dewar, and J. J. O'Brien, 2004: Dynamical response of the oceanic eddy field to the North Atlantic Oscillation : A model – data comparison. *Journal of Physical Oceanography*, **34** (12), 2615–2629.

- Penduff, T., M. Juza, B. Barnier, J. Zika, W. K. Dewar, A.-M. Treguier, J.-M. Molines, and N. Audiffren, 2011: Sea level expression of intrinsic and forced ocean variabilities at interannual time scales. *Journal of Climate*, **24** (21), 5652–5670.
- Polzin, K. L., 1997: Spatial variability of turbulent mixing in the abyssal ocean. *Science*, **276** (5309), 93–96.
- Qiu, B., 1999: Seasonal eddy field modulation of the North Pacific Subtropical Countercurrent : TOPEX / Poseidon observations and theory. *Journal of Physical Oceanography*, **29** (10), 2471–2486.
- Qiu, B. and S. Chen, 2005: Variability of the Kuroshio extension jet, recirculation gyre, and mesoscale eddies on decadal time scales. *Journal of Physical Oceanography*, **35** (11), 2090–2103.
- Qiu, B. and S. Chen, 2010: Eddy-mean flow interaction in the decadally modulating Kuroshio Extension system. *Deep Sea Research Part II: Topical Studies in Oceanography*, **57** (13-14), 1098–1110.
- Qiu, B. and S. Chen, 2013: Concurrent decadal mesoscale eddy modulations in the western North Pacific subtropical gyre. *Journal of Physical Oceanography*, **43** (2), 344–358.
- Richardson, P. L., 1983: Eddy kinetic energy in the North Atlantic from surface drifters. *Journal of Geophysical Research*, **88** (C7), 4355 – 4367.
- Robinson, E. A., 1984: Eddies in marine sciences. *International Journal of Biometeorology*, **28** (4), 326.
- Rodrigues, R. R., E. J. D. Campos, and R. Haarsma, 2015: The impact of ENSO on the South Atlantic Subtropical Dipole Mode. *Journal of Climate*, (in press).
- Roemmich, D. and J. Gilson, 2001: Eddy transport of heat and thermocline waters in the North Pacific : A key to interannual / decadal climate variability ? *Journal of Physical Oceanography*, **31** (3), 675–688.
- Sallée, J. B., K. Speer, and R. Morrow, 2008: Response of the Antarctic Circumpolar Current to atmospheric variability. *Journal of Climate*, **21** (12), 3020–3039.
- Sasaki, Y. N. and N. Schneider, 2011: Interannual to decadal Gulf Stream variability in an eddy-resolving ocean model. *Ocean Modelling*, **39** (3-4), 209–219.
- Scharffenberg, M. G. and D. Stammer, 2010: Seasonal variations of the large-scale geostrophic flow field and eddy kinetic energy inferred from the TOPEX/Poseidon and Jason-1 tandem mission data. *Journal of Geophysical Research*, **115** (C2), C02 008.
- Schwarzkopf, F. U. and C. W. Böning, 2011: Contribution of Pacific wind stress to multi-decadal variations in upper-ocean heat content and sea level in the tropical south Indian Ocean. *Geophysical Research Letters*, **38** (12), L12 602.

- Screen, J. a., N. P. Gillett, D. P. Stevens, G. J. Marshall, and H. K. Roscoe, 2009: The role of eddies in the Southern Ocean temperature response to the Southern Annular Mode. *Journal of Climate*, **22** (3), 806–818.
- Sebille, E., J. Sprintall, F. U. Schwarzkopf, A. Sen Gupta, M. H. Santoso, A., England, and C. W. Böning, 2014: PacificoIndian Ocean connectivity: Tasman leakage, Indonesian Throughflow, and the role of ENSO. *Journal of Geophysical Research : Oceans*, **119** (2), 1365–1382.
- Shroyer, E. L. and A. J. Plueddemann, 2012: Wind-driven modification of the Alaskan coastal current. *Journal of Geophysical Research: Oceans (1978-2012)*, **117** (C3), C03 031.
- Slingo, J., 1998: The 1997 / 98 El Niño. *Weather*, **53** (9), 274–281.
- Spence, P., J. C. Fyfe, A. Montenegro, and A. J. Weaver, 2010: Southern Ocean response to strengthening winds in an eddy-permitting global climate model. *Journal of Climate*, **23** (19), 5332–5343.
- Sprintall, J., et al., 2004: INSTANT : A new international array to measure the Indonesian Throughflow. *Eos, Transactions American Geophysical Union*, **85** (39), 369–376.
- Stammer, D., C. Böning, and C. Dieterich, 2001: The role of variable wind forcing in generating eddy energy in the North Atlantic. *Progress in Oceanography*, **48** (2-3), 289–311.
- Stammer, D. and C. Wunsch, 1999: Temporal changes in eddy energy of the oceans. *Deep Sea Research Part II: Topical Studies in Oceanography*, **46** (1), 77–108.
- Stammer, D., C. Wunsch, and K. Ueyoshi, 2006: Temporal changes in ocean eddy transports. *Journal of Physical Oceanography*, **36** (3), 543–550.
- Strub, P. and C. James, 2000: Altimeter-derived variability of surface velocities in the California Current System: 2. Seasonal circulation and eddy statistics. *Deep Sea Research Part II: Topical Studies in Oceanography*, **47** (5-6), 831–870.
- Taylor, A. H. and J. A. Stephens, 1998: The North Atlantic Oscillation and the latitude of the Gulf Stream. *Tellus A*, **50** (1), 134–142.
- Thompson, D. W. and J. Wallace, 2000: Annular modes in the extratropical circulation . Part I : month-to-month variability *. *Journal of Climate*, **13** (5), 1000–1016.
- Treguier, A. M. and B. L. Hua, 1988: Influence of bottom topography on stratified quasi-geostrophic turbulence in the ocean. *Geophysical & Astrophysical Fluid Dynamics*, **43** (3-4), 265 – 305.
- Trenberth, K. E. and T. J. Hoar, 1996: The 1990–1995 El NiñoSouthern Oscillation event: Longest on record. *Geophysical Research Letters*, **23** (1), 57–60.

- Venegas, S. A., L. A. Mysak, and D. N. Straub, 1997: Atmosphere – Ocean coupled variability in the South Atlantic. *Journal of Climate*, **10** (11), 2904–2920.
- Volkov, D. L., 2005: Interannual variability of the altimetry-derived eddy field and surface circulation in the extratropical North Atlantic Ocean in 1993–2001. *Journal of Physical Oceanography*, **35** (4), 405–426.
- Volkov, D. L. and L.-L. Fu, 2011: Interannual variability of the Azores Current strength and eddy energy in relation to atmospheric forcing. *Journal of Geophysical Research*, **116** (C11), C11011.
- Von Storch, H. and F. W. Zwiers, 2001: *Statistical analysis in climate research*. Cambridge university press.
- Wallace, J. M. and D. S. Gutzler, 1981: Teleconnections in the geopotential height field during the Northern Hemisphere winter. *Monthly Weather Review*, **109** (4), 784–812.
- White, A. and K. J. Heywood, 1995: Seasonal and interannual changes in the North Atlantic subpolar gyre from Geosat and TOPEX / POSEIDON altimetry. **100**, 931–941.
- Wijffels, S. and G. Meyers, 2004: An intersection of oceanic waveguides : Variability in the Indonesian Throughflow region. *Journal of Physical Oceanography*, **34** (5), 1232–1253.
- Wolff, J.-O., E. Maier-Reimer, and D. J. Olbers, 1991: Wind-driven flow over topography in a zonal β -plane channel: A quasi-geostrophic model of the Antarctic Circumpolar Current. *Journal of Oceanography*, **21** (2), 236–264.
- Wyrtki, K., 1975: Fluctuations of the dynamic topography in the Pacific Ocean. *Journal of Physical Oceanography*, **5** (3), 450 – 459.
- Wyrtki, K., L. Magaard, and J. Hager, 1976: Eddy energy in the oceans. *Journal of Geophysical Research*, **81** (15), 2641–2646.
- Yoshida, S., B. Qiu, and P. Hacker, 2011: Low-frequency eddy modulations in the Hawaiian Lee Countercurrent: Observations and connection to the Pacific Decadal Oscillation. *Journal of Geophysical Research*, **116** (C12), C12009.
- Yuan, D., et al., 2011: Forcing of the Indian Ocean Dipole on the interannual variations of the Tropical Pacific Ocean: Roles of the Indonesian Throughflow. *Journal of Climate*, **24** (14), 3593–3608.
- Yuan, X., 2004: ENSO-related impacts on Antarctic sea ice: a synthesis of phenomenon and mechanisms. *Antarctic Science*, **16** (4), 415–425.
- Zhai, X., R. J. Greatbatch, and J.-D. Kohlmann, 2008: On the seasonal variability of eddy kinetic energy in the Gulf Stream region. *Geophysical Research Letters*, **35** (24), L24609.

- Zhai, X. and C. Wunsch, 2013: On the variability of wind power input to the oceans with a focus on the subpolar North Atlantic. *Journal of Climate*, **26** (11), 3892–3903.
- Zlotnicki, V., L. Fu, and W. Patzert, 1989: Seasonal variability in global sea level observed with Geosat altimetry. *Journal of Geophysical Research: Oceans (1978-2012)*, **94** (C12), 17 959 – 17 969.